KAUNAS UNIVERSITY OF TECHNOLOGY

AGNĖ ŠMIGELSKYTĖ

# SYNTHESIS, PROPERTIES, AND APPLICATION OF RANKINITE IN THE PRODUCTION OF $CO_2$ CURED CONCRETE

Doctoral dissertation
Technological Sciences, Chemical Engineering (T 005)

2019, Kaunas

This doctoral dissertation was prepared at Kaunas University of Technology, Faculty of Chemical Technology, Department of Silicate Technology during the period of 2015–2019. The studies were supported by the Research Council of Lithuania.

**Scientific Supervisor:**
Prof. dr. Raimundas ŠIAUČIŪNAS (Kaunas University of Technology, Technological Sciences, Chemical Engineering, T 005).

Doctoral dissertation has been published in:
http://ktu.edu

Edited by: Armandas Rumšas (Publishing Office "Technologija").



ISBN 978-609-02-1650-7

The bibliographic information about the publication is available in the National Bibliographic Data Bank (NBDB) of Martynas Mažvydas National Library of Lithuania.

KAUNO TECHNOLOGIJOS UNIVERSITETAS

AGNĖ ŠMIGELSKYTĖ

# RANKINITO SINTEZĖ, SAVYBĖS IR PANAUDOJIMAS $CO_2$ APLINKOJE KIETĖJANČIO BETONO GAMYBOJE

Daktaro disertacija
Technologiniai mokslai, Chemijos inžinerija (T 005)

2019, Kaunas

Disertacija rengta 2015-2019 metais Kauno technologijos universiteto Cheminės technologijos fakultete Silikatų Technologijos katedroje. Mokslinius tyrimus rėmė Lietuvos mokslo taryba.

**Mokslinis vadovas:**

Prof. dr. Raimundas ŠIAUČIŪNAS (Kauno technologijos universitetas, technologijos mokslai, chemijos inžinerija, T 005)

Interneto svetainės, kurioje skelbiama disertacija, adresas:
http://ktu.edu

Redagavo: Armandas Rumšas (leidykla "Technologija").



ISBN 978-609-02-1650-7

Leidinio bibliografinė informacija pateikiama Lietuvos nacionalinės Martyno Mažvydo bibliotekos Nacionalinės bibliografijos duomenų banke (NBDB).

**Table of contents**

**Notations and Abbreviations**

OPC – ordinary Portland cement
C – CaO
S – $SiO_2$
A – $Al_2O_3$
Fe – $Fe_2O_3$
H – $H_2O$
C/S – $CaO/SiO_2$ molar ratio
$C_3S$ – $Ca_3SiO_5$ tricalcium silicate – alite
$C_2S$ – $Ca_2SiO_4$ dicalcium silicate – belite
$C_3S_2$ – $Ca_3Si_2O_7$ tricalcium disilicate – rankinite
CS – $CaSiO_3$ calcium silicate – wollastonite
$C_3A$ – calcium aluminate
$C_4AF$ – calcium aluminoferrite
C-S-H – calcium silicate hydrate
α-$C_2SH$ – dicalcium silicate hydrate
$CaO_{free}$ – free calcium oxide
SC – super critical
RH – relative humidity
w/c – water to cement (binder) ratio
w/s – water to solid ratio
ITZ – interfacial transition zone
CSC –calcium silicate cement
LOI – loss on ignition
XRD – X-ray diffraction analysis
XRF – X-ray fluorescence spectroscopy
STA – simultaneous thermal analysis
TG – thermogravimetry
DSC – differential scanning calorimetry
FTIR – Fourier transform infrared spectroscopy
SEM – scanning electron microscopy
EDX – energy dispersive X-ray spectrometry
BSE – backscatter electron
MIP – mercury intrusion porosimetry
CT – computer tomography
LA-ICP-MS – laser ablation inductively coupled plasma mass spectrometry
$^{29}Si$ MAS NMR – 29Si magic angle spinning nuclear magnetic resonance

## Introduction

Concrete is the second largest commodity after water consumed annually by the population of Earth. Due to such vast demand for building materials, cement industry is responsible for about 5–7% of the global anthropogenic greenhouse gas emissions, as, in the course of production of one tonne of cement, an almost equal amount of $CO_2$ is emitted into the atmosphere. Accordingly, the scientific community is struggling to find a solution for greenhouse gas mitigation and for reduction of the negative effect caused by the cement production. Even though in the last decades many solutions to alleviate the adverse effect of cement production to the environment have been proposed, recent studies have shown that such strategies as clinker substitutions, alternative fuels and/or improved energy efficiency alone will not be sufficient to meet the target $CO_2$ reductions. Thus finding alternative cementitious materials with a lower $CO_2$ footprint than the ordinary cement is one of the major challenges for the building material industry and the scientific community. One of the most promising approaches is the production of low-lime calcium silicate cement (CSC). This type of binding material not only requires lower amounts of limestone but, on top of that, is denoted by a lower production temperature thereby resulting in much lower $CO_2$ emissions. Moreover, such binders are environmentally amicable not only due to lower $CO_2$ emissions but also because of the capacity to permanently store $CO_2$ in the concrete structure in their carbonation hardening process. Implementation of such efficient carbonation technologies can potentially lead to cementitious materials becoming one of the largest global $CO_2$ sequestration sectors.

Rankinite – $Ca_3Si_2O_7$ – is one of such low lime calcium silicates that can be used as an alternative binder. Since the $CaO/SiO_2$ ratio of rankinite is almost two times lower than ordinary cement, it requires lower amounts of calcareous raw materials. The fuel and energy requirements for this type of binder are also reduced since the synthesis temperature of rankinite is 200 °C lower than that of cement clinker and it does not require any additional processing, such as rapid cooling, either. Moreover, rankinite can be produced from the same raw materials as cement clinker – therefore, the already operating production plants are also suitable for its production. Thus no major adjustments would be necessary. Since calcium silicates can be synthesized from a broad range of raw materials, it is economically conducive to use local materials. One of such materials, which is abundant in Lithuania, is *opoka* – a silica-calcite sedimentary rock that, together with limestone, whose resources are also readily available in Lithuania, can be used for the production of a rankinite binder.

Most importantly, rankinite is a non-hydraulic material that hardens in the $CO_2$ atmosphere, which results in a highly durable structure of calcium carbonates and silica gel. Since carbonation is a diffusion limited process, it relies on many process parameters, such as $CO_2$ pressure, exposure duration, temperature, moisture content, and properties of the concrete itself, all of which must be taken into account and efficiently combined.

Due to this, **the aim of this work** is to determine the influence of synthesis parameters on the rankinite formation process and mineral composition, to investigate

the mechanism of its curing in the $CO_2$ atmosphere and to determine the properties of the obtained concrete.

**The goals of this work are:**

1. To investigate the influence of applied compaction on the raw material mixture for Portland cement clinker, its calcination temperature, mineral composition, and hydration.
2. To investigate the impact of high temperature syntehsis conditions on the calcium silicate formation process, its mineral composition, and structural stability, and to determine the optimum parameters for rankinite synthesis.
3. To determine the influence of the carbonation parameters on the hardening process and performance of rankinite binder concrete.
4. To investigate the rankinite binder carbonation process kinetics and reaction product impact on the properties of hardened cement stone.
5. To prepare recommendations for the production of calcium silicate binder and its curing in the $CO_2$ atmosphere.

**Statements presented for defense:**

1. Rankinite formation is a multi-stage process including the formation of intermediate compounds, mainly larnite and wollastonite, that recrystallize to rankinite only at 1250–1275 °C.
2. Rankinite binder paste and mortar carbonation results in different reaction products as, in pastes, three polymorphs of crystalline $CaCO_3$, including meta-stable vaterite and aragonite, were observed, while mortars only contained calcite.
3. Rankinite binder carbonation includes diffusion and phase boundary limited stages which determine the course of the curing process and the mechanical properties of the obtained carbonated concrete.

**Scientific novelty of the research:**

Compaction of the raw mixture for OPC clinker results in the reduction of $CaO_{free}$ in the clinker composition by ~30%, while the heat release during the hydration increases by 2.5% after calcination at 1400 °C thus increasing clinker reactivity.

$CaCO_3$ formation in the rankinite binder carbonation reactions highly depends on the system composition since calcium carbonate polymorphs obtained in the single binder and complex mortar systems are different as pastes contained calcite, vaterite, and aragonite, while mortars only contained calcite.

**Practical significance of the scientific research:**

Locally available materials – Stoniškių-Žemaitkiemio opoka and Karpėnai quarry limestone – are suitable raw materials for calcium silicate synthesis: rankinite formation occurs at 1250 °C, which is 200 °C lower than OPC clinker formation. In addition, the production of rankinite binder requires 2 times less calcareous raw materials and ~20% less fuel, which results in lower $CO_2$ emissions, while the emitted

gas can be sequestered in stable carbonates in the concrete structure during the hardening process.

The obtained binder satisfies the essential requirements with regard to the currently existing state of the art technologies and can be characterized by the required physico-chemical and mechanical properties. After the hardening process in the water and $CO_2$ environment, silicate cement forms $CaCO_3$ thus increasing product density and reducing porosity. This results in enhanced durability and strength.

**Approval and publication of the research results:**

The results of the doctoral dissertation were published in 3 scientific publications included in the *Clarivate Analytics Web of Science* database – two papers were published in the *Journal of Thermal Analysis and Calorimetry*, while the third one was published in the *Romanian Journal of Materials/Revista Romana de Materiale*.

The results were presented in 9 scientific international conferences: *15th International Congress on the Chemistry of Cement* (ICCC'19) 2019, Czech Republic, *Chemistry and Chemical Technology 2019*, Lithuania, *12th European Symposium on Thermal Analysis and Calorimetry* (ESTAC 2019) 2019, Romania, *38th Cement and Concrete Science Conference* (CCS 2018) 2018, United Kingdom, *BaltSilica 2018*, Latvia, *Chemistry and Chemical Technology 2017*, Lithuania, *BaltSilica 2016*, Lithuania, *Chemistry and Chemical Technology 2016*, Lithuania, *International Conference on Thermal Analysis and Calorimetry* (RTAC-2016) 2016, Russia.

**Structure and content of the dissertation:**

The dissertation consists of introduction, literature review, experimental part, results and discussion, conclusions, a list of references and publications on the dissertation topic. The list of references includes 189 bibliographic sources. The main results are discussed in 56 pages and illustrated in 8 tables and 45 figures.

**The contribution of the author and co-authors:**

The author investigated and described the influence of the compaction pressure of clinker mineral formation as well as the rankinite binder synthesis process; the author also examined its carbonation hardening process. Raimundas Šiaučiūnas advised on the progress of the experiment that was carried out at Kaunas University of Technology and on the preparation of the manuscripts. Liudvikas Urbonas advised on the progress of the experiment that was carried out at Technical University of Munich and on the preparation of the manuscript. Matthias Wagner helped with X-ray diffraction analysis results and the preparation of the manuscript as well.

# 1. Literature Review

## 1.1. Ordinary Portland cement production: obstacles, solutions and alternatives

Ordinary Portland cement (OPC) based concrete is the most extensively manufactured building material on Earth in terms of volume (1), while its annual worldwide production is already approaching 4 billion tonnes (2). OPC is the most popular binder material used in concrete for construction because of its durability, efficient natural resource usage, strength, and relatively low cost. Nonetheless, all stages of OPC manufacturing have an adverse effect on the environment, in particular, regarding high energy consumption and air pollution. Cement plants cause 5–7% of global anthropogenic $CO_2$ emissions, while ~0.9–1 t of $CO_2$ is emitted into the atmosphere while producing one tonne of cement (3–5). Furthermore, about 110 kWh of electric energy is used to produce one tonne of cement, and most of this energy is related to the thermal treatment of the clinker (6). Even though the cement production technology is constantly changing and improving to meet the demand for cement quality and quantity, fuel efficiency and pollution limitations, there still is a matter of great importance to seek for alternative approaches so that to reduce the adverse effect of the OPC manufacture in order to pursue sustainable development. In the recent decades, attention has been directed to the environmental impact caused by production of construction and building materials. Therefore, the scientific community, along with the cement industry, has been seeking for such approaches that could include usage of industrial waste as a raw material in the production of OPC, substitution of conventional fuels with alternatives, advanced engineering solutions, and development of alternative cementitious products.

Minimizing the industrial waste and reduction of natural resource consumption are in the primary focus regarding the achievement of a cleaner production. Reusing industrial by-products is considered as one of the most promising and practical solutions thus allowing to scale down the accumulation of by-products produced by industries. Due to their inert nature, a broad range of waste materials can be incorporated into the concrete mixture as supplementary cementitious materials (SCM) with minimal impact on the properties of concrete; some waste even provides enhancement in concrete performance (7). Such wastes include granulated ground blast furnace slag (8; 9), fly ash (10), silica fume (11; 12), palm oil fuel ash (13–15), foundry waste (16–18), fibres from pre- and post-consumer wastes (13; 19), agricultural wastes (such as rice husk ash, wheat straw ash, sugarcane bagasse ash, hazel nutshell ashes, etc. (20)). Up to 30% of raw materials can be replaced with waste without significant influence on the properties of concrete (21; 22). Industrial waste utilization in concrete leads to sustainable, green, and environmentally friendly construction materials as well as to the reduction of the price of the components, improvement of the durability of concrete structures, and reduction of the energy usage as well as reduction of landfilling and disposal of waste.

Since approximately half of the $CO_2$ emission from OPC clinker burning is a result of fossil fuel combustion, another action to minimize this negative effect is displacement of the conventional fuel, such as coal or petroleum coke, with waste

materials. Utilizing low carbon content fuel with a high hydrogen-to-carbon (H/C) ratio instead of the conventional fossil fuels can remarkably diminish the rate of $CO_2$ emissions in the process (23). Potential alternative materials include vegetable compounds or natural products (oil shale, peat, barks, sawdust, waste wood, etc.), synthetic products (used tyres, rubber waste, waste plastics, etc.) and others (parts of shredded cars, fuels derived from rejects, household garbage, etc.) (24). Blending of different fuels with fossil fuel has economic, environmental, and chemical benefits. However, there are many factors to be considered before using alternative fuels. Such factors include moisture and ash content, calorific value, volatile content, reactivity, potential for ambient air pollution, slagging and fouling, and corrosion (25; 26). Reduction of fuel consumption can significantly contribute in reducing the global emissions of pollutant, greenhouse gases, and solid particles. Moreover, fuel and energy saving is also an effective strategy to slow down depletion of fossil fuels, and this can be achieved by many different approaches, such as process modification and integration, plant optimization, maintenance, insulation, energy recovery, etc.

What regards the engineering solutions, cement has been globally manufactured by employing three different processes, specifically, the wet, semi-wet and dry processes. The wet process uses raw materials that typically contain 30–40% of moisture. This raw material stream is directly fed to the kiln without any drying or preheating. Therefore, a big part of energy is consumed to evaporate this moisture and to prepare the materials for calcination reactions. In the semi-wet process, 10–20% of water is removed before feeding the raw materials to the kiln by preheating them on the conveyor by the kiln's exhaust gases. Therefore, feed materials reach the kiln with only 15–20% of moisture remaining. In the dry process, the raw materials are first dried, preheated, and only then transported to the kiln. It is possible to save up to 50% of the required energy and to reduce 20% of $CO_2$ emissions by shifting to the dry process (3). However, the dry process of the raw material requires more electrical energy compared to the wet process. Other solutions to reduce energy losses include applied insulation layers, proper sealing methods, and heat recovery from exhaust streams or implementation of a new design of the pyro-processing unit in cement factories. In the latter case, decomposition reactions are separated from other reactions, which results in pure $CO_2$ production. As a result of such novelties, the new process may reduce 66% of $CO_2$ emission and 2.3% of the energy consumption compared to the conventional process (27). In terms of the heat recovery, up to 20% of fuel can be saved, and, consequently, the $CO_2$ emissions can be mitigated by 8%.

Even though the OPC clinker production technology is rather well developed and optimized, the improvement possibilities of the already existing technology should not be excluded. It is well known that synthesis reactions are intensified when the contact surface area of the reactants is increased. Thus, if the compaction pressure is used, clinker particles are forced to compress, and the space between the particles is physically reduced. Therefore, point contacts between the particles are transformed into interfaces, this way affecting the water-to-solids ratio and porosity, and thus altering the mechanism of hydration reactions. Due to the applied force, clinker mineral formation reactions are accelerated and intensified as the particles need to overcome smaller inner distances. Compaction also has an impact on the free lime

content which subsequently exerts a major impact on the clinker produced in the kiln processes. Free CaO content in a range of 1–1.5% leads to optimized energy consumption with maximum kiln reactivity, improved fuel consumption, and ultimately to a decrease in $CO_2$ emissions (28).

An additional way to achieve lower $CO_2$ emissions and energy consumption is to reduce the lime saturation factor of the raw mixture. This may lead to an increase in the belite amount and a decrease in the alite phase content in the clinker. The reduction of the $CaCO_3$ content in the raw mixture (when belite-rich cement is produced) decreases the energy demand by 15–20% (29) and reduces $CO_2$ emissions by 20–30% (30). However, the mechanical strength of belite cement is very low in the initial hardening stage due to the slow hydration of the belite phase. This weakness can be avoided by stabilizing hydraulically reactive forms of belite and its chemical activation (30–32).

Another way to decrease the cement $CaO/SiO_2$ (C/S) ratio is by using low-lime calcium silicates such as rankinite ($3CaO{\cdot}2SiO_2$ or $C_3S_2$) (33–37), wollastonite and pseudowollastonite ($CaO{\cdot}SiO_2$ or CS) (34; 38–41) instead of the conventional OPC clinker minerals. The amounts of limestone required to produce these low-lime calcium silicates are almost two times lower than those of OPC; hence it contributes to the reduction of the $CO_2$ emission from the calcination process involved in the cement production (42). Moreover, these materials not only contain a lower amount of lime, they also have a lower production temperature, which also contributes to the lower $CO_2$ emissions. However, unlike conventional hydraulic calcium silicates, the aforementioned ones are non-hydraulic binders, and therefore one of the ways to readily activate and harden them is carbonation curing. These binder systems can store a substantial amount of $CO_2$ through the hardening process, which helps to alleviate the greenhouse effect. A recent addition to this carbonated binder system is a commercially available cement referred to as “calcium silicate based cement (CSC)” (34; 42).

Owing to this, one of the most viable options that can greatly reduce the $CO_2$ emission is the capture, storage, and sequestration of the emitted $CO_2$ in the concrete materials (43). The carbon dioxide capture and storage (CCS) in one of the major recent research studies regarding industrial greenhouse gas emission mitigation, where potential storage methods include geological storage, ocean storage, and $CO_2$ mineralization (i.e., mineral carbonation) (44–47). The method that seems to be most useful for the cement industry is mineral carbonation – that is a process in which $CO_2$ is chemically stored in solid inorganic carbonates by carbonation reactions of alkaline materials containing calcium oxides and silicates (45) and includes natural and accelerated processes. Concrete and other cementitious materials absorb $CO_2$ through a natural process (48). One of the main consequences of the carbonation reaction of concrete is the modification and reduction of pH in the pore solution (49). Therefore, conventionally, the carbonation reaction of concrete is considered as an unfavourable effect since it decreases the durability performances of such materials (50); moreover, it is also known as a very slow process due to the low $CO_2$ concentration in the atmosphere. Nevertheless, concrete carbonation has a positive impact on the mechanical properties of the material. Recent research has shown that concrete can be

treated with carbonation curing at early age for accelerated strength gain and improved durability (51–53). OPC concrete carbonation has been widely discussed in the literature (54–62) and is regarded as an opportunity to create a sustainable concrete industry by storing $CO_2$ in cement-based materials and utilizing carbonate binders with a low $CO_2$ footprint.

Even though, low $CO_2$ carbonated binders gained major interest in the recent years, there are only a few of them that have already reached the stage of manufacturing and are commercially available, including *Solidia* cement (34), carbonated concrete named $CO_2$-SUICOM that can achieve a $CO_2$ emission level below zero (63), *Calera* calcium carbonate (64) and *Novacem* magnesium silicate (65).

## 1.2. Alternative low-lime binder materials

### 1.2.1. Belite cements

Belite ($Ca_2SiO_4$ or $C_2S$) is the second largest clinker phase in OPC and its hydration products develop a similar strength in cement to that of alite ($Ca_3SiO_4$ or $C_3S$) in the final stage – it only matures much slower and significantly contributes to strength only after 28 days of hydration (66). Compared to OPC, low-lime chemistry of $C_2S$ extends a variety of manufacturing and materials benefits to the cement industry, such as the use of lower-grade limestone and lower calorific value alternative fuels, lower kiln temperatures, and more efficient heat management.

There are five $C_2S$ polymorphs that are stable in different temperature ranges, have different structures and hydraulic properties – α, $\alpha'_L$, $\alpha'_H$, β, and γ (67; 68). The α′ polymorphs are the most hydraulic forms of belite, while β-belite is slightly less hydraulic, whereas γ-belite is a non-hydraulic polymorph that does account for the setting and hardening of cement (69). Generally, none of the forms of α polymorphs is present in the final cement clinkers because they are readily transformed to β-$C_2S$ and γ-$C_2S$ during the cooling process. The β and γ polymorphs coexist because of the reversible polymorphic transition that takes place below 500 °C, and this β → γ polymorphic transformation occurs when cooling and is disruptive with a change in volume by 12 % (70). This effect is called ‘dusting’ and causes the material to disintegrate spontaneously to powder (71), although it can be avoided by fast cooling or by inclusion of an appropriate stabilizer. The β-$C_2S$ polymorph is the most important considering its hydraulic properties, and the γ-$C_2S$, as a non-hydraulic polymorph is used in production of low-lime carbonated cement since it hardens in $CO_2$ atmosphere.

Hydraulically active low-energy cement based on belite-rich clinker is a highly prospective cementitious binder, but the main problem is to find a way to produce belite cement with properties of standard OPC while using the existing production lines. Since the hydraulic reactivity of β-$C_2S$ is substantially slower than that of $C_3S$, therefore, studies based on stabilizing hydraulically active forms of belite were conducted. High reactive forms of $C_2S$ can be stabilized by ‘remelting reaction’ and by adding controlled amounts of stabilizers, such as NaF, $SO_3$, and $B_2O_3$ (33).

Stanek and Sulovsky (31) state that chemical stabilization by suitable admixtures, usually complemented by fast quenching, is one of the possibilities to

stabilize the reactive form of belite. The principle of belite activation is the formation of a belite clinker with an increased ratio of $CaO:SiO_2$ in the structure of dicalcium silicate by substitution of $SiO_4$ groups with $SO_4$ groups. It is claimed that $SO_3$ considerably decreases the viscosity and surface tension of the clinker melt, postpones the start of alite formation, and also decreases its nucleation and its overall content in the clinker. Stanek and Sulovsky achieved hydraulically active low-energy belite cement by burning clinker at a temperature of 1350 °C and activating it by addition of about 5 wt.% of $SO_3$. The authors claim that this type of cement has the same fineness of grinding as alite-rich cements, and, on top of that, short-term strengths exceeding 20 MPa, and lower heat of hydration after 7 days of hardening.

Bouzidi *et al*. (30) used quick cooling associated to four different mineralizations (i.e., 2% NaF; 2% LiF; 1% NaF + 1% $CaSO_4$; 1% LiF+1% $CaSO_4$) in order to synthesize environmentally friendly cements of a very low lime saturation factor and hydraulic reactivity compared to alite cement. The use of the aforementioned mineralizers made it possible to reduce the burning temperature of cement by about 300–350 °C compared to alite cement and also to significantly reduce the energy consumption as well as the emission of greenhouse gas during the manufacturing process. The use of mineralizers improved the crystallization of the belite phases, which led to an improvement of the hydraulic reactivity of cement thus helping it to reach compressive strength of cement Class 32.5 according to NF P 15-301, which is an ordinary Portland (alite) cement. Kacimi *et al*. (32) obtained a belite clinker with hydraulic reactivity similar to that of alite clinker, by burning a raw mixture containing 2% of NaF at 1150 °C and cooling quickly by water quenching, of which, hydration heat and compressive strength evolve quickly to reach the values of 28 days, similar to those of alite clinker.

$B_2O_3$ can also be used to stabilize $\beta$-$C_2S$ and to prevent its transformation into $\gamma$-$C_2S$. Davraz (72) investigated the effects of boron compounds in the hydration process of various cement types and the controllability of these effects. He determined that the highest $B_2O_3$/cement ratio to reach the closest workability and other properties of OPC is 0.3.

Even though belite-based cement offers a considerable opportunity to mitigate the cement production impact on the environment, however, there is still much effort needed to obtain significant results in this development.

### 1.2.2. $\alpha$-$C_2SH$ binders

Another promising approach to the production of highly reactive belite binders at lower temperatures is the hydrothermal synthesis of intermediate calcium silicate hydrates (C-S-H) followed by thermal or mechanical activation. Hydraulically active C-S-H can be obtained by intensive tribochemical activation of hydrothermally synthesized dicalcium silicate hydrate $\alpha$-$C_2SH$ ($\alpha$-$Ca_2[HSiO_4]OH$) together with quartz (73). By using such materials, the consumption of lime and energy are highly reduced in comparison to OPC, and it is possible to reduce the $CO_2$ emissions in production by 50%.

$\alpha$-$C_2SH$ is an orthorhombic nesosilicate which can be easily produced from calcium oxide and silicic acid by means of autoclaving between 95 and 200 °C (74).

However, it is difficult to obtain pure α-$C_2SH$ by using natural raw materials since it often forms together with other calcium silicates and portlandite (75). Another difficulty is dehydration because this material is highly dependent on the annealing temperature and yields different phase compositions of dehydrated material. Therefore, many researches have struggled to achieve a hydraulically active form of $C_2S$.

Garbev *et al*. (76) were the first ones to propose a hydraulic binder synthesized from α-$C_2SH$ activated by milling with sand. The authors (76; 77) synthesized a novel cementitious material referred to as 'calcium–oxide-hydroxide–silicate' (C–CH–S) that is amorphous and was produced via mechanical and thermal treatment of a mixture of quartz and hydrothermally synthesized calcium silicate hydrates – α-$C_2SH$ and jaffeite. The material was formed independently of the type of mill used after thermal treatment of the ground materials at 360–420 °C and demonstrated very high hydraulic reactivity, which was beyond that of typical $C_2S$-like materials. The same authors (78) later on investigated the stability and structural relations between α-$C_2SH$, killalaite, dellaite, and x-$C_2S$ that have an impact and stabilize β-$C_2S$ as the final product.

Link *et al*. (79) synthesized α-$C_2SH$ by mixing $Ca(OH)_2$ and highly dispersive $SiO_2$ (molar ratio of $Ca(OH)_2/SiO_2$ = 2), with the addition of 5% α-$C_2SH$ seeds as a precursor and as crystallization centres. The solids were suspended in de-ionised water (water/solid = 10) and autoclaved at 200 °C for 16 h. During the autoclaving process, the suspension was stirred at 200 rpm. The resulting α-$C_2SH$ was filtered and dried at 80 °C. α-$C_2SH$ was annealed at temperatures between 400 and 800 °C to produce highly reactive binders, which led to a multiphase binder consisting of X-ray-amorphous material, x-$C_2S$, γ-$C_2S$ and β-$C_2S$ (above 600 °C). The amorphous content was the most reactive constituent, while the x-$C_2S$ was the most reactive crystalline $C_2S$ polymorph. The authors determined that criteria for the production of highly reactive binders are the annealing temperatures below 500 °C.

Šiaučiūnas *et al*. (80; 81; 82) synthesized α-$C_2SH$ from limestone and quartz sand (C/S = 2) with 5 wt% addition of sodium oxide. According to the authors, α-$C_2SH$ was the dominant compound in the product after 8 h of hydrothermal synthesis at 200 °C in stirred (50 rpm) suspensions. It was established that tribochemical activation must be combined with thermal treatment in order to obtain a hydraulically active cementitious binder from the mixture of synthesised α-$C_2SH$ and quartz sand (83). The hydraulic binder material was prepared by mixing α-$C_2SH$ and quartz sand (1:1), activating it in a vibratory disc mill for 5 min at 950 rpm, and thermally treating at 450°C for 30 min. The manufactured binder material obtained a compressive strength of 10.3 MPa after 3 d and 19.4 MPa after 28 d of hydration.

The production of such materials is not only less costly in terms of energy, it is also less harmful to the environment since $CO_2$ is emitted only during the calcination process of the raw materials.

### 1.2.3. Rankinite

Rankinite is a low-lime non-hydraulic calcium silicate ($3CaO{\cdot}2SiO_2$ or $C_3S_2$). It was first described from the dolerite-chalk contact at Scwat Hill, Co., Antrim, and was

named in honour of dr. G.A. Rankin of the Geophystical Laboratory, Carnegie Institution of Washington (84). It is a very rare mineral that can be found in natural melt rocks (41) and is considered to be dimorhpous to kilchoanite. Natural rankinite varies little in composition from pure $Ca_3Si_2O_7$ and shows only a small amount of other ions which may be present only as impurities. In the rankinite crystal, the Si and O atoms are arranged in sorosilicate groups $[Si_2O_7]^{-6}$, in which, the central O connects two $SiO_3$ units (85). The interatomic distances between Ca and O have the values from 2.25 to 2.90 Å, while the angles O-Ca-O are all from 60 to 87 degrees. The $Si_2O_7$ groups have shapes of nearly regular tetrahedrons like other silicates, and the distance between Si-O is from 106° to 115° (86). The rankinite structure is ordered in successive layers of Ca atoms and $Si_2O_7$ groups parallel to the z direction, with the $Si_2O_7$ units oriented towards the z direction and resulting in the lower compressibility of the mineral in this direction (85).

This type of material is not usually used in conventional OPC based systems, but can rather be used as an alternative binder material readily activated during the carbonation reaction in the presence of moisture. However, the potential applications of $C_3S_2$ in cement-based materials have not yet been thoroughly explored, and literature on this topic is rather scarce.

Rankinite can be produced from the same calcareous and siliceous raw materials as OPC clinker, and its manufacturing needs neither specialized equipment nor additional unit operations; thus already existing OPC plants can be used without almost any modification. Since the rankinite calcination temperature is about 200–250 °C (34; 87; 88; 89) lower than that of OPC, alternative fuels of lower calorific value can be used for its production. The absence of $C_3S$ in this type of cement makes it less sensitive to the cooling rate, therefore, rapid cooling is not necessary, and thus the heat losses from the cooler can be considerably reduced. Additionally, the non-hydraulic nature of rankinite eliminates the usage of gypsum as a set-controlling component, and since it is not prone to hydration, no special storage arrangements are needed, either. Moreover, the hardening or carbonation curing of rankinite is a relatively speedy process. It can be conducted at ambient pressures and at moderate temperatures of 20 to 60 °C, and the concrete products can be cured within a 24-hour period, which makes this process much more productive and efficient compared to the 28-day curing cycle required for OPC-based concretes. Above all, rankinite curing via a reaction with gaseous $CO_2$ opens up the possibility for the permanent sequestration of $CO_2$ in a hardened concrete structure.

Qian *et al*. (38) determined the optimal formation temperature and sintering time of $C_3S_2$, which was approximately 1300 °C and 4 h, respectively. The materials used for the synthesis were industrial raw materials of limestone and quartzite. The authors claim that, at temperatures above 1300 °C, the formation of rankinite no longer occurred, and the slight decomposition of this mineral could take place when sintered for a considerable time – more than approximately 8 h – according to the authors. At lower sintering temperatures (1200 °C), the formation of $C_3S_2$ was time controlled, while higher temperatures accelerated the formation of $C_3S_2$. With a prolonged sintering time, $C_3S_2$ formed via consumption of $\beta$-$C_2S$ and $\gamma$-$C_2S$.

Wang *et al*. (90) synthesised pure rankinite by calcining a C-S-H gel precursor at a temperature of 1300 °C. The C-S-H precursor was prepared by exposing the mixtures of CaO and amorphous $SiO_2$ (at 3:2 molar ratios) to a hydrothermal process. The water-to-solid ratio was 10, and the mixtures were sealed at 60 °C for 6 h to allow the complete reaction at ambient pressure. Then, the prepared C-S-H gel precursor was dried in a vacuum oven at 100 °C for 24 h, and the dried C-S-H gel precursor was later calcined at 1300 °C for 2 h. Zwang *et al*. (91) prepared $C_3S_2$ from the mixture of raw materials of $CaCO_3$ and $SiO_2$ (at 3:2 molar ratios) that was calcined at a temperature of 1440 °C for 2 h. Lu *et al*. (92) prepared a low calcium clinker containing rankinite by sintering the stoichiometric mixture of calcium oxide, amorphous silica, aluminum oxide and ferroferric oxide. The mixtures were heated to the target temperature of 1250–1320 °C for 2 h. Lu and his team determined that the sintering laboratory temperature for this type of clinker was about 1320 °C, and the product included mostly $C_3S_2$, γ-$C_2S$, and a low amount of $C_2AS$. Ashraf and Olek (93) synthesised rankinite form CaO and amorphous (fumed) silica with a molar ratio of 3:2 at a heating temperature of 1250 °C.

Even though the rankinite synthesis temperature varies quite greatly depending (1250–1440 °C) on the system, it still offers a great potential for the reduction of carbon footprint when compared to OPC clinker which is produced at around 1450 °C.

### 1.2.4. Wollastonite

Wollastonite is a single-chain low-pressure polymorph of calcium metasilicate ($CaSiO_3$ or CS), with a chain repeat unit of three tetrahedrons. Its formation is a two-step process: larnite ($C_2S$) appears in the first step and then reacts with the $SiO_2$ excess to form wollastonite. Under all conditions, rankinite ($C_3S_2$) seems to be the precursor of wollastonite (94). $CaSiO_3$ exists in two primary mineral phases, including β-wollastonite (or simply wollastonite), and α-wollastonite (pseudowollastonite). β-wollastonite mineral is obtained as a natural silicate material, whereas α-wollastonite is rarely found in nature (41; 95). Wollastonite can also be synthesized from various raw and waste materials, similar or the same to those used for OPC production from limestone and silica (95) to calcium hydroxide and zirconium-containing silicon slag (96) at temperatures of 1000–1450 °C.

Wollastonite is commonly used in ceramics and plastics as a filler, in coating materials, metallurgy, wood-composites, rubber, paper fillers, paints, etc. due to its low water and oil capacity, low shrinkage, and chemical stability (96), as well as due to good fluxing properties, less volatile components and needle-like shapes that give it a reinforcing capability (33). This low lime calcium silicate is non hydraulic, but it still reacts with $CO_2$ in the presence of moisture (97). Due to the presence of calcium oxide and rapid dissolution rate, wollastonite is considered to be one of the most suitable minerals for geological sequestration of $CO_2$ (40). $CO_2$ is sequestered in wollastonite by the process of mineral carbonation where this calcium silicate reacts with $CO_2$ to form calcium carbonate and silica gel.

## 1.3. Carbonation of cementitious materials

### 1.3.1. Natural vs. accelerated

Concrete and other cement-based materials absorb $CO_2$ through a natural process known as mineral carbonation that results in permanent $CO_2$ sequestration in these materials. About 19% of the $CO_2$ produced during manufacturing of cement is reabsorbed by concrete over its lifecycle (48). However, the natural process of carbonation in concrete is very slow – about 1 mm/year – due to the low $CO_2$ concentration in the atmosphere (400 ppm or 0.04% (50)). Moreover, in natural carbonation, the amount of $CO_2$ dissolved in the pore water is restricted by the low solubility of atmospheric $CO_2$ in water (98) and the slow rate of diffusion of $CO_2$ into the mortar structure (55).

Carbonation is a diffusion process either by $CO_2$ or by carbonate ions, which in turn is controlled by water saturation in the capillary system (99). Over time, THE carbonation rate decreases as $CO_2$ must pass through a thickening layer of its alteration products. The speed of transportation is mainly governed by concentration gradients, porosity and thickness of the already formed layer of carbonation products (99). On the other hand, the carbonation rates of accelerated carbonation are considerably higher than those of natural carbonation. The higher carbonation rates are obtained by using higher $CO_2$ concentration and controlled environment, among which, humidity is one of the most important factors in the progress of the carbonation front and the amount of $CO_2$ combined.

Natural carbonation of concrete takes place when $CO_2$ from the atmosphere reacts with alkaline components of concrete, mainly portlandite, and/or with the C-S-H gel, resulting in the formation of $CaCO_3$. This reaction generally leads to a decrease in the pH of the aqueous phase of the concrete pores, i.e., from highly alkaline values greater than 12 to values below 8 (58). If the reaction reaches the steel reinforcement, its passive layer may disappear thus exposing the steel surface to corrosion, therefore, carbonation is generally regarded as a deterioration mechanism for concrete. The deleterious effect of atmospheric $CO_2$ on modern concretes and mortars is known as ‘weathering carbonation’ (100). Another important consequence of carbonation is the change of the effective permeability due to volume changes and microcracking caused by the chemical reactions. The permeability change can be an increase, as in concrete containing blast furnace slag or fly ash, or a decrease as in OPC (101). Accelerated carbonation, on the other hand, may be used to achieve accelerated strength gain and improved durability of the concrete products. Among other differences, researches reported that the reaction products formed during natural and accelerated carbonation are considerably different due to the dependence of the alkali-carbonate phase equilibrium on the $CO_2$ concentration (102). Goni *et al*. (103) compared $CaCO_3$ polymorphs formed in natural and 100% carbonation and detected that, in natural carbonation calcite, vaterite and aragonite formed, while at 100% $CO_2$ calcite was the only polymorph present.

Accelerated carbonation curing has several important benefits over moisture curing (98). Accelerated carbonation curing can lead to high early age strength and rapid strength gain due to the more densified crystalline structure. Carbonation curing

has been found to increase durability by decreasing capillary water uptake, chloride resistance, and by showing better sulphate resistance (104).

### 1.3.2. Parameters influencing the carbonation process

In theory, the carbonation process seems fairly simple, however, in reality, it is a complex process that depends on many and various parameters. The carbonation reaction of hydrated Portland cement in air is generally a slow process that is dependent on the relative humidity of the environment, temperature, permeability of the concrete, and the concentration of $CO_2$ available (48). In accelerated carbonation, the pressure value is an additional variable. According to Bertos *et al*. (55), the main factors that affect the carbonation process are the diffusivity and reactivity of $CO_2$, while the following scheme combines the carbonation-dependent factors:

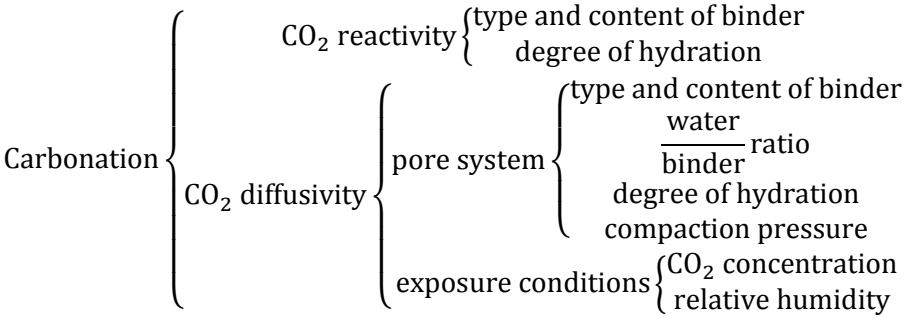


**Fig. 1.1** Factors on which the carbonation process depends (55)

***Reactivity of $CO_2$***

For $CO_2$ to be reactive in order to achieve effective carbonation, the solid material has to possess certain chemical properties. First of all, materials must be inorganic in nature, containing calcium and/or silicon salts, or they may be hydraulic, pozzolanic, lime-bearing or other $CO_2$-reactive calcium-containing material heavy metals (55). The higher is the concentration of Ca in the material, the better is the result of carbonation, therefore, the higher is the Ca/Si ratio, the higher is the degree of carbonation as well.

The water content in the material in also very important since it is necessary to promote the carbonation reaction by dissolving $CO_2$ and releasing $CO_3^{2-}$ ions. $CO_2$ in the gaseous form cannot react directly with the cementitious material; for carbonation, $CO_2$ gas has to first dissolve in water to form carbonate ions (carbonic acid) which, in turn, react with the calcium ions of pore water. However, an excess of water may limit the rate of carbonation by clogging the pores and reducing the diffusion of $CO_2$, which subsequently leads to the faster accumulation of precipitations on the surface. At low water-to-cement (w/c) ratios, the gas permeability is increased, and the $CO_2$ effectively diffuses into the material, therefore, the optimum water-to-solids (w/s) ratio has been found to be between 0.06 and 0.20 (105). Even so, a different water content may be required for different cement types in order to achieve the same degree of carbonation.

***Diffusivity of $CO_2$***

Diffusivity of $CO_2$ is constrained by the physical properties of the solid (55). The higher is the surface area of the material, the greater is the degree of carbonation. A high degree of compaction (mechanical or due to a higher surface area) leads to a lower porosity and, therefore, to a higher strength, however, it may prevent $CO_2$ diffusion. Carbonation of cement-based materials is largely controlled by the diffusion rate of $CO_2$ through the microstructure if it is already hardened. Therefore, a higher microporosity of the hydration products leads to a better-carbonated material (55).

Shao *et al*. (106) suggest that, theoretically, with 100% carbonation efficiency, 1 t of cement could absorb 0.5 t of $CO_2$ to form 1.5 t of solid calcium carbonates and silica gels. In practise, however, this is limited by strength and diffusivity consideration. In reality, $CO_2$ uptake of 9–20% by mass of cement has been achieved (107).

***Pressure***

$CO_2$ partial pressure can control the carbonation process which can be carried out at various pressure values from atmospheric to super-critical $CO_2$ ($scCO_2$). $CO_2$ pressure along with other process parameters determines the course of the reaction and, depending on the individual system, all the parameters should be set individually as well. By increasing the temperature and pressure, it is possible to increase the rate at which carbonation occurs in concrete.

Shi and Wu (108) state that accelerated reactions between $CO_2$ and cement minerals happen mainly during the initial 15 minutes of curing regardless of the $CO_2$ pressure and pre-conditioning environment. Furthermore, they found that an increase in the $CO_2$ pressure increases the $CO_2$ consumption but does not show any significant effect on the strength of concrete.

Some authors have taken into account the carbonation process using $scCO_2$. Supercritical carbon dioxide is a fluid state of carbon dioxide where it is held at or above its critical temperature and critical pressure. Taylor *et al*. (109) states: "as the container is heated, the density of the liquid decreases because of normal thermal expansion. Simultaneously, the density of the vapor increases as more molecules leave the liquid and enter the gas phase. If the heating continues, a temperature will be reached called the critical temperature, where the density of the liquid is so reduced, and that of the vapor is so increased that the density of the two phases becomes equal. When this occurs, then since the density and temperature inside the container is everywhere equal, and the pressure is everywhere equal, we have reached a supercritical fluid". For $CO_2$, the critical point is 31.1 °C (around 304 K) and 7.39 MPa (around 74 bar). Supercritical $CO_2$ has liquid-like density but gas-like transport properties and no surface tension, which enables it to penetrate into very fine pores of the cement paste (98). In natural carbonation, the amount of $CO_2$ dissolved in the pore water is restricted by the low solubility of atmospheric $CO_2$ in water. High pressure helps to increase the amount of $CO_2$ molecules dissolved into the pore water, therefore, $CO_2$ is able to penetrate even small pores with ease thus providing continuous availability of fresh $CO_2$ (110). Therefore, carbonation of cement under supercritical conditions is not diffusion controlled (111).

***Relative humidity***

The carbonation reaction rate is the highest within a relative humidity (RH) range of 50–70%, and it decreases at higher and lower relative humidity (99). The relatively narrow range of RH is due to the fact that the progress of carbonation reaches its maximum at an RH of about 60% (57). At RH > 70%, capillary condensation as an additional parameter seems to be pore size-dependent, and, with it, cement-specific influence on carbonation resistance is maintained (112).

Galan *et al*. (113) determined that, at a very low RH, there is not enough water in the pores to dissolve the phases involved and to allow their reaction. At an intermediate RH, the optimal conditions for carbonation are reached: enough water for the reaction, as well as enough space for $CO_2$ diffusion. From a certain value of RH, the pores start to be saturated with water, complicating the diffusion.

***Temperature***

The effect of temperature is usually complicated. A higher temperature could promote the ion leaching and chemical reaction, yet it reduces the solubility of $CO_2$. At low temperatures, superficial carbonation temperatures are favored thus promoting the formation of a carbonate shell over the particles' surface, while at higher temperatures, diffusion processes are more effective, and the carbonation can proceed through the bulk material; thus, through higher temperature carbonation, $CO_2$ can quickly cure and be permanently stored in the concrete structure. Considering the application on an industrial scale, it may be more convenient to operate at high temperatures rather than at a high pressure (46).

According to Bertos *et al*. (55) the uptake of $CO_2$ increases with the increasing temperature up to 60 °C (at atmospheric pressure). This is most likely due to the leaching of $Ca^{2+}$ ions from the particles of the solid. Higher temperatures decrease the solubility of $CO_2$ in water thus decreasing the rate of carbonation. However, as the carbonation reaction is exothermic, the heat of the reaction promotes the formation of meta-stable polymorphs of $CaCO_3$. To obtain the desired stable polymorph (i.e., calcite), the process should be maintained at low temperatures – in a range of 0–10 °C. Asavapisit *et al*. (114) showed that more calcite is formed if very cold carbonic acid is used. Wang *et al*. (110) determined that the rise of the temperature to 40 °C results in a significant increase of the initial reaction rate and the total $CO_2$ uptake capacity, but the further increment to 60 °C presented a negative effect (at 15 bar and w/c of 0.16). Contrarily, Liu *et al*. (115) showed that the temperature increase up to 60 °C resulted in a higher $CO_2$ content in the solidified material, while an increase of the reaction temperature above 60 °C resulted in a decreased $CO_2$ content due to the decreased $CO_2$ solubility in water at elevated temperatures.

Mazzella *et al*. (46) states that increasing the temperature from 25 to 45 °C resulted in twice as high $CO_2$ uptake at 2.5 bar and even almost three times higher uptake at 7.5 bar $CO_2$ pressure, therefore, it is evident that the temperature plays an important role in the carbonation process.

Considering the complexity and abundance of carbonation affecting parameters, the most important aspect is to find and investigate the coexistence and interaction of these factors upon the reaction course and kinetics. Since the carbonation process is mostly diffusion-based, some of the factors affect the reaction path in a positive way,

while the others act contrarily. Thus this is a major obstacle for the scientist to reach the desired parameter synergy.

### 1.3.3. OPC carbonation

Carbonation of cementitious materials is a natural phenomenon that is caused by carbon dioxide in the atmosphere. About 19% of the carbon dioxide produced during manufacture of cement is reabsorbed by the concrete over its lifecycle (48). According to the literature (116-126), carbonation is the result of the neutralization reaction between the basic compounds of calcium silicates and $H_2CO_3$ producing thermodynamically stable carbonates and water, which leads to the drop in pH. Carbonation of concrete can be described as a physical-chemical process, in which, a series of chemical reactions occur. $CO_2$ dissolves in the aqueous pore solution and produces carbonic acid ($H_2CO_3$). $CO_2$, which penetrates concrete through a diffusion mechanism, slowly proceeds from the surface inwards, with the depth of carbonated cement concrete front increasing with time. The rate of carbonation depends on many factors, such as moisture content, permeability of concrete, the environment's $CO_2$ content, and the relative humidity. Theoretically, due to the instability of hydration compounds in the presence of $CO_2$, concrete is able to absorb over time almost the same amount of $CO_2$ as that which was chemically released during the reverse reaction of limestone calcination in the cement kiln (127). The reaction of $CO_2$ with calcium bearing phases in the cement paste can also cause chemo-mechanical changes in the microstructure and porosity (98). These changes are usually considered as passive since they occur spontaneously when cement paste reacts with $CO_2$, therefore, they are commonly considered as deterioration effects even though some properties, such as compressive strength, can be improved during the carbonation. On the other hand, an active carbonation process stems from a procedure designed to intentionally take advantage of the ability of calcium bearing phases of the cement paste to react with carbon dioxide for different applications. Active or accelerated carbonation curing is a way to capture and store atmospheric $CO_2$. This procedure involves exposure of the freshly cast cement paste or concrete to a pure or $CO_2$ rich environment. With fresh pastes and high concentrations of $CO_2$, the hydration process of OPC is greatly accelerated as well. Accelerated carbonation curing has several important benefits – it can lead to high early age strength and rapid strength gain. This is due to pore filling by $CaCO_3$, as well as due to changes in the C-S-H microstructure.

The process of OPC carbonation is strongly exothermic and diffusion-controlled. Carbon dioxide dissolves in water to form carbonic acid, while this reaction involves the evolution of considerable quantities of heat, specifically, $669.9\times10^3$ J/mol (55). $CO_2$ gas diffuses into the solid resulting in a growing front of carbonated material surrounding the inner zone of non-carbonated material. The penetration of carbonation is formulated by considering the following successive steps which are generally involved in the reactive-transport mechanism (55):

1. Diffusion of $CO_2$ in the air.
2. Permeation of $CO_2$ through the solid.
3. Solvation of $CO_{2(g)}$ in the water to $CO_{2(aq)}$.
4. Hydration of $CO_{2(aq)}$ to $H_2CO_3$.

5. Ionization of $H_2CO_3$ to $H^+$, $HCO_3^-$ and $CO_3^{2-}$. During this stage, pH typically drops from 11 to 8.

6. Dissolution of cementitious phases $C_3S$ and $C_2S$. This step is rapid and extensive, calcium silicate grains are covered by a loose layer of calcium silicate hydrate gel which is quickly dissolved, releasing $Ca^{2+}$ and $SiO_4^{4-}$ ions.

7. Nucleation of $CaCO_3$, C-S-H, which is favored by slightly higher temperatures and the presence of finely derived material that acts like heterogeneous nuclei.

8. Precipitation of solid phases. At the beginning, vaterite and aragonite can be formed, but these polymorphs of $CaCO_3$ ultimately revert to calcite. Amorphous calcium carbonate can also be found in the final product.

9. Secondary carbonation. C-S-H gel forms and progressively decalcifies, converting ultimately to silica gel and $CaCO_3$.

During the carbonation reaction of calcium silicates, the primary reaction product is $CaCO_3$. Major chemical reactions governing carbonation curing of cement-based materials are the following:

$$Ca(OH)_2 + CO_2 \rightarrow CaCO_3 + H_2O \quad (1.1)$$

This reaction occurs because calcium is the most common element among the Portland cement hydrates, and calcium hydroxide has the highest water solubility compared to the other calcium compounds; thus, the reaction with $CO_2$ readily proceeds. Even though this reaction is between a gas and a solid, water plays an important role – ion dissolution of calcium hydroxide and $CO_2$ dissolved in pore water is necessary for the carbonation to proceed. Calcium hydroxide dissolved in the pore solution can react with carbonic acid to produce calcium carbonate (43; 128):

$$Ca(OH)_2 + H_2CO_3 \rightarrow CaCO_3 + 2H_2O \quad (1.2)$$

The formation of both carbonic acid and crystalline $CaCO_3$ are exothermic reactions which release 160 kcal and 288 kcal of heat per mole, respectively (129). As the reaction continues, the calcium hydroxide content in the cement paste decreases, and the production of calcium carbonate increases and subsequently reduces the pH of the hardened paste.

The hydration reaction of cement clinker minerals constantly occurs as time proceeds. The carbonation reaction of unreacted $C_3S$ and $C_2S$ can produce calcite and C-S-H in the early stage, but calcite and silica gel are produced instead in the final stage:

$$3CaO \cdot SiO_2 + 3CO_2 + nH_2O \rightarrow SiO_2 \cdot nH_2O + 3CaCO_3 \quad (1.3)$$

$$2CaO \cdot SiO_2 + 2CO_2 + nH_2O \rightarrow SiO_2 \cdot nH_2O + 2CaCO_3 \quad (1.4)$$

Belite phases can be present as $\beta$-$C_2S$ and $\gamma$-$C_2S$, with the $CO_2$ uptake capacity of $\gamma$-$C_2S$ higher than that of $\beta$-$C_2S$ and the formation of different $CaCO_3$ polymorphs is present (67).

The carbonation of C-S-H phase leads to the formation of a silica gel network accompanied with a significant decrease in porosity and a substantial increase in compressive strength. The carbonation of C-S-H is initiated when a sufficient degree of carbonation is reached, thus occurring only after most of the calcium hydroxide has been consumed. When carbonation lowers the content of $Ca^{2+}$ in the pore solution, it is compensated by the release of $Ca^{2+}$ from C-S-H. This changes the composition of

the C-S-H and gives it a lower C/S ratio. When this ratio drops to less than 1 and the pH is around 10, C-S-H completely decalcifies and finally transforms into calcium carbonate and a highly polymerised silica gel which is acid stable and maintains a similar morphology to the original hydrate. Since the exact stoichiometry of C-S-H has not yet been clearly defined, the carbonation reaction of C-S-H gel can be expressed as follows (130; 99; 131):

$$xCaO \cdot ySiO_2 \cdot zH_2O + xCO_2 \rightarrow xCaCO_3 + y(SiO_2 \cdot nH_2O) + (z\text{-}nt)H_2O \quad (1.5)$$

Ettringite and aluminates are also effectively carbonates at low partial $CO_2$ pressures. Ettringite decomposes upon reaction with $CO_2$, resulting in the formation of gypsum and alumina gel (132):

$$3CaO \cdot Al_2O_3 \cdot 3CaSO_4 \cdot 32H_2O + 3CO_2 \rightarrow 3CaCO_3 + 3(CaSO_4 \cdot 2H_2O) + Al_2O_3 \cdot xH_2O + (26 - x)H_2O \quad (1.6)$$

The released sulphate ions can either precipitate as gypsum or diffuse inwards and react with aluminate ions from decomposed monosulphate thus forming new ettringite. This phenomenon is due to the decreasing pH. However, the end result is that most of the $Ca^{2+}$ ions from the aluminate phases will form carbonate and that the aluminate and ferrite phases will form stable metal hydroxides (99).

### 1.3.4. Belite cement carbonation

Another approach to a more sustainable cement production is carbonation curing of belite rich cement, which can not only modify belite cement but also sequestrate $CO_2$ into chemically stable carbonates over a long-term period of time. Jang and Lee (133) determined that a higher belite content in cement increases the $CO_2$ uptake during carbonation curing while promoting microstructural densification. Mechanical strength of belite-rich cement mortar cured by carbonation for 28 days was significantly improved in comparison with normally cured cement for an identical period of time as it is denoted by reduced pore connectivity and more instances of pore closure, which results in a complex microstructure. $CO_2$ uptake capacity increases with the increasing belite content; this subsequently leads to a higher amount of formed calcite. A direct consequence of this process is the increased strength of the ultimate product. Fang and Chang (134) also investigated the hardening behavior of $\beta$-$C_2S$ by accelerated carbonation and reached a carbonation degree of 21.6 % and compressive strength of 85.7 MPa after 6 h of carbonation in 99.9 % $CO_2$ concentration.

Moreover, not only hydraulically active forms of belite can be carbonated – activation and hardening of $\gamma$-$C_2S$ by carbonation reaction is considered as an effective approach towards production of low-lime cement (63). Guan *et al*. (135) produced mortars based on $\gamma$-$C_2S$ binder which demonstrated similar or even superior strength compared to OPC that could fully harden within 24 h by using accelerated carbonation. The $CO_2$ footprint associated with the manufacturing and use of $\gamma$-$C_2S$ binder can be reduced by up to 53% compared to OPC. Chang *et al*. (67) compared carbonation of $\beta$-$C_2S$ and $\gamma$-$C_2S$ in order to examine the strength development in the accelerated carbonation process and the microstructural changes induced by carbonation. The authors determined that $\beta$-$C_2S$ absorbs less $CO_2$ than $\gamma$-$C_2S$ but presents a higher compressive strength as well as different $CaCO_3$ polymorphs formed

in carbonated systems. A number of researchers (136; 137; 138) reported that the addition of γ-$C_2S$ to the OPC system leads not only to densified surface layers, lower porosity, and higher compressive strengths, but also to an increased resistance to leaching after accelerated carbonation curing.

### 1.3.5. Rankinite carbonation

The carbonation process of rankinite is similar to that of OPC: at the beginning of carbonation, the dissolution of $CO_2$ gas into water forms carbonic acid, which then ionizes $H^+$, $HCO^-_3$ and $CO_3^{2-}$. As the $H^+$ concentration significantly increases, the pH value drops, and thus leaching of $Ca^{2+}$ from $C_3S_2$ structure is induced. This results in the immediate precipitation or formation of insoluble $CaCO_3$, which is considered as a rate-limiting step of the carbonation reaction. Calcite occurs as a compact, continuous coating of small crystals having a major effect on the carbonation extent (38). The carbonation reaction products of the rankinite binder system include calcium carbonate, silica gel (or Ca-modified silica gel), and a composite phase containing intermixed the two former phases (107; 85; 139). At this point, the reaction path that seems to be the most accurate for the rankinite carbonation system is proposed by Ashraf *et al*. (33):

$$5(3CaO{\cdot}2SiO_2) + 11CO_2 + 2.5H_2O \rightarrow 11CaCO_3 + 4CaO{\cdot}10SiO_2{\cdot}2.5H_2O \quad (1.7)$$

As the solvation of the $Ca^{2+}$ ions from the $C_3S_2$ structure occurs, simultaneously, the polymerization of the remaining silicon tetrahedral monomers ($H_2SiO_4$) starts to form highly polymerized silica gels (90). The stiffness of this produced polymerized silica gel phase is determined to be substantially higher than that of the C-S-H gel, the primary binding phase of the hydrated OPC system (42). The formation of a Ca-modified silica gel was proposed by Ashraf and Olek (140). The authors state that this type of silica gel phase can be considered to consist of semi-spherical clusters of silica gel with silanol (Si–OH) bonds located primarily on their surfaces (140). Also, it is suggested that calcium might be present inside the gel clusters which are not accessible to moisture. Due to this inaccessibility, calcium is not removed from the Ca-modified silica gel during the carbonation process and does not convert to $CaCO_3$. In their previous study (33), the same authors observed that, during the carbonation reaction of $C_3S_2$, the initial gel phase to form is C–S–H which eventually decomposes and forms a highly polymerized Ca-modified silica gel.

Carbonation of calcium silicates involves two distinct stages – (1) the initial fast carbonation reaction that is controlled by the chemical kinetics, followed by (2) a slower reaction which is controlled by product-layer diffusion (140). Since diffusion is the major limiting process during the carbonation curing, it is controlled by the pore system and pore saturation, and thus it plays a significant role in determining the extent of carbonation. Carbonation of calcium silicates causes loss of pore connectivity and shifts the pore size distribution curve towards smaller pore diameters as porosity changes are caused by dissolution of cementitious phases. Carbonation significantly affects the transport properties by modifying and densifying the microstructure of concrete. Concrete porosity drops with an increasing $CO_2$ pressure, as previously large open pores fill with calcium carbonate and silica gel – which have a bigger molar volume than the initial components (141; 142). As the coating of

$CaCO_3$ on the binder particle becomes thicker, the whole structure is surrounded by a densified layer of reaction products hence preventing further permeation and diffusion of $CO_2$ into the unreacted clinker and thus limiting the carbonation extent of rankinite (38). Even though the compressive as well as flexural strength of the concrete structure is improved, the carbonation process is confined and cannot reach 100% if the structure is overly dense or if the pores are overly saturated with water. Therefore, the importance of moisture during the carbonation reaction should also be emphasized. Even though no water is consumed in the reaction, it acts as a catalyst and is necessary to promote the reaction of $CO_2$; however, too much water can limit the reaction due to blockage of the pores in the solid material. Moreover, the curing reaction is exothermic, and it releases a considerable amount of heat which is dissipated by the evaporation of water. If all of the pores, water evaporates, and there is no medium for the $CO_2$ to dissolve into. Thus the carbonation reaction is hindered. Therefore, it is greatly necessary to find the optimum water (w/c ratio) amount for each individual system so that to reach the highest possible carbonation degree.

### 1.3.6. Wollastonite carbonation

Among the Ca-bearing silicates, wollastonite is one of the most reactive minerals (40). Itsts carbonation is an exothermic process, $\Delta H_r = -87$ kJ/mol (143), which can potentially reduce the overall energy consumption and the cost of carbon sequestration. Carbonation of Ca-bearing silicates occurs in a gas-solid-water slurry, which increases the reaction rate substantially compared to direct gas-solid carbonation (144).

Wollastonite carbonates rapidly with a maximum conversion in 15 min of 70% at relatively mild conditions ($d < 38$ μm, $T = 200$ °C and $p_{CO2} = 20$ bar) (144). Daval *et al*. (40) investigated the kinetics of wollastonite carbonation and used kinetic modelling. They proved that the rate-limiting step of the overall reaction is wollastonite dissolution. However, Min *et al*. (145) researched CS carbonation in water-bearing supercritical $CO_2$ and determined that the carbonation reaction is not controlled by the kinetics of the surface reactions but rather by the diffusion of water-bearing $scCO_2$ through the surface layer. Therefore, the state and medium in which $CO_2$ approaches the material is very important. Wollastonite carbonation is intensified with the increasing water content, temperature, and pressure. According to Miller *et al*. (146), it is possible to achieve almost 50% wollastonite conversion to carbonate at 70 °C, 160 bar, with no less than 24 h carbonation. Similar carbonation degrees (~50%) were achieved by Daval *et al*. (39) at 250 bar and 90 °C and by Whitfield and Mitchell (147) at 79.2 bar and 60 °C.

Wang *et al*. (110) investigated the influence of the CS addition to the OPC system carbonation and determined that the reaction rates, as well as the $CO_2$ uptake capacity, were significantly enhanced. The additive CS content promoted the carbonation conversion of OPC components during the curing process and acted mainly on the gaseous diffusion properties thus enhancing gas permeability during the reaction.

**********

To sum up the literature review data, it is evident that OPC production has a major negative effect on the environment and that critical changes need to be implemented to reduce this effect. Even though there are numerous suggestions to achieve lower greenhouse gas emissions, only a small fraction of them have real-life sizable possibility to achieve the desired results. One of these options is the production of alternative low-lime calcium silicate binder materials that, in conjunction with accelerated $CO_2$ carbonation, can significantly reduce the greenhouse emissions and thus the adverse effect of the OPC manufacture on the environment. One of the most promising alternative binders is rankinite since its contribution to emission reductions is threefold: it requires lower amounts of raw materials due to the lower C/S ratio, its synthesis temperature is at least 200 °C lower than that of OPC clinker, and it is able to store a considerable amount of $CO_2$ in the concrete structure in the form of stable carbonates. However, the rankinite hardening process by mineral carbonation requires careful and thorough research since the process highly relies on many factors and parameters that need to be adequately combined in order to obtain both ecologically and economically viable production.

## 2. Materials And Methods

### 2.1. Materials

1. **Initial mixture for OPC clinker burning** (SC "Akmenės cementas", Lithuania). Oxide composition is provided in Table 2.1.
2. **Clay –** "Nikiforovo" (Ukraine). Oxide composition is provided in Table 2.1.
3. **Opoka** – Stoniškių-Žemaitkiemio quarry (Lithuania). Dried for 24 h at 100±5 °C and ground in a ball mill (45 rpm, grounding bodies (round, steel) and dry material ratio 1:0.8) for 2 h (specific surface area $S$ = 755 $m^2$/kg). Oxide composition is provided in Table 2.2. Opoka was chosen due to its relatively large reserves in Lithuania and a suitable composition for silicate binder production. Opoka is mainly composed of opal silica and calcium carbonate, which makes it a highly suitable raw material and a source of both silica and lime. The composition and properties of Stoniškių-Žemaitkiemio quarry opoka has already been extensively discussed by other authors; the relevant data can be found in (148).
4. **Limestone** – "Naujasis Kalcitas" (Lithuania). Dried for 24 h at 100±5 °C and ground in a ball mill (45 rpm, grounding bodies (round, steel) and dry material ratio 1:0.8) for 2 h. Calcined at 1000 °C for 2 h (specific surface area $S$ = 550 $m^2$/kg). Oxide composition is provided in Table 2.2.
5. CEN Standard **sand** EN 196-1 (Germany).
6. **Portland cement** CEM I 42.5 R (Lithuania).
7. 3% NaCl solution

**Table 2.1** Oxide composition of the raw materials, wt%

| | **CaO** | **$SiO_2$** | **MgO** | **$Fe_2O_3$** | **$Al_2O_3$** |
|---|---|---|---|---|---|
| Mixture for OPC clinker | 42.04 | 12.47 | 2.87 | 2.30 | 3.38 |
| Clay | 1.06 | 58.5 | 1.08 | 7.16 | 20.8 |
| | **$K_2O$** | **$Na_2O$** | **$SO_3^{2-}$** | **Others** | **LOI** |
| Mixture for OPC clinker | 0.80 | 0.09 | 0.40 | - | 35.65 |
| Clay | 2.39 | 0.72 | 0.11 | 1.66 | 6.53 |

**Table 2.2** Oxide composition of the raw materials, wt%

| | **CaO** | **$SiO_2$** | **MgO** | **$Fe_2O_3$** | **$Al_2O_3$** | **$SO_3^{2-}$** |
|---|---|---|---|---|---|---|
| Opoka | 34.1 | 42.8 | 0.35 | 1.54 | 1.73 | 0.59 |
| Limestone | 49.2 | 3.27 | 3.31 | 1.08 | 0.93 | 0.38 |
| | **$K_2O$** | **$P_2O_5$** | **$TiO_2$** | **Others** | **LOI** | **C/S** |
| Opoka | 0.55 | 0.14 | 0.12 | 0.18 | 17.9 | 0.79 |
| Limestone | 0.37 | 0.044 | 0.056 | 0.16 | 41.2 | 15.05 |

## 2.2. Sample preparation and characterization methods

For the determination of compaction influence on the OPC clinker formation, the initial mixture for OPC clinker burning and heavy clay were used. The samples were prepared by mixing 98.34% of the initial mixture with 1.66% of clay.

The Nikiforovo quarry clay was used to achieve clinker saturation coefficient $K_p$ = 0.93, which is the same as the one used in *SC Akmenės Cementas*. This clay was chosen due to the relatively high amount of $Al_2O_3$ (Table 2.1). The prevailing mineral composition of the clay was determined by XRD and STA analysis (Fig. 2.1). The obtained results showed that the main compounds of the clay were kaolinite ((*d-spacing*: 0.716, 0.356 nm) and illite (*d-spacing*: 0.997, 0.446, 0.246 nm), although a relatively high amount of quartz (*d-spacing*: 0.425, 0.334, 0.245, 0.228, 0.181 nm) was determined as well, along with traces of K, Na-feldspars (*d-spacing*: 0.319, 0.411, 0.295 nm), and dolomite (*d-spacing*: 0.289, 0.219, 0.179 nm) (Fig. 2.1, *a*). According to the obtained STA results, the first endothermic effect at 100 °C is attributed to the loss of the physically bound water. The next smaller effect at around 303 °C is also most likely due to water release from the clay components, such as limonite, an iron-bearing oxyhydroxide mineral, that loses its free water at temperatures around 250–350 °C since it is followed by a mass loss (149). A third clear endothermic effect is visible at the temperature range of 440–560 °C, where clay minerals lose the interlayer (crystal) and chemically bound water (150), at this point, the determined mass loss was equal to 2.43%. However, it is rather difficult to identify the clay mineral group since the dehydration temperatures of kaolinite, illite, and feldspars are similar and tend to overlap. A small shoulder on this peak at around 573 °C is typical to α-$SiO_2$ conversion to β-$SiO_2$ (151), however, this effect can also be attributed to the decomposition of kaolinite as well (152). The next small scale effect at around 734 °C is attributed to the decomposition of dolomite (153), and the last endothermic effect at 915 °C indicates the disintegration of the crystal lattice of illite (154).

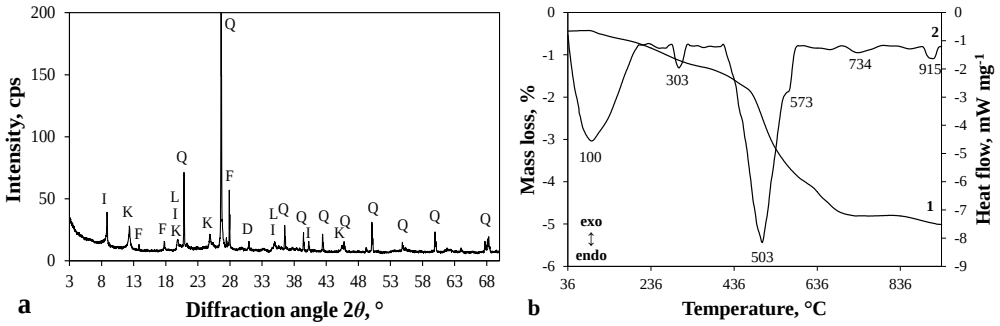


**Fig. 2.1** XRD pattern (*a*) and STA curves (*b*, *curve 1* – TG, *curve 2* – DSC) of Nikiforovo clay. Indexes: *Q* – quartz, *K* – kaolinite, *I* – illite, *D* – dolomite, *F* – K, Na-feldspars, *L* – limonite

The raw materials were homogenized for 2 h at 49 rpm in a homogenizer *Turbula Type T2F* (*Glen Mills Inc.*, USA). 1 kg of the raw materials was placed in the homogenizer of 2 l capacity with the addition of 200 g of homogenization bodies of

10-15 mm diameter. Afterwards, the obtained raw meal samples of 10 g were pressed with a hydraulic desktop pellet press *MP15* (*Across International LLC*) to 4–20 MPa (with steps at every 2 MPa) to form cylindrical pellets (h ≈ 4 mm, D = 40 mm) and, together with one sample of non-compressed powder, were calcined at temperatures of 1300, 1350, 1400, and 1450 °C for 20, 40, and 60 min in a laboratory kiln *Nabertherm LHT* 08/16 (Germany). The calcined samples were cooled down to an ambient temperature in 5 min by forced airflow and ground in a vibratory disc mill *Pulverisette 9* (*Fritsch*, Germany) at 900 rpm for 3 min in order to pass an 80 μm sieve. Rietveld analysis materials were ground for additional 3 min at the same conditions and passed through a 40 μm sieve.

For rankinite binder synthesis, opoka (source of silica and CaO) and limestone (source of CaO) were chosen as the primary materials for the initial mixture with $CaO/SiO_2$ = 1.5 (C/S = 1.5) composition. A stoichiometric mixture of the primary materials was homogenized in a *Turbula Type T2F* mixer at 34 rpm for 2 h. The homogenized mixture afterwards was moistened with distilled water to form a plastic dough and manually granulated to round ~15-20 mm diameter pellets. After drying the pellets at 100±5 °C for 24 h, they were ***calcined*** in a *Nabertherm LTH* 08/16 laboratory furnace in platinum plates at a temperature range of 900–1300 °C for 60 min to determine the optimum conditions for the rankinite synthesis. After the calcination, pellets were ***ground*** in a vibratory disc mill *Pulverisette 9* at 900 rpm for 6 min to fine powder < 80 μm.

The ***specific surface area*** of the materials was determined by laser particle size analyser *CILAS LD 1090* (France) that features a sensitivity range from 0.04 to 500 μm. Water was used as a carrier liquid. The particles were dispersed with ultrasound for 2 min, while the obstruction of the particles in water reached 14%. The standard operating procedure in use was the Fraunhofer method.

The ***density*** was determined by using a pycnometer *AccuPyc 1330 V2.02* (*Micromeritics*, USA). The volume of the sample was calculated according to Boyle's law. Analysis was carried out in the inert gas (helium) atmosphere.

The ***amount of free CaO*** was determined following the standard ASTM C114–11b.

The ***formation of the samples*** and determination of the ***compressive and tensile splitting strength*** were performed according to EN 196-1 and EN 12390-6 respectively, while using a universal testing machine *FORM+TEST MEGA 10-400-50* (Germany) at a loading rage of 1 kN/s (for forming) and 1.5 kN/s (for compressive strength).

***Carbonation curing*** was carried out in a *Parr Instruments* (USA) pressure reactor, model *4555*, with the maximum working pressure of 131 bar, volume – 18.75 l, temperature range – -10–+350 °C. The reactor was first twice purged with $CO_2$ gas up to ~2 bar and immediately depressurized to atmospheric pressure to eliminate the presence of air, and afterwards the pressure of $CO_2$ (99.9% concentration) was increased (and ultimately decreased) by 2.5 bar/min to the required value.

The ***Heat evolution*** rate of the manufactured binder during the hydration was investigated by using an eight-channel isothermal calorimeter *TAM Air III* (*TA Instruments*). Glass ampoules (20 ml), each containing 3 g of the dry material, were

placed in the calorimeter and the injection units for each ampoule filled with 1.5 g of water. Having reached the isothermal conditions (25±0.1 °C), the water was injected into the ampoules and mixed inside the calorimeter with the dry material for 20 s (frequency 2–3 $s^{-1}$). The heat evolution rate was measured over a period of 72 h.

Analysis of the material composition was determined by ***X-ray diffraction*** (XRD) performed on a *D8 Advance diffractometer* (*Bruker AXS*, Germany) operating at the tube voltage of 40 kV and tube current of 40 mA. The X-ray beam was filtered with a Ni 0.02 mm filter which was set to select the Cu-Kα wavelength. The diffraction patterns were recorded in *Bragg-Brentano geometry* by using a fast counting detector *Bruker LynxEye* based on silicon strip technology. The specimens were scanned over the range 2θ = 3–70° at a scanning speed of 6° $min^{-1}$ while using the coupled two theta/theta scan type.

Spatially resolved ***X-ray diffraction*** analysis was performed with a *Bruker D8 Advance* diffractometer by using CuKα radiation (λ = 1.54 Å, 40 kV, 40 mA) in θ-θ configuration with a *LynxEye XE-T* silicon strip detector and an automatic divergence slit (fixed radiation spot of 1 mm). The measurement range was 5–50° 2θ with steps of 0.03° 2θ with a measurement duration of 2 s/step. A cross section (d = 3 mm) of the original sample was prepared by using a *Buehler IsoMet 5000* precision saw. A motorized sample stage (*Bruker Compact UMC*, software controlled XYZ positioning) was used for creating X-ray diffraction profiles along the cross section of the sample. XRD analysis was complimented by Rietveld refinement. For this, 10% of ZnO was added to the sample as an internal standard for the quantitative determination of the amorphous phase. The samples for XRD and Rietveld analysis were dried at 40 °C for 48 h and ground to pass a 32 μm sieve.

Quantitative analysis of the material composition was determined by ***X-ray Fluorescence Spectroscopy*** (XRF) performed on a *Bruker X-ray S8 Tiger WD* (Germany) spectrometer equipped with a Rh tube with the energy of up to 60 keV. Powder samples (passed through a 63 μm sieve and pressed to cylindrical tablets of 5×40 mm) were measured in He atmosphere, and the data was analyzed with *SPECTRAPlus QUANT EXPRESS* standardless software.

***Simultaneous thermal analysis*** (STA: thermogravimetric analysis – TG and differential scanning calorimetry – DSC) was performed by two types of equipment:

1. *Linseis STA PT 1000* (Germany). Heating rate of 10 °C$min^{-1}$; temperature range from 30 to 950 °C under nitrogen atmosphere. Ceramic sample handlers and crucibles of Pt–Rh were used.
2. *Netzsch STA 449F3* (Germany). Temperature range from 25 to 1100 °C at the heating rate of 20 °C$min^{-1}$ under air atmosphere.

***Fourier transform infrared spectroscopy*** (FTIR) spectra were carried out with the spectrometer Perkin Elmer FT-IR system *Spectrum X* (USA). The specimens were prepared by mixing 1 mg of the sample material in 200 mg of KBr. Spectral analysis was performed in the range of 4000–400 $cm^{-1}$ with the spectral resolution of 1 $cm^{-1}$.

The microstructure of the materials was observed by using ***scanning electron microscopy*** (SEM) *(Model JSM-7600F, JEOL Co.*, Japan) coupled with ***energy dispersive X-ray spectrometry*** (EDX) (*Inca Energy 350*, *Oxford Instruments*, *Silicon Drift type detector X-Max20*) performed by using accelerated voltage of 10kV, the

working distance of 8.6 and 8.7 mm for SEM observation, and 200 s accumulation time for EDX analysis. The samples were affixed to the SEM specimen holder by using epoxy resin and then sputter-coated with gold aimed to promote electrical conductivity.

For the mortar microstructure observations, the carbonated samples were cut in half using a precision saw. The cutting planes afterwards were sanded and polished using Tegramin-25 (Struers ApS, Danija) equipment. For sanding, a SiC paper (#320) was used and for polishing, 9, 3, and 1 μm diamond suspensions and corresponding polishing substrates (Struers ApS) were used. To ensure surface electrical conductivity, the samples were coated with 20-30 nm carbon layer using a Q150T ES (Quorum Technologies Ltd.) system. Sample surface structure and elemental composition was investigated by scanning electron microscopy (SEM) using Helios Nanolab 650 (FEI) scanning electron microscope coupled with energy dispersive X-ray (EDX) spectrometer (Oxford Instruments, Xmax 20 $mm^2$ detector, INCA 4.15 software). Surface images were obtained by recording secondary electrons at 5 kV accelerating voltage and 0.8 nA current. The elemental composition and distribution maps were obtained at 20 kV accelerated voltage and 3.2 nA current.

The porosity and pore size distribution of the materials was determined by using ***mercury intrusion porosimetry*** (MIP) (*AutoPore III*, *Micromeritics*, USA). Isopropanol was used to stop the reactions of the sample fragments remaining from the strength measurements.

***High resolution X-ray computed tomography*** (CT) as a visual and non-destructive method was performed on a *Rayscan 250 E* instrument with high resolution, micro-focus X-ray tube 1 operating at a voltage range of 10–230 kV featuring the maximum power of 320 W and a resolution from 3 μm, and high penetration, a high power X-ray tube 2 operating at a voltage range of 50–450 kV, the maximum power of 700 W and a resolution from 100 μm. *Fei Avizo Inspect* (*VGStudio MAX*) advanced software was used for the visualization of volume and analysis of computed tomography data.

***Water absorption by immersion, freeze-thaw, and abrasion resistance*** was determined according to the Standard EN 1338:2003+AC:2006. The samples used for these experiments were prepared with the binder-to-sand ratio of 1:3; for the OPC samples, the w/c = 0.35, while for rankinite the binder samples were w/c = 0.25. The samples were compacted by using 12.5 $N/mm^2$ pressure to reach 100×100×20 mm dimensions. After the formation, the samples were immediately cured at 15 bar $CO_2$ pressure for 24 h, at 45 °C.

***Laser ablation inductively coupled plasma mass spectrometry*** (LA-ICP-MS) was performed by an *ESI NWR 213* (*ESI New Wave Research*, USA) laser, providing 10, 60 μm broad and 20000 μm long, lines, and a *NexION 300D Perkin Elmer* (USA) spectrometer with *NexION ICP MS* Software, Version 1.5; carrier gas 0.7 $lmin^{-1}$ He + 0.92 $lmin^{-1}$ Ar.

***$^{29}$Si Nuclear magnetic resonance*** (NMR) experiments were performed with a *Bruker Advance 300* spectrometer (magnetic field strength 7.0455 T, resonance frequency for 29Si: 59.63 MHz) in MAS (magic angle spinning) mode using the single pulse technique (90° pulse). The samples were packed in 7 mm zirconia rotors and

spun with 5 kHz. About 2,000 scans were recorded for each spectrum with a repetition time of 45 s. The chemical shifts were set relative to external tetramethylsilane. The signal patterns of the spectra were deconvoluted with *Bruker WINNMR* software.

***Chemical determination of the elements***:

From the cut sample half cylinders, smaller pieces of the material were removed with a hammer and then ground. After careful mixing, the sample material was subjected to a representative subsample of approximately 0.5 g. Together with 1.5 g of lithium metaborate, the material was placed in a weighed platinum crucible and annealed at 1000 °C for 0.5 h. The loss on ignition (LOI) of the crucible was determined by weighing the crucible including the melting tablet after cooling. The fused tablet was then removed, mixed with 1 molar nitric acid and filled up to 100 ml with ultrapure water and measured by using inductively coupled plasma optical emission spectrometry (*ICP-OES, Jobin Yvon Ultima II*).

***Thermodynamic calculations***

For the thermodynamic calculations of the hypothetical reaction parameters, the values of standard formation enthalpy ($\Delta_r H^{0,f}_{298}$), entropy ($\Delta_r S^{0,f}_{298}$), and specific heat capacity ($C_p$) values for reactive compounds and the reaction products are provided in Table 2.3. For the calculations, the method of absolute entropies was used, according to which, the change of the reaction standard free Gibbs energy was calculated by the following equation:

$$\Delta_r G^0_T = \Delta_r H^0_T - T\Delta_r S^0_T \quad (2.1)$$

where $\Delta_r H^0_T$ and $\Delta_r S^0_T$ are the variations of reaction enthalpy and entropy at temperature $T$. Enthalpy and entropy for the reactions were calculated by the following equation:

$$\Delta_r H^0_T = \Delta_r H^0_{298} + \Delta_r C_p(T_r - 298) \quad (2.2)$$

$$\Delta_T S^0_T = \Delta_r S^0_{298} + \Delta_r C_p(T_r/298) \quad (2.3)$$

where $\Delta_r H^0_{298}$ is the standard enthalpy change of the reaction, J/mol and $\Delta_r S^0_{298}$ is the standard entropy change of the reaction, J/(molK) (Table 2.3).

**Table 2.3** Thermodynamic parameter values at 25 °C (1 bar)

| Component | | $\Delta H^{0,f}_{298}$, kJ/mol | $S^{0,f}_{298}$, J/(molK) | $C_p$, J/(molK) | Reference |
|---|---|---|---|---|---|
| Calcium oxide | CaO | -635.1 | 37.75 | 51.03 | (155) |
| Silica | $SiO_2$ | -910.7 | 41.46 | 66.09 | (155) |
| Magnesium oxide | MgO | -601.6 | 26.95 | 37.20 | (156) |
| Wollastonite | $CaSiO_3$ | -1632.7 | 81.81 | 116.01 | (155) |
| Larnite | $Ca_2SiO_4$ | -2280.4 | 143.25 | 169.02 | (155) |
| Rankinite | $Ca_3Si_2O_7$ | -3943.0 | 210.90 | 282.84 | (157) |
| Akermanite | $Ca_2MgSi_2O_7$ | -3867.5 | 208.20 | 205.30 | (155) |

## 3. Results and Discussion

### 3.1. Influence of raw meal compaction pressure on OPC clinker formation

Since the initial mixture for OPC clinker burning density dependency on the compaction pressure so far has been rather scarcely investigated, the main objective of the experimental part was to research the compaction influence of the clinker mineral formation reactions while estimating the calcination temperature and duration.

For this reason, the compacted raw meal samples were calcined in the temperature range of 1300–1450 °C for 20 to 60 min. The materials in use and the sample preparation as well as the calcination process are described in Section 2.2.

**Table 3.1** Effect of pressure on the density of the compressed samples

| Pressure, MPa | 4 | 6 | 8 | 10 | 12 | 14 | 16 | 20 |
|---|---|---|---|---|---|---|---|---|
| Sample density, kg/m$^3$ | 1760 | 1820 | 1850 | 1870 | 1920 | 1960 | 1980 | 2010 |

Compacted calcined raw meal samples were investigated by chemical analysis, XRD, and micro-calorimetry. The density of the compressed samples is provided in Table 3.1. As it can be seen, with an increasing compaction pressure, the density of the samples gradually increased as well thus improving the particle surface contact area. While increasing the compaction pressure from 4 to 20 MPa, the density of the samples increased by 14.2%.

After calcination, chemical analysis was carried out in order to determine the amount of free CaO ($CaO_{free}$) in the samples as it plays an important role in optimizing the clinker synthesis process. The completed chemical analysis showed that the non-compacted calcined powder samples contained the highest amount of $CaO_{free}$ at all the calcination temperatures (Fig. 3.1), except for the sample compacted at 8 MPa (calcined at 1300 °C for 20 min). Even though this sample contained the highest amount of $CaO_{free}$, the obtained result is most likely due to an operational error and does not reflect the prevailing tendency. Compacting the raw meal with the lowest pressure of 4 MPa, the amount of $CaO_{free}$ decreased from 8.25% to 8.04% after 1300 °C and 20 min calcination. However, when further increasing the pressure, no major influence on the amount of $CaO_{free}$ was observed since, at all of the pressure values, the amount of free calcium oxide was around 8%. Similar observations were made with an extended calcination duration: the duration was prolonged from 20 to 60 min; this led to a 12.36% decrease in the $CaO_{free}$ value (at 1300 °C). However, after calcination for 40 and 60 min, the total amount of $CaO_{free}$ remained at around 6.5%.

The increased temperature had a considerable influence on the amount of $CaO_{free}$ remaining in the samples. As expected, the amount of $CaO_{free}$ decreased gradually with the calcination temperature increment. While increasing the calcination temperature from 1300 to 1450 °C, the amount of $CaO_{free}$ decreased dramatically by 90.91%, from 8% to 1%, for non-compacted samples. The applied compaction led to a decrease in the amount of $CaO_{free}$ from 3.3% to 2.5% after calcination at 1350 °C, from 2.3% to 1.6% after calcination at 1400 °C, and remained

similar at around 1% for samples calcined at 1450 °C. Although the 1% change in the $CaO_{free}$ value does not seem major, it is a considerable difference, since, with the amount of $CaO_{free}$ is in a range of 1–1.5%, the kiln processes are believed to be optimal. However, if CaO is overcalcined, its reaction with water in the cement hydration process occurs very slowly, which could take up to a month or even longer. Due to this, the final hydration reaction of CaO occurs in an already hardened cement stone, thus leading to material deterioration and scaling caused by volume expansion.

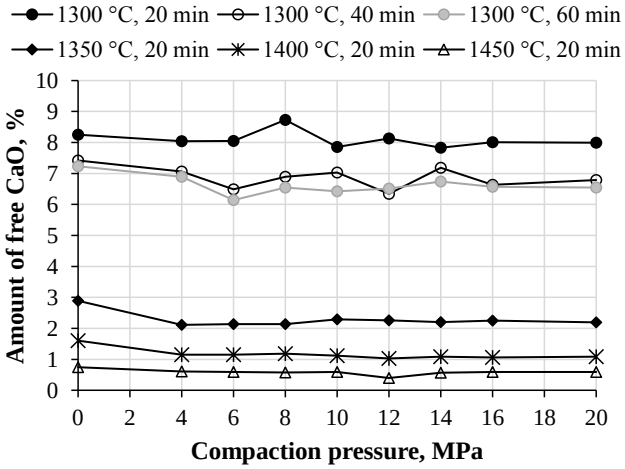


**Fig. 3.1** Compaction pressure, temperature, and calcination duration influence on the amount of $CaO_{free}$

The obtained XRD patterns of the samples calcined at 1300 °C for 20–60 min and at 1300–1450 °C for 20 min, with and without compaction, are provided in Figures 3.2 and 3.3. It is evident that neither the extended calcination duration, nor the increased compaction seemed to have a significant effect on the clinker mineral composition of the samples calcined at the lowest temperature of 1300 °C (Fig. 3.2), whereas the increase of the temperature up to 1450 °C led to enhanced development of the main clinker component – alite ($C_3S$) (Fig. 3.3). However, even with the increased calcination temperature, compaction at 10 MPa does seem to affect the mineral composition (Fig. 3.3, *b*).

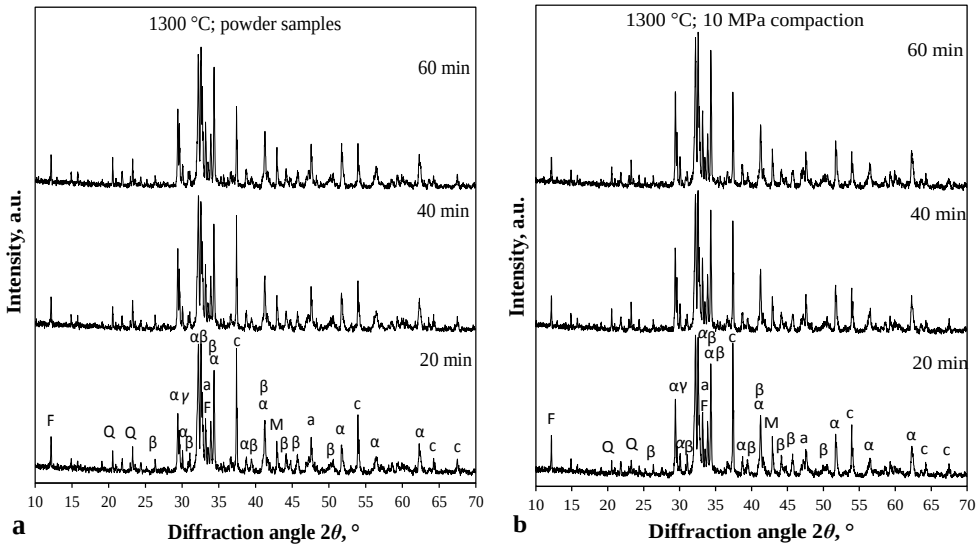


**Fig. 3.2** XRD patterns of powder (a) and pressed (b) to 10 MPa samples calcined at 1300 °C for 20 min, 40 min, and 60 min. Indexes: Q – $SiO_2$, c – CaO, M – MgO, a – $C_3A$, F – $C_4AF$, α – $C_3S$, β – β-$C_2S$, γ – γ-$C_2S$

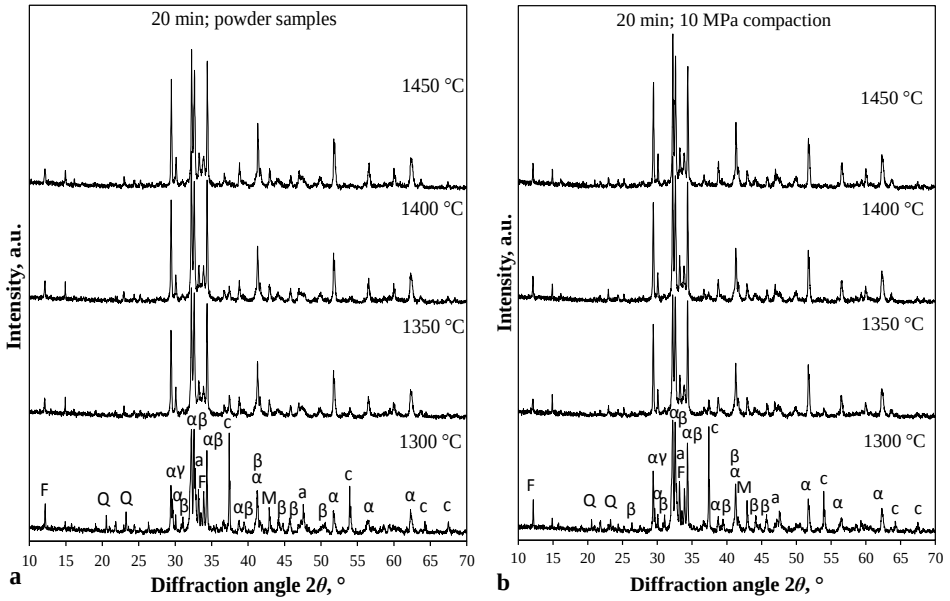


**Fig. 3.3** XRD patterns of powder (a) and pressed (b) to 10 MPa samples calcined at 1300–1450 °C for 20 min. Indexes: Q – $SiO_2$, c – CaO, M – MgO, a – $C_3A$, F – $C_4AF$, α – $C_3S$, β – β-$C_2S$, γ – γ-$C_2S$

In order to obtain quantitative results of the mineral composition, the XRD data was supplemented with Rietveld refinement to determine the prevailing mineral composition of the clinker and its alterations with regard to the applied compaction

pressure. The obtained Rietveld refinement results are provided in Tables 3.2 and 3.3. As it can be seen, in the samples calcined at 1300 °C for 20 min, two modifications of dicalcium silicate – β-$C_2S$ and γ-$C_2S$ – were determined (Table 3.2). β-$C_2S$ is the most common polymorph in the industrial Portland cement (66), while γ-$C_2S$ is an unfavorable polymorph due to its lower density and non-hydraulic properties. Moreover, γ-$C_2S$ causes cracking of β-$C_2S$ crystals while forming a voluminous powder, a phenomenon known as 'dusting' (66; 158), since the transformation of monoclinic β-$C_2S$ to orthorhombic γ-$C_2S$ is followed by volume expansion of about 12% (159). Formation of γ-$C_2S$ can be avoided by rapid cooling, thus for higher temperature calcinations it was applied, and the formation of γ-$C_2S$ was averted (159). Additionally, typical OPC minerals formed at all the calcination temperatures, including, $C_3S$, $C_3A$, $C_4AF$, as well as, MgO and CaO. Considering the compaction, in the samples calcined at 1300 °C for 20 min, the amount of the main clinker mineral – alite ($C_3S$) – seems to reach its highest value at compaction of 10 MPa, while a further increase of the pressure led to lower extent of this mineral (Table 3.3).

Since alite is the main mineral responsible for the initial and final strength of cement, a higher extent of its formation is highly favorable. This was achieved with an increase of the calcination temperature – an increase of only 50 °C led to an almost 90% increase in the alite content (Table 3.3). However, a further increase of the temperature up to 1450 °C led to an only ~9% increase in the alite content. Considering the compaction, an increase of the applied pressure from 0 to 20 MPa led to an only ~1% increase in the alite content in all the calcination scenarios, thus indicating that compaction does not exert a significant influence on the clinker mineral formation. In addition, the remaining clinker mineral composition alters only insignificantly thus increasing the calcination temperature and/or compaction. Still, according to the obtained results, it is evident that compaction at a pressure no higher than 10 MPa seems to offer the most beneficial results, since, at such conditions, the formation of CaO is minimal.

**Table 3.2** Clinker mineral composition of samples calcined at 1300 °C for 20 min

| Composition | Compaction pressure, MPa | | | | | | | | |
|---|---|---|---|---|---|---|---|---|---|
| | 0 | 4 | 6 | 8 | 10 | 12 | 14 | 16 | 20 |
| $C_3S$ | 29.3 | 31.8 | 33.5 | 29.1 | 33.4 | 29.5 | 32.1 | 30.2 | 30.3 |
| β-$C_2S$ | 29.1 | 29.4 | 29.5 | 33.5 | 29.6 | 32.6 | 31.9 | 32.4 | 32.6 |
| γ-$C_2S$ | 12.9 | 9.7 | 9.1 | 8.3 | 8.2 | 8.8 | 7.6 | 8.6 | 8.9 |
| $C_3A$ | 6.7 | 7.4 | 6.9 | 7.0 | 7.2 | 7.1 | 6.5 | 6.9 | 6.7 |
| $C_4AF$ | 10.8 | 10.6 | 10.1 | 11.0 | 10.3 | 10.4 | 10.8 | 10.9 | 10.4 |
| MgO | 3.6 | 3.8 | 3.9 | 3.6 | 4.0 | 4.1 | 3.9 | 4.0 | 3.9 |
| CaO | 7.6 | 7.2 | 7.0 | 7.6 | 7.3 | 7.5 | 7.2 | 7.0 | 7.3 |

**Table 3.3** Clinker mineral composition of samples calcined at 1350–1450 °C for 20 min

| Composition | 1350 °C | | | 1400 °C | | | 1450 °C | | |
|---|---|---|---|---|---|---|---|---|---|
| | 0 MPa | 10 MPa | 20 MPa | 0 MPa | 10 MPa | 20 MPa | 0 MPa | 10 MPa | 20 MPa |
| $C_3S$ | 55.4 | 53.8 | 56.4 | 59.3 | 59.1 | 60.8 | 59.4 | 59.7 | 61.7 |
| β-$C_2S$ | 20.0 | 22.7 | 20.3 | 17.5 | 18.2 | 16.7 | 18.0 | 18.0 | 17.3 |
| $C_3A$ | 7.9 | 5.3 | 7.3 | 6.5 | 6.3 | 7.6 | 4.4 | 5.4 | 6.7 |
| $C_4AF$ | 10.1 | 12.7 | 10.2 | 11.2 | 11.8 | 10.1 | 14.4 | 13.3 | 10.8 |
| MgO | 3.1 | 3.1 | 3.3 | 3.2 | 3.2 | 3.2 | 2.9 | 2.9 | 2.4 |
| CaO | 3.3 | 2.5 | 2.6 | 2.4 | 1.5 | 1.6 | 0.9 | 0.8 | 1.0 |

OPC hydration, in which cement undergoes chemical and mechanical changes, is a complex process that includes dissolution and precipitation reactions. Cement hydration is usually described by the fast initial reaction (i.e., the initial period) lasting up to ~1 h, followed by an induction period that can last for several hours and is followed by acceleration and deceleration periods and the final period of slow continued reaction lasting up to several days. Since OPC hydration reactions are exothermic, the influence of various factors on the hydration kinetics can be described by typical heat flow diagrams (160). Since the compaction pressure as well as the calcination temperature and duration have an impact on the mineral composition of the sample, it also influences the heat release during hydration. The heat release from the products during the hydration reactions was investigated by isothermal micro-calorimetry. The obtained results are provided in Figures 3.4–3.7.

As it can be seen in Figures 3.4 and 3.5, calcining the samples at the lowest temperature led to the lowest heat formation. The highest value of heat flow in the initial period was observed in the samples calcined for 20 min – 0.0698 W/g, while with extended calcination this value decreased to 0.0552 and 0.0428 W/g for 40 and 60 min, respectively (Fig. 3.4, *a*). With applied compaction, the heat flow for the samples calcined for 20 min increased to 0.07969 W/g, whereas for the samples calcined for a longer duration, it slightly decreased to 0.042 and 0.0372 W/g for 40 and 60 min, respectively (Fig. 3.5, *a*). However, with an extended calcination duration, the heat flow curves shifted to prolonged hydration durations. The highest amount of cumulative heat released during the hydration reactions reached ~200 J/g and was obtained in the samples calcined at 1300 °C for 20 min and decreased with extended calcination duration, similarly to the powder and compressed samples (Figs. 3.4 and 3.5, *b*).

With an increased calcination temperature, the heat evolution rate as well as the total released heat significantly increased (Fig. 3.6). In the dissolution period of the hydration of the powder samples, the highest value of the heat flow, i.e., 0.0935 W/g, was reached by the samples calcined at 1400 °C for 20 min. After applied compaction at the same calcination temperature and duration, there was only a minor increase in the heat flow value to 0.0938 W/g (Fig. 3.7, *a*). Furthermore, the highest amount of

the heat flow in the acceleration period of the powder samples – 0.00341 W/g – was obtained by the samples calcined at 1350 °C for 20 min (Fig. 3.6, *a*). The amount of the heat flow during this period in the compacted samples (10 MPa) increased in the samples calcined at 1300 °C from 0.00178 to 0.00206 W/g (Fig. 3.7, *a*), yet, it remained similar to the powder ones calcined at 1400 °C and 1450 °C. The highest total amount of the cumulative heat was obtained by the powder samples calcined at 1400 °C for 20 min, and it reached a value of 324.06 J/g, while, with increased compaction, the total amount of heat further increased to 331.86 J/g (Fig. 3.8, *b*). The time of the maximum heat flow achieved in the acceleration period decreased from ~10 to 9.7 h in the samples calcined at 1300 °C and remained similar at 7.5, 9.2, and 12 h in the samples compacted by 10 MPa and calcined at 1350, 1400, and 1450 °C, respectively, in comparison to the non-compacted powder samples.

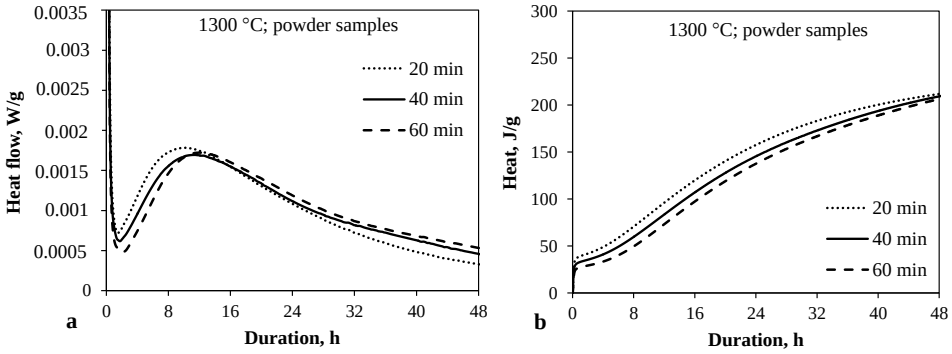


**Fig. 3.4** Heat evolution rate (a) and cumulative heat (b) of the powder samples calcined at 1300 °C for 20, 40, and 60 min

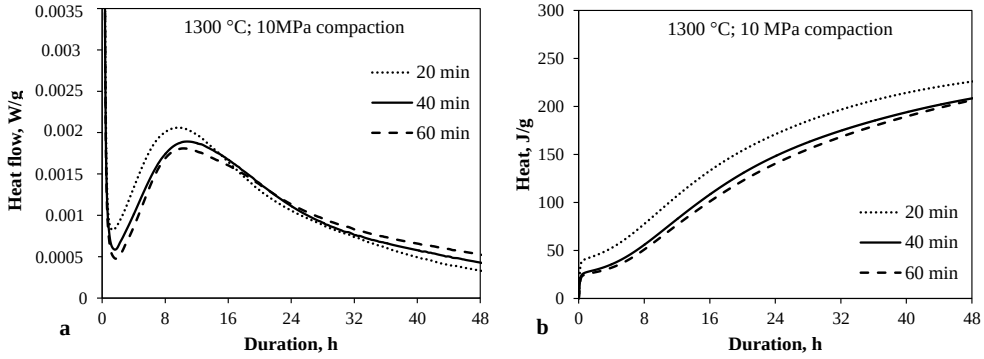


**Fig. 3.5** Heat evolution rate (a) and cumulative heat (b) of samples with 10 MPa compaction calcined at 1300 °C for 20, 40, and 60 min

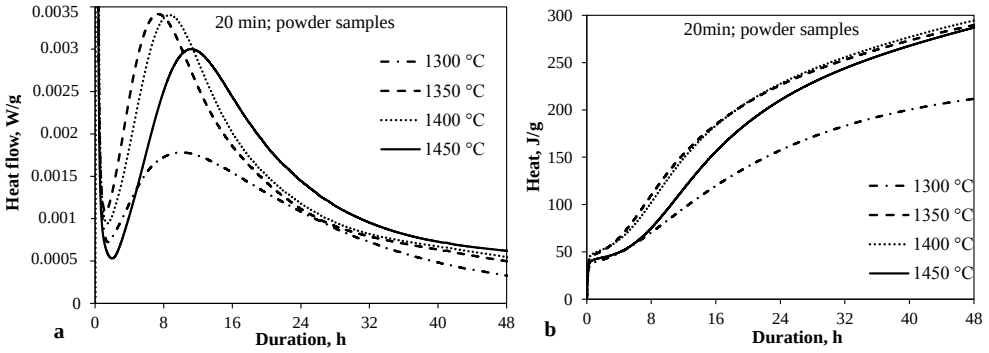


**Fig. 3.6** Heat evolution rate (a) and cumulative heat (b) of the powder samples calcined at 1300, 1350, 1400, and 1450 °C for 20 min

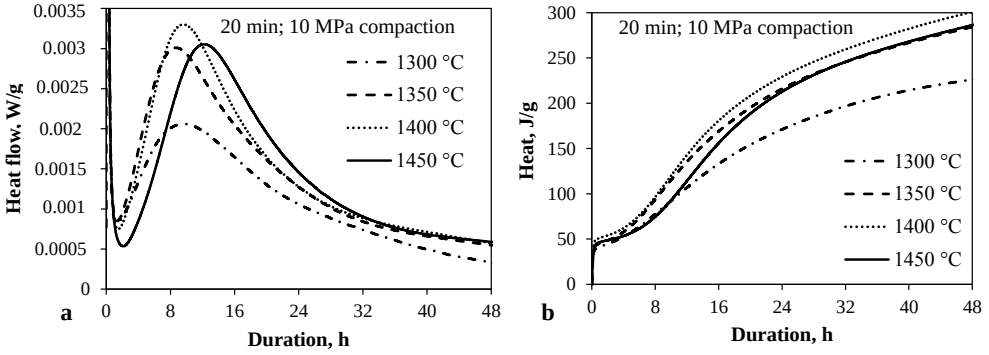


**Fig. 3.7** Heat evolution rate (a) and cumulative heat (b) of samples with 10 MPa compaction calcined at 1300, 1350, 1400, and 1450 °C for 20 min

It can be concluded that compaction of the raw meal for the OPC clinker burning influences clinker mineral formation reactions by slightly accelerating them. Moreover, the amount of $CaO_{free}$ in the compacted samples is lower than in the samples without any compaction. Compaction had a minor impact on the remaining mineral composition of the clinker – after applied compaction of 10 MPa, the amount of the main clinker mineral $C_3S$ increased by ~14 % (at 1300 °C). The applied compaction also had some positive influence on the heat release during the hydration reactions of the products. The amount of heat flow during the acceleration period in the samples calcined at 1300 °C for 20 min increased by ~14%, and the highest amount of the cumulative heat obtained in the samples calcined at 1400 °C for 20 min increased by more than 2% after compaction by 10 MPa; the amount of $CaO_{free}$ in these compacted samples was ~30% lower. Therefore, it could be beneficial to apply a relatively low compaction pressure so that to lower the clinker calcination temperature by 50 °C and achieve some positive effect on the OPC clinker mineral formation and kiln process optimization. Considering the practical implementation, this would not require major changes in the existing clinker production line since only one additional piece of equipment would be necessary.

### 3.2. Low-lime calcium silicate cement – rankinite binder – synthesis

As already discussed in the literature review, one of the most promising ways to reduce the adverse effect of the OPC clinker manufacturing is replacing it with low-lime calcium silicates, such as rankinite, since their production not only requires lower energy amounts, but, most importantly, they harden in the $CO_2$ atmosphere thus encapsulating it in the concrete structure and minimising the emissions. Therefore, the main objective of this part of the research was to synthesize an environmentally friendly binder of low C/S ratio with $CO_2$ reactive properties based on rankinite ($C_3S_2$). Rankinite was chosen due to its almost two times lower C/S ratio in comparison to OPC and still a relatively high amount of CaO that opens up a possibility of a higher absorbed $CO_2$ content if compared, for example, to wollastonite.

Details regarding the materials in use and the synthesis methods are already described in Section 2.2, thus they will not be further discussed.

XRD analysis was carried out to determine the prevailing mineral composition in the obtained product after the calcinations at 900–1300 °C, and the obtained results are provided in Figure 3.8.

As it can be seen in Figure 3.8, curves *1* and *2*, when calcining the sample pellets at a rather low temperature of 900–1000 °C, the main compounds were unreacted silica and calcium oxide with small amounts of formed calcium monosilicate $CaSiO_3$ (wollastonite, CS) and dicalcium silicate $Ca_2SiO_4$ (larnite, $C_2S$). The reaction path, according to the stoichiometric composition $CaO:SiO_2 = 3:2$, of the mineral formation can be described by the following equations (Eqs. 3.1–3.8):

$$3CaO + 2SiO_2 \rightarrow 2CaSiO_3 + CaO \quad (3.1)$$

$$3CaO + 2SiO_2 \rightarrow CaSiO_3 + Ca_2SiO_4 \quad (3.2)$$

$$CaSiO_3 + CaO \rightarrow Ca_2SiO_4 \quad (3.3)$$

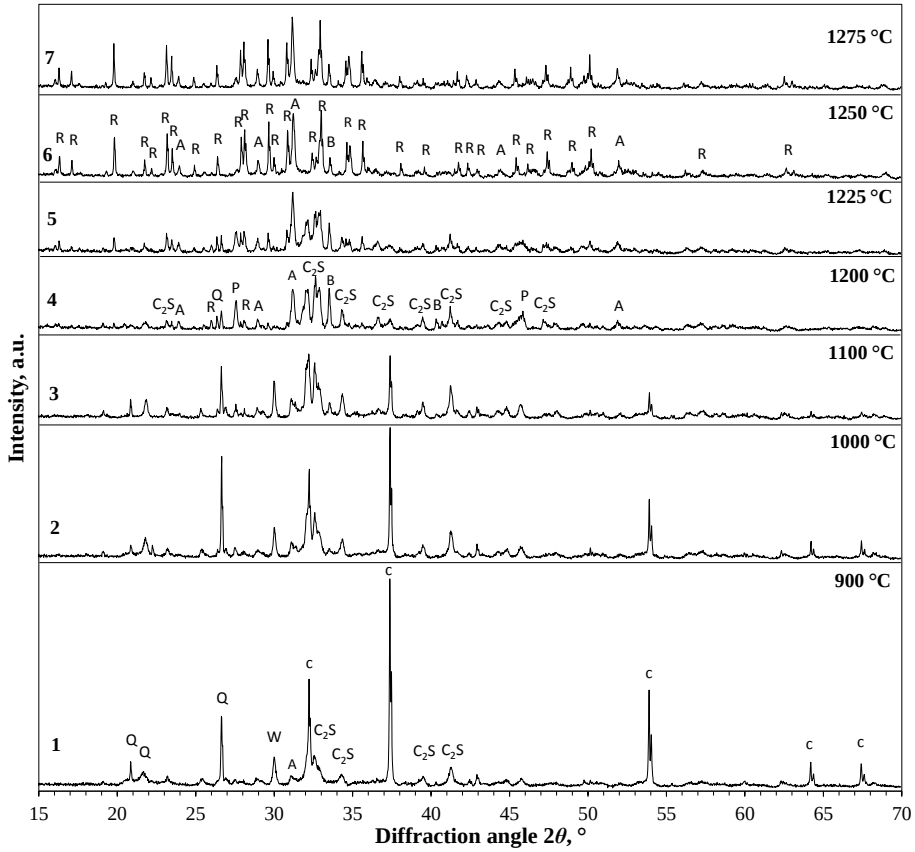


**Fig. 3.8** XRD patterns of high temperature synthesis products after calcinations at 900–1275 °C (curves 1–7) for 60 min. Indexes: Q – $SiO_2$, W – wollastonite, P – pseudowollastonite, A – akermanite, B – bredigite, R – rankinite, $C_2S$ – larnite, c – calcium oxide

When increasing the calcination temperature up to 1100 °C, the amounts of unreacted CaO and silica decreased with the further development of $C_2S$ and CS (Fig. 3.8, curve *3*; Eqs. 3.1–3.3). After the calcination at 1200–1225 °C, both CaO and silica seem to be fully reacted, which results in further formation of calcium silicates ($C_2S$ and CS) with newly formed calcium-magnesium silicates (Fig. 3.8, curves *4* and *5*; Eqs. 3.4, 3.5) – akermanite $Ca_2MgSi_2O_7$ and bredigite $Ca_7Mg(SiO_4)_4$. Yet, the formation of akermanite may have already started earlier, at 900 °C:

$$2CaSiO_3 + MgO \rightarrow Ca_2MgSi_2O_7 \quad (3.4)$$

$$MgSiO_3 + 2SiO_2 + Ca_2SiO_4 + 5CaO \rightarrow Ca_7MgSi_4O_{16} \quad (3.5)$$

Akermanite formation is considered to be occurring in the (pseudo)binary system of MgO-$CaSiO_3$ (161), while bredigite formation involves the formation of transitional intermediate compounds, such as wollastonite, larnite, merwinite and calcium magnesium silicate (162). Even though these Ca, Mg silicates are formed due to a relatively high amount of magnesium in the initial mixture, considering their low amount in the final product, they should not affect the properties of the final material.

Apart from this, small scale peaks attributed to rankinite start to appear at 1200 °C as well thus indicating that reactions of rankinite formation are starting to develop. Furthermore, at 1200 °C, wollastonite transition to pseaudowollastonite – a high temperature polymorph of wollastonite (163) – occurs.

A further increase of the calcination temperature up to 1250–1275 °C led to full recrystallization of CS and $C_2S$ to rankinite – $Ca_3Si_2O_7$ ($C_3S_2$) (Fig. 3.8, curves *6* and *7*; Eqs. 3.6–3.8) (164), while the peak intensities of the Ca, Mg silicates did not seem to further develop.

$$3CaSiO_3 \rightarrow Ca_3Si_2O_7 + SiO_2 \quad (3.6)$$

$$3Ca_2SiO_4 + SiO_2 \rightarrow 2Ca_3Si_2O_7 \quad (3.7)$$

$$CaSiO_3 + Ca_2SiO_4 \rightarrow Ca_3Si_2O_7 \quad (3.8)$$

When increasing the calcination temperature up to 1300 °C, the material, however, started to melt, thus indicating that higher temperatures are no longer acceptable for the proper synthesis. Since no further formation of $C_3S_2$ was observed above 1250 °C, as most reactants had been transformed to rankinite during the heating process, formation of $C_3S_2$ seems to be stabilized at 1250 °C, which leads to drawing a conclusion regarding the optimum temperature for the rankinite binder synthesis. Summarizing the results, compound formation at 900–1275 °C for a system with C/S = 1.5 can be described by the following sequence:

$$\underset{CaO/SiO_2=1.5}{Opoka+limestone} \xrightarrow{900-1100\,^{\circ}C} \begin{cases} CaSiO_3 \\ Ca_2SiO_4 \\ Ca_2MgSi_2O_7 \end{cases} \xrightarrow{1200-1225^{\circ}C} \begin{cases} CaSiO_3 \\ Ca_2SiO_4 \\ Ca_3Si_2O_7 \\ Ca_2MgSi_2O_7 \\ Ca_7MgSi_4O_{16} \end{cases}$$

$$\xrightarrow{1250-1275^{\circ}C} \begin{cases} Ca_3Si_2O_7 \\ Ca_2MgSi_2O_7 \\ Ca_7MgSi_4O_{16} \end{cases} \quad (3.9)$$

The experimental data and theoretical reaction formation sequence was supplemented with thermodynamic calculations. For this reason, the method of absolute entropies was used which is described in Section 2.2.

The thermodynamic properties of mineral formation reactions for the molar ratio C/S = 1.5 of the initial materials is presented in $\Delta_r G_T = f(T)$ plot (Fig. 3.9). The executed thermodynamic calculations showed that mineral formation Reactions 3.1–3.3 are exothermic processes with a decreasing entropy of the system, thus they should be spontaneous at all temperatures since $\Delta_r G_T < 0$. In the case of akermanite (Eq. 3.4), the path of the formation reaction is given directly from wollastonite and MgO and not from the initial components, while in a complex system it may occur gradually, through intermediate compounds, thus the given reaction may not accurately describe the actual path of this mineral formation. Reaction 3.6 corresponds to the endothermic process with a decreasing entropy of the system, thus it should only be spontaneous at high temperatures, while Reactions 3.7 and 3.8 should be spontaneous at a low temperature. Reactions 3.1–3.3 and 3.7–3.8 have negative values of free Gibbs energy, while Reactions 3.4 and 3.6 have a positive $\Delta_r G_T$ value thus indicating that they are the least likely to occur and should not take place spontaneously. Thus the rankinite formation reaction from wollastonite (Eq. 3.6) cannot be of great accuracy

either due to wollastonite transformation to pseudowollastonite at higher temperatures or due its rather limited extent.

It should also be noted that, due to a complex path of formation and also by considering its negligible amount after the calcination process, the formation reaction of bredigite (Eq. 3.5) was not taken into account.

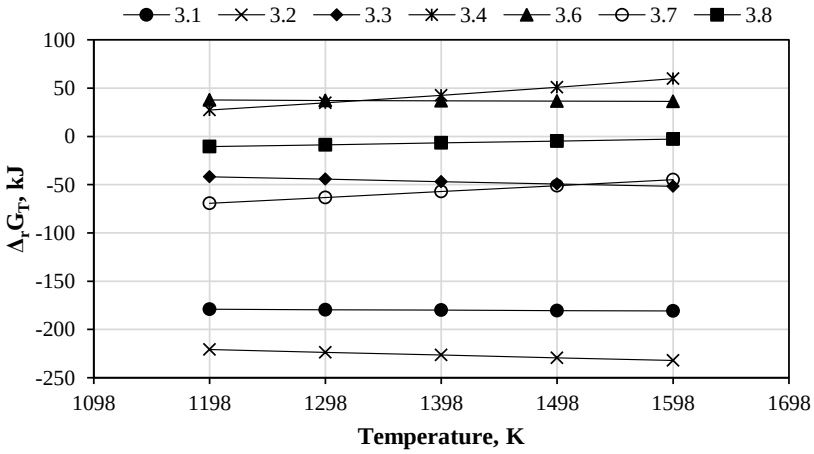


**Fig. 3.9** Gibbs free energy dependence on the temperature for reactions 3.1–3.4, 3.6–3.8 at 900–1300 °C (1198–1598 K)

Figure 3.10 illustrates the FTIR spectra of initial mixture pellets calcined at different temperatures. i.e., at 1000, 1200 and 1250 °C for 60 min. The spectra were collected across a range of 400–4000 $cm^{-1}$.

The sharp stretching band at around 3645 $cm^{-1}$ in the sample calcined at 1000 °C is assigned to the structural OH groups of $Ca(OH)_2$. Since the samples calcined at this temperature contained a fairly high amount of CaO, the appearance of $Ca(OH)_2$ indicates that the sample has reacted with the atmospheric moisture, which resulted in the formation of hydroxide.

The broad bands at around 3450 $cm^{-1}$ and the small bands at around 1635 $cm^{-1}$ are attributed to the stretching and bending bands of water molecules. These bands appear due to the presence of absorbed moisture remaining in the samples.

The band at around 1470 $cm^{-1}$ corresponds to the asymmetrical stretching of the C-O bond present in the $CaCO_3$ thus indicating that the samples absorbed carbon dioxide from the environment.

The FTIR spectra of silicate compounds show large absorptions in the range of 800 and 1200 $cm^{-1}$, which corresponds to the asymmetrical stretching vibration of the Si-O bond (165). $C_2S$ exhibits a strong band at around 996 $cm^{-1}$ and a smaller one at around 840 $cm^{-1}$ due to the stretching Si-O bond of the silicon tetrahedron and the bending out-of-plane skeletal vibration band appearing at around 520 $cm^{-1}$ and a shoulder at around 540 $cm^{-1}$ (166). $C_3S_2$ exhibits four absorption bands at around 846, 906, 940, and 996 $cm^{-1}$, and the bands attributed to CS can be found around 896, 963, 1010, and 1058 $cm^{-1}$ (33). The sharp absorption band around 655 $cm^{-1}$ is most likely attributed to the O-Si-O bending vibrations in the silicate compounds (167). Bands of

akermanite can be found at around 415 $cm^{-1}$ attributed to O-Ca-O bending and at around 486 $cm^{-1}$ attributed to O-Mg-O bending (168).

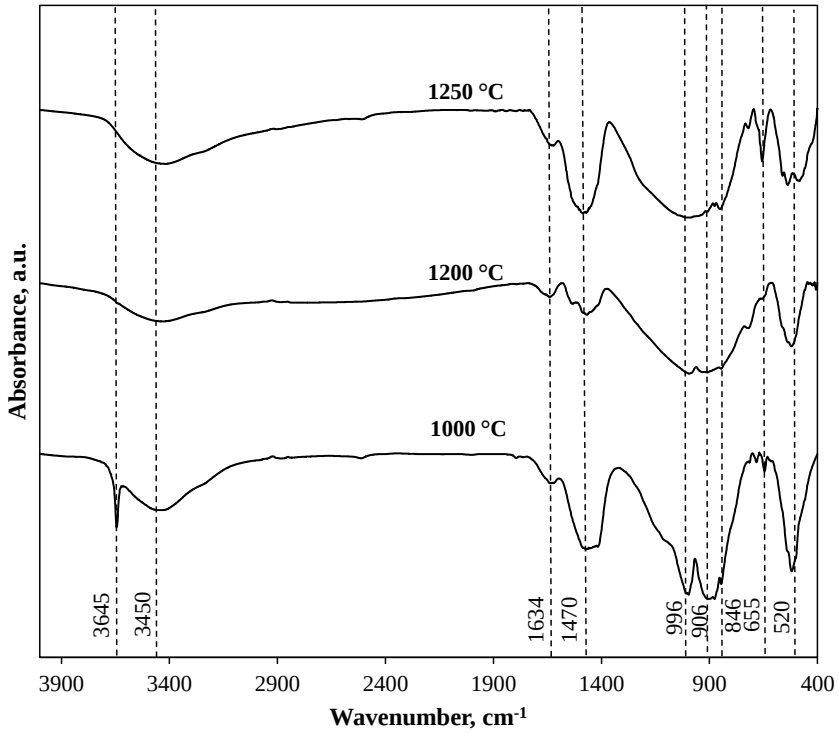


**Fig. 3.10** FTIR spectra of high temperature synthesis products after calcinations at 1000, 1200, and 1250 °C for 60 min

However, the optimization of both duration and temperature is necessary to improve the yield of $C_3S_2$ and to achieve the most economically viable process parameters. Since calcination was only carried out for 60 min, further experiments were performed to determine the possibility of decreasing the synthesis duration. For this reason, the calcination duration at 1250 °C was decreased from 60 to 15 min (with steps of every 15 min).

As it can be seen in Figure 3.11, changes in the calcination duration did not seem to have a significant effect on the final composition of the material, except for the formation of pseudowollastonite. Pseudowollastonite peaks are visible in the shortest calcination (15 min) case, the highest intensity is reached after 45 min, while the increase of the calcination duration up to 60 min led to full recrystallization of pseudowollastonite to rankinite. Since the intensity of the peaks attributed to rankinite does not seem to change accordingly with the increase of the duration (up to 45 min) and since pseudowollastonite is also a desirable component of the low-lime cements, 45 min appears to provide the most economically viable option of duration.

Thus, according to the obtained analysis data, it can be concluded that the optimum conditions for the synthesis of an environmentally friendly binder based on rankinite is 1250 °C and 45 min at laboratory conditions.

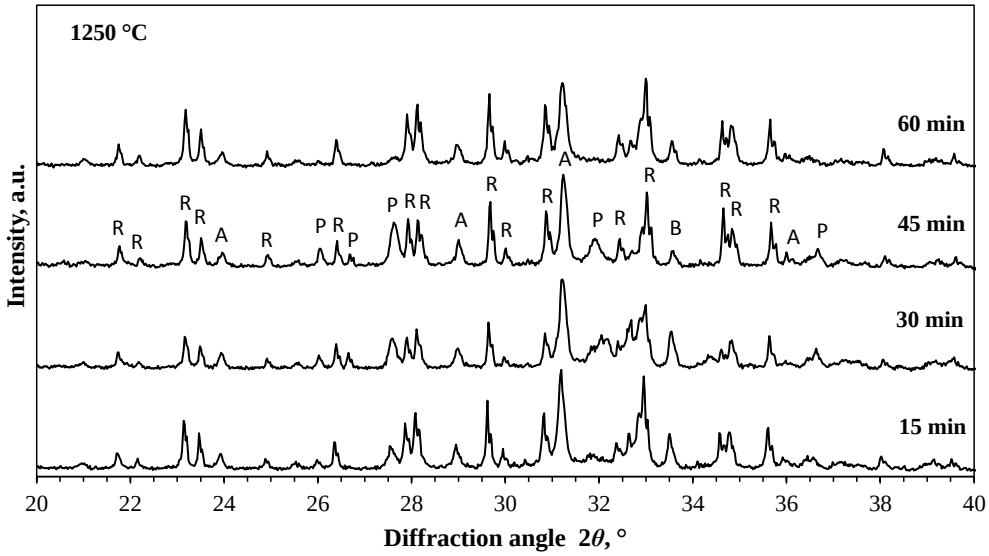


**Fig. 3.11** XRD patterns of the initial mixture pellets exposed to different duration from 15 to 60 min at 1250 °C. Indexes: R – rankinite, P – pseudowollastonite, A – akermanite, B – bredigite

Scanning electron microscopy (SEM) was performed to determine the morphology of the material synthesized at 1250 °C with various exposure durations (15–60 min). Figure 3.12 shows that, at all the durations, the visible crystals can be characterized by an irregular shape. Large scale (around 10–20 μm) rough surface rankinite crystals seem to be covered with relatively large amounts of dispersed small scale (< 1 μm) crystals, most likely, Ca, Mg silicates (169). An increase of the synthesis duration does not seem to significantly affect the crystallinity of the materials, however, since the material had been ground prior to the analysis, this may have affected the size of the particles.

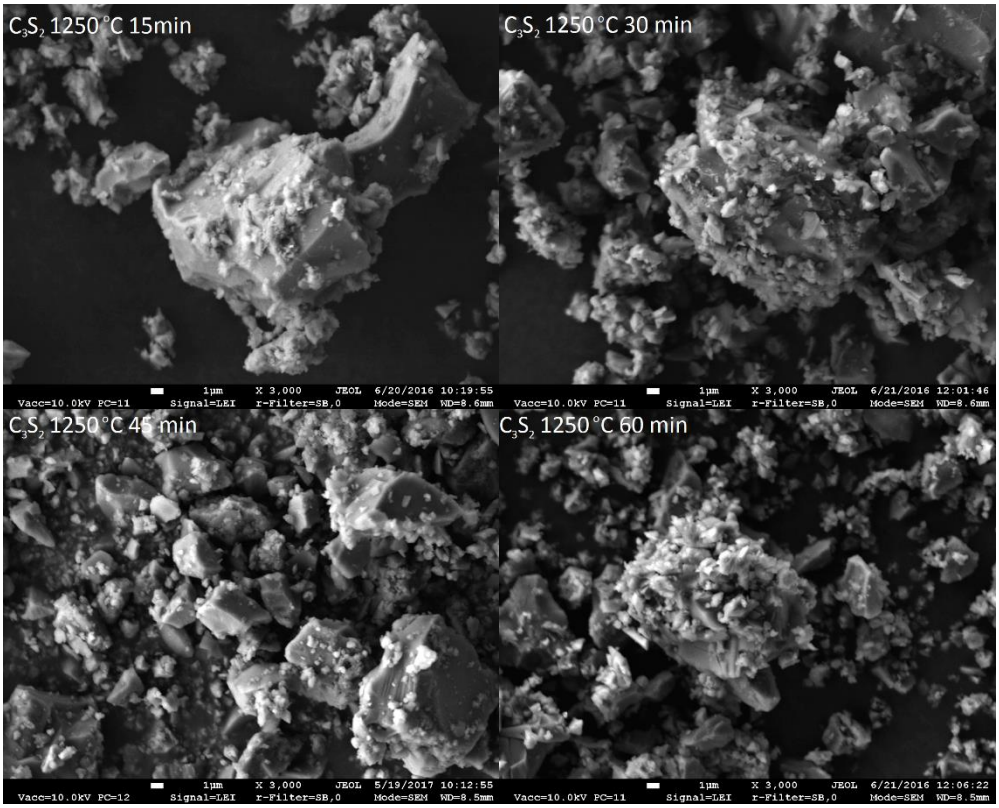


**Fig. 3.12** SEM micrographs of rankinite binder synthesised at 1250 °C for 15–60 min

## 3.3. Technological recommendations for the production of rankinite binder from opoka and limestone

According to the results obtained in Section 3.2, a sequence of technological operations for the production of the rankinite binder from opoka and limestone based on high temperature synthesis was proposed.

The rankinite binder is produced from locally available raw materials – opoka and limestone – with a mixture C/S = 1.5 at 1250 °C for 45 min. The binder production consists of the following stages: raw material processing, raw material mixture preparation and homogenization, binder calcination and processing. The principal technological production scheme is provided in Figure 3.13.

The raw materials – opoka and limestone – are transported from the quarries by dump trucks and discharged into the receiving hoppers *1*. From the receiving hoppers, the raw materials are fed to the jaw crushers *2* by an apron feeder to reach < 300 mm fraction. After the coarse crushing, the raw materials are transported to the ball mills *3* by belt conveyers for fine milling. After milling, a bucket elevator transports the raw materials to the driers *4* where they are dried at 100±5 °C for 2 h. The exhausted gas from the driers *4* enters the cyclone separators *13*, where the deducted dust is transmitted to the silos *5* by an air slide.

After processing, both raw materials are transported to the silos *5* by spiral feeders for raw material dosing. From the silos, the raw materials are transported to the mixer *6* for homogenization by weight feeders. The homogenized raw material mixture is then transported to an intermediate hopper *7*, from which, the mixture is conveyed to a five-degree preheater *8* with a bucket elevator and an air slide. The hot air for the pre-heater is provided from the end of the rotary kiln *9* and is ~900–1000°C – that is enough for limestone to completely decalcify. After pre-heating, the material is fed to a rotary kiln *9*, where it is calcined at 1250 °C for 45 min. The fuel to the kiln is fed through a hopper *16*. After calcination, the obtained binder pellets are transported through the air beam grate coolers *10* to the binder silo *11* via the bucker chain conveyor. From the binder silo *11*, the pellets are transported by a belt conveyor to the binder ball mill *12*, where they are ground to a fine powder. The obtained fine binder powder is then transported to the binder silos *14* by air slides for storage before packing and transportation. The aeration system installed at the bottom of the silos aerates the binder before discharging to the air slide by the discharging system. Then, the binder will be carried to the packing and bulk binder loading department.

The used air from the kiln is provided to the pre-heater *8*, after which, it is transferred to a cooling tower *15* and electric dust removers *17*. The removed dust is transported back to the raw material hopper *7*, the air is sent to the emission monitoring and afterwards emitted into the atmosphere. The same procedure is performed for the air from the rotary kiln. The dust from the binder mill *12* is supplied to a cyclone *13*, after which, the material is transported to the binder storage silos *14*.

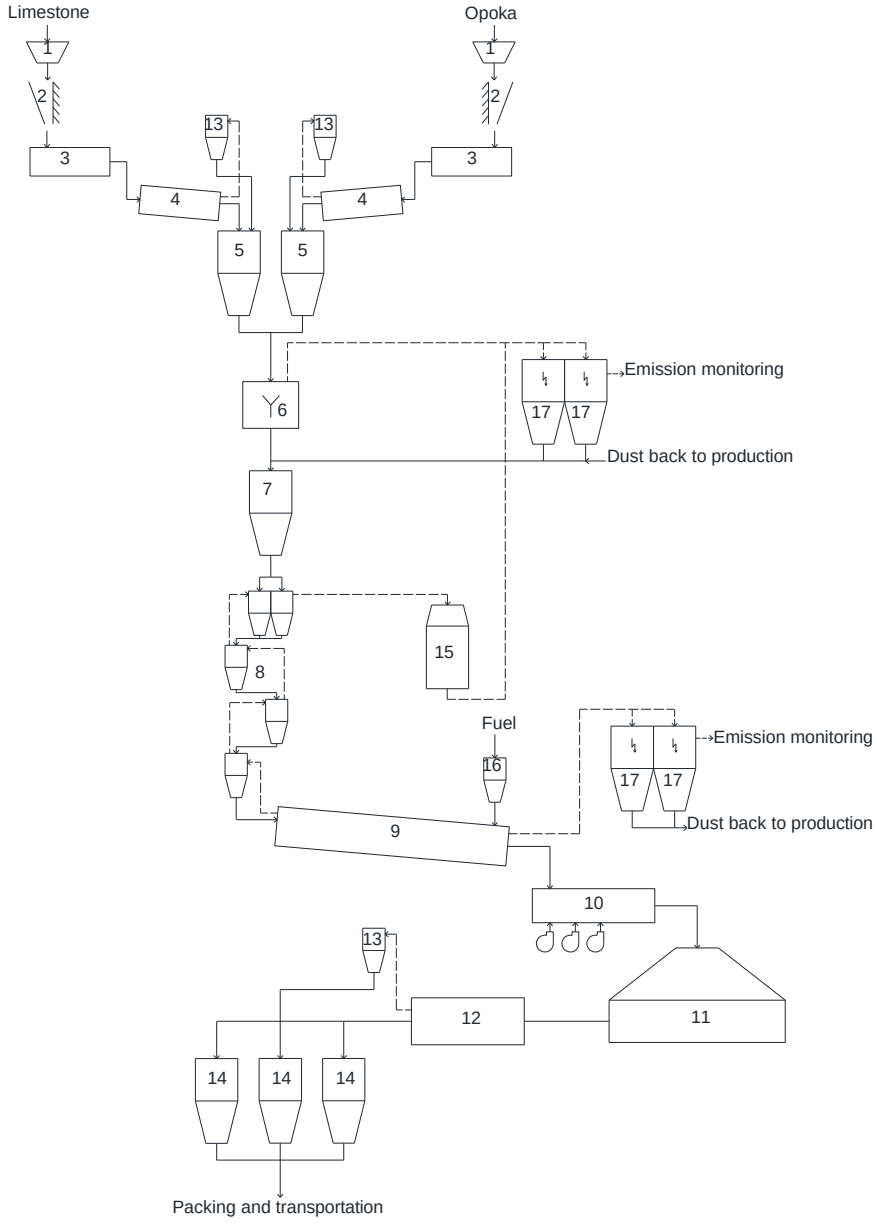


**Fig. 3.13** Principal technological scheme of the rankinite binder production from opoka and limestone. Solid line – material flow, dashed line – gas flow. 1 – receiving hoppers, 2 – jaw crushers, 3 – ball mills, 4 – driers, 5 – raw material silos, 6 – mixer, 7 – intermediate hopper, 8 – pre-heater, 9 – rotary kiln, 10 – grate coolers, 11 – binder silo, 12 – binder ball mill, 13 – cyclones, 14 – final product silos, 15 – cooling tower, 16 – fuel hopper, 17 – electric dust removers

### 3.4. Process parameter influence on rankinite binder carbonation

Since the carbonation process is highly dependent on many parameters, it is rather difficult to construct the experiment, especially due to the fact that many parameters are interdependent and can interfere with each other's effect. For this reason, in the first part of the synthesized rankinite binder carbonation curing experiments*, a fairly wide range of the primary process parameters was chosen in order to examine the rankinite binder reaction to carbonation. One of the primary parameters affecting the reaction kinetics is $CO_2$ pressure. Since the pressure highly influences the course of carbonation, it was decided to choose the uttermost pressure values, i.e., 5 bar as the minimum, 50 bar as an intermediate value, and 150 bar as the highest pressure value. The carbonation process was also carried out for a considerably minor duration – 4 h – and a high interval of 24 h. Also, as carbonation is a diffusion-limited process, the temperature should have a considerable affect as well. For this reason, a part of the experiments was carried out at room temperature, whereas the next part was carried out at an elevated temperature (50 °C).

For carbonation curing, two types of samples – mortars and pastes – were used. The mortar samples were prepared by mixing the binder with sand (15:85 wt%) and adding distilled water for the water-to-binder (w/c) ratio of 0.35 (water-to-solid ratio, w/s = 0.05). The mixture was then moulded and pressed (by using 19.630 kN (10 $N/mm^2$) pressure, at a speed of 2 $N/mm^2$ with 10 s exposure at the highest pressure) to form 50×50 mm cylindrical samples. After the formation, the samples were immediately transported to the pressure reactor. For each experiment of the carbonation curing, an additional sample of only rankinite binder paste with the same w/s as the mortars was prepared. The paste was prepared right before the curing experiment, spread onto a ceramic plate without any compaction and transported to the pressure reactor immediately afterwards.

The prepared samples were hardened in the pressure reactor with gaseous and supercritical (SC) $CO_2$, by procedure described in Section 2.2. The carbonation curing was carried out at 5, 50, 100, and 150 bar, for 4 and 24 h, at 20 and 50 °C.

Compressive and tensile splitting strength of the samples was determined immediately after the curing. The remains from the crushed samples were used for the porosity determination. For better determination of the mortar mineral composition, the binder was separated from the sand grains as best as possible, by gently crushing the sample remains from the strength determination by pestle into smaller pieces and sieving those through a 32 μm mesh sieve. The obtained powder, along with the paste sample, was dried at 40 °C for 48 h and was used for further determination of the mineral composition.



*this part of the research was completed at the Centre of Building Materials, Technical University of Munich in Germany, under supervision of dr. Ing. L. Urbonas

### 3.4.1. Compressive and tensile splitting strength of carbonated rankinite binder mortars

The obtained compressive and tensile splitting strength results of the rankinite binder mortars carbonated at the investigated conditions is presented in Figures 3.14 and 3.15.

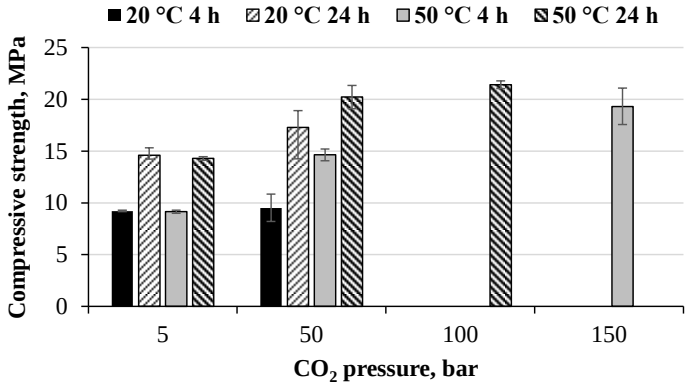


**Fig. 3.14** Compressive strength development of rankinite binder mortars carbonated at different pressure, duration, and temperature conditions; w/c = 0.35

As it can be seen in Fig. 3.14, when carbonating the rankinite binder mortars at the lowest conditions for 4 h at 20 °C, regardless of the pressure (5 and 50 bar), a strength of around 10 MPa was reached. When increasing the carbonation duration from 4 to 24 h (at 20 °C), rankinite binder mortar strength increased by 37% and 45%, at 5 and 50 bar, respectively. Similar increases were reached when the process temperature was increased up to 50 °C at 50 bar carbonation, however, the temperature had no impact on the mortars carbonated at 5 bar. As expected, the highest compressive strength of rankinite binder mortars was reached when carbonating at SC conditions – 19 and 21 MPa, at 150 bar (4 h) and 100 bar (24 h), respectively.

Since the rankinite carbonation reaction results in the formation of calcium carbonate, it is believed to be the main component contributing to the compressive strength development. However, the increase in the strength values of the SC carbonated samples may not be only due to the higher extent of calcium carbonate formation. It has been stated that in the samples carbonated at SC conditions the silica gel polymerization is higher with lower amounts of Ca incorporated in its structure (98). This may indicate that a highly polymerized silica gel also contributes to a higher strength of the carbonated samples. Purnell *et al*. (170) stated that the modification of the silica gel by SC carbonation is of primary importance for the improvement of mechanical properties of the cement matrix.

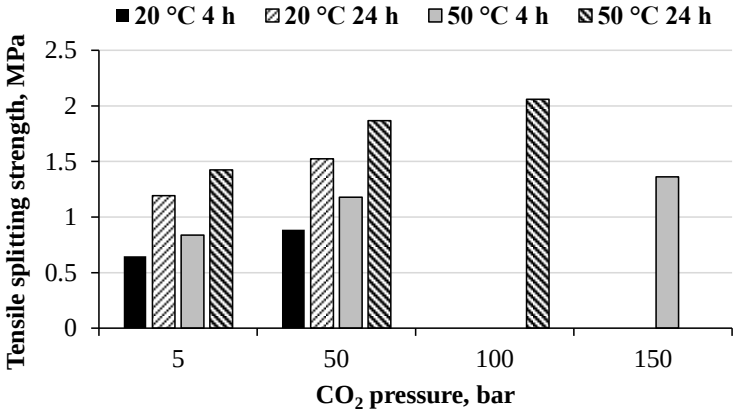


**Fig. 3.15** Tensile splitting strength development of rankinite binder mortars carbonated at different pressure, duration, and temperature conditions; w/c = 0.35

The obtained tensile splitting strength results of the rankinite binder mortars are provided in Figure 3.15. Similarly as above, the tensile splitting strength of rankinite binder mortars increased accordingly with the increasing pressure, duration and/or temperature, and, as with the compressive strength, the highest value of the tensile splitting strength was reached after the carbonation at 100 bar for 24 h at 50 °C.

### 3.4.2. Microstructure of carbonated rankinite binder mortars

Mercury intrusion porosimetry (MIP) was used to determine the porosity of the carbonated rankinite binder mortars. The total porosity of rankinite binder mortars is provided in Table 3.4, while the pore size distribution is shown in Fig. 3.16. As it can be seen in Table 3.4, the total porosity of the samples carbonated for 4 h decreases with the increasing $CO_2$ pressure; when increasing the pressure from 5 to 150 bar, the total porosity decreased by 1.5% (at 50 °C). Figure 3.16 demonstrates the pore size evolution of the mortar samples carbonated at 50 °C. The samples carbonated at 5 and 50 bar are shown to have pores of similar dimensions, while the ones carbonated at SC conditions are detected to have relatively lower pore volumes. That is associated with an increasing amount of calcium carbonate accumulated in the pore structure or a thicker layer of carbonation reaction products including calcium carbonate and silica gel. Since SC $CO_2$ features liquid-like density and gas-like transport properties, it can penetrate into very fine pores (171) thus providing continuous availability of fresh $CO_2$ and rendering carbonation into a non-diffusion controlled process (98). The reduction of the total porosity and pore volume is related to the compressive strength development thus indicating that the formation of carbonates contributes to a denser microstructure because of the reduced capillary porosity which is likely to account for a higher compressive strength. MIP results are in good agreement with the obtained compressive and tensile splitting data where the highest strength was obtained by samples carbonated at SC conditions.

**Table 3.4** Total porosity of rankinite binder mortar samples cured at different curing conditions for 4 h, %

| % | w/c = 0.35 | |
|---|---|---|
| $CO_2$ pressure, bar | 20 °C | 50 °C |
| 5 | 24.53 | 22.64 |
| 50 | 22.53 | 22.96 |
| 150 | - | 21.25 |

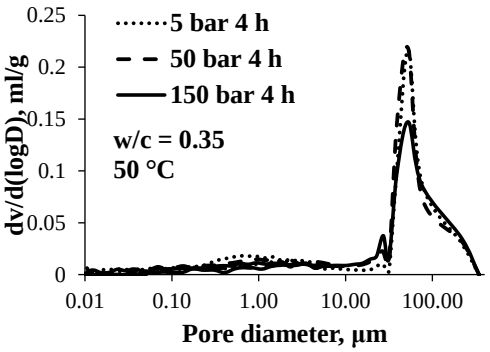


**Fig. 3.16** Pore size distribution of rankinite binder mortars after carbonation at different conditions

X-ray computed tomography (CT) as a non-destructive method was also used to further investigate the pore structure of the carbonated material. Two samples were used for the determination – 5 bar/4 h as a reference of the least carbonated sample and 50 bar/24 h as a most carbonated sample cured at 50 °C. CT scan images in the gray scale of the samples are provided in Fig. 3.17 – with those featuring the clearer tones representing a higher density being attributed to the aggregates, sand in this case, and the darker tones corresponding to the lower densities being attributed to the reaction products and pores. Even though there are no visual differences in the images and as the structures of both of the samples seem rather evenly distributed, the total calculated amount of pores was equal to $71.9 \cdot 10^3$ and $67 \cdot 10^3$ units for 5 and 50 bar, respectively, which corresponded to 11.3% and 10.9% of 3D volume, yielding a 4% difference. The obtained results further complemented the MIP results thus indicating that a higher $CO_2$ pressure and a longer carbonation duration determines a lower porosity thus leading to a higher mechanical strength of the samples.

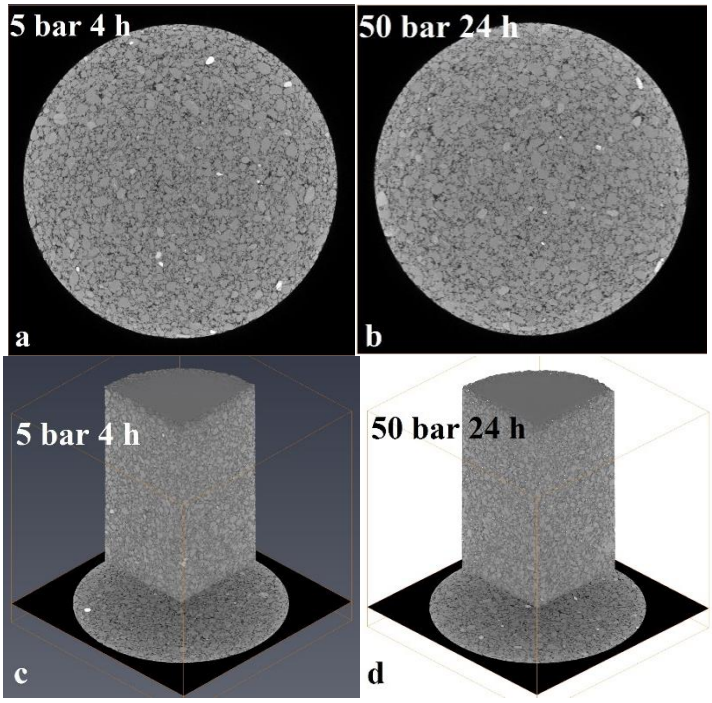


**Fig. 3.17** X-ray CT scan images of rankinite binder mortar samples carbonated at different conditions; w/c = 0.35, 50 °C

### 3.4.3. Mineral composition of carbonated rankinite binder samples

XRD patterns of carbonated rankinite binder pastes and mortars are provided in Figures 3.18–3.20. As it can be seen in Fig. 3.18, the carbonation at low parameter values, i.e., 5 bar for 4 h at 20 °C, did not have any major impact on the mineral composition of the carbonated sample since it is almost identical to the unreacted rankinite binder (Fig. 3.18, *untreated*). However, with the increased process parameter values, the obtained XRD patterns are different – the main calcium carbonate – calcite – peak at around 0.304 nm is visible in all of the curves and is much broader and of a higher intensity at higher carbonation parameter values. The curing experiments carried out at 20 and 50 °C showed similar tendencies (Figs. 3.18–3.19). However, in contrast to any other conditions, the samples carbonated at 5 bar for 24 h at 50 °C surprisingly showed formation of aragonite and vaterite, metastable calcium carbonate polymorphs, rather than calcite (Fig. 3.19, *5 bar 24 h*). Possibly, the increase of the temperature at a lower pressure and a prolonged carbonation duration led to the formation of the metastable forms of calcium carbonate, which, with an increased pressure, recrystallized to a more stable form of calcite. Apart from this, no other mineral, besides rankinite, from the binder composition seems to be involved in the carbonation reaction – peaks of Ca, Mg carbonates, akermanite and bredigite remain stable, while the absence of any peaks attributed to the silica gel confirms the amorphous state of this component.

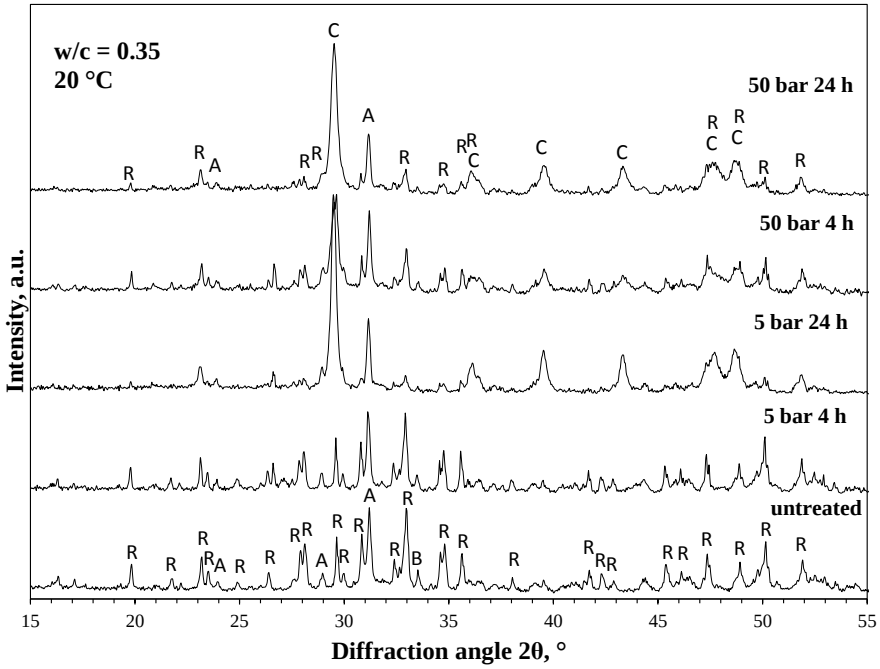


**Fig. 3.18** XRD patterns of carbonated rankinite binder paste samples. Indexes: R – rankinite, A – akermanite, B – bredigite, C – calcite

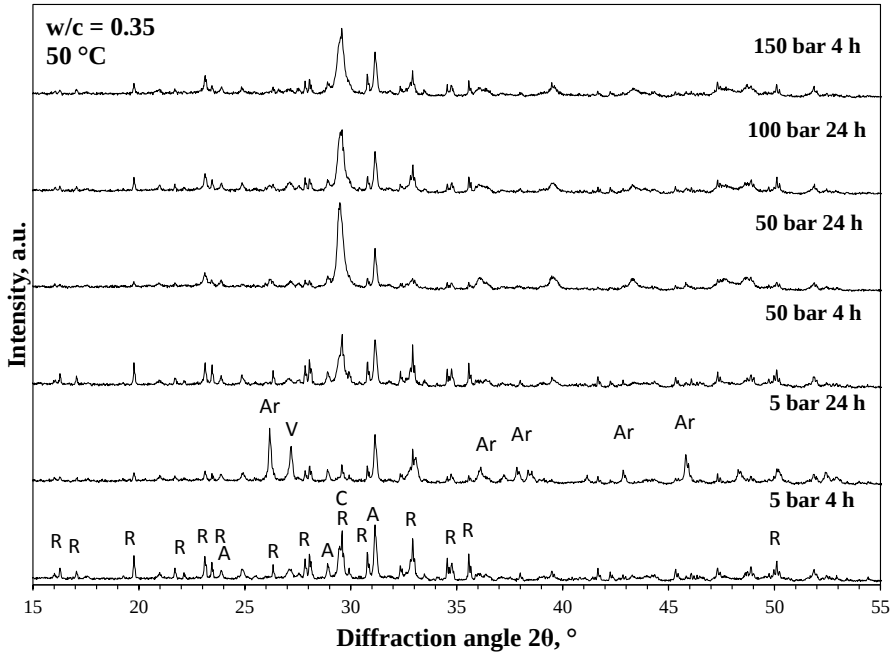


**Fig. 3.19** XRD patterns of carbonated rankinite binder paste samples. Indexes: R – rankinite, A – akermanite, B – bredigite, C – calcite, Ar – aragonite, V – vaterite

On the contrary, entirely different patterns of XRD curves are visible in the mortar samples (Fig. 3.20). The relatively large peaks attributed to quartz are due to the complicated separation process discussed previously in the introduction of Section 3.4. Other than that, the mortars seem to have reached a much higher degree of carbonation, since, even at low process parameter values (e.g., 5 bar and 4 h), the peaks attributed to rankinite are insignificantly small-scale or not evident at all. The highest carbonate peak intensities are visible in the samples carbonated for 24 h or at SC conditions, which is consistent with the expected carbonation reaction.

Accordingly, these considerable differences in the mortar and paste sample carbonation could be explained by the differences in the sample microstructure. Since mortars were prepared with a considerably large amount of fine aggregates, i.e., sand, the microstructure of such samples is markedly porous thus allowing $CO_2$ gas to penetrate the system with ease. The porous structure of the mortar also supports water maintained in the pores so that it does not evaporate too quickly. Paste, on the other hand, being prepared without any compaction, does not maintain water, and it can easily evaporate into the atmosphere thus hindering $CO_2$ gas from reacting with binder particles. Since the carbonation reaction is an exothermic process where increases in temperature of up to 58 °C for concrete and 70 °C for cement paste have been recorded at room temperature (100), water evaporation in the loose system is further induced. Another possible explanation is also associated with water scarcity: even though mortars and pastes were prepared with the same water-to-solids ratio, in the mortars, a higher amount of water is attributed to the binder since sand does not react with water and is not included in the carbonation reaction. Contrarily, in the pastes, the same w/s ratio leads to a lower amount of water attributed to the binder, thus, again, leading to a possible water shortage. Since water is an essential element for carbonation, its presence needs to be adequately proportioned and sealed to allow $CO_2$ to efficiently dissolve and to allow the carbonation reaction to proceed.

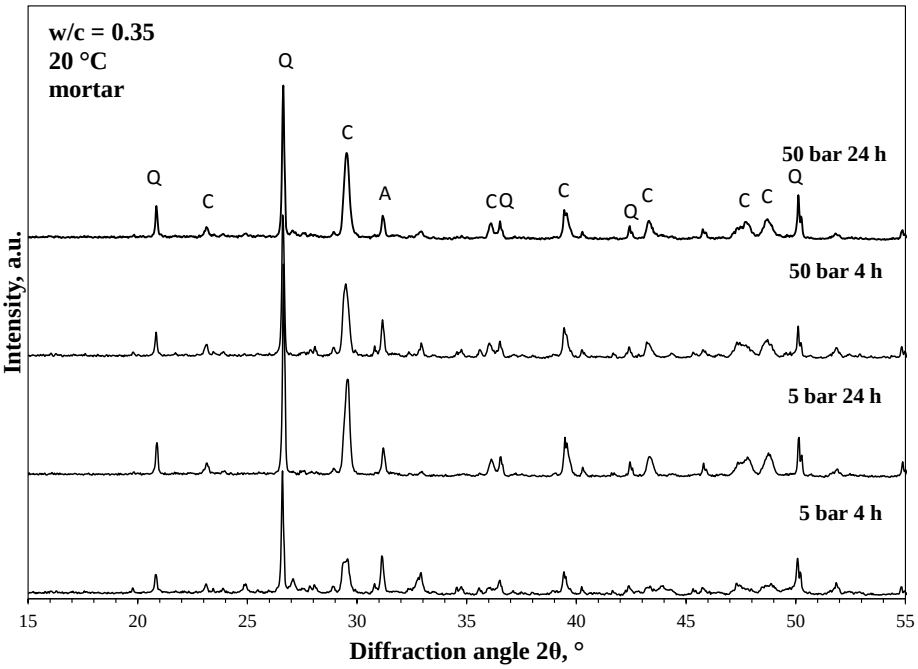


**Fig. 3.20** XRD patterns of carbonated rankinite binder mortar samples. Indexes: C – calcite, A – akermanite, Q – quartz

FTIR spectra of carbonated rankinite binder paste samples with w/c = 0.35 are shown in Figure 3.21. FTIR spectra of carbonated samples tend to show a broad strong carbonate band at around 1300–1600 $cm^{-1}$. This band appears stronger for samples carbonated for a longer duration or at a higher $CO_2$ pressure thus confirming the results obtained from the XRD analysis that showed the same tendencies. The asymmetrical stretching band of the C-O bond in the carbonate molecule – a broad shoulder – centred around 1430–1490 $cm^{-1}$ – indicates the formation of the main calcium carbonate – calcite. The split in-plane bending vibrations of the carbonate band at around 875 $cm^{-1}$ have different relative intensities depending on the carbonation parameter values – at a higher pressure and/or duration, the peak is much sharper. The third band attributed to carbonates can be found at around 715 $cm^{-1}$ and is associated with the out-of-plane bending vibration of the C-O bond.

The absorption bands of uncarbonated rankinite can be found at around 850, 940 and 985 $cm^{-1}$ (Fig. 3.21, *b untreated*). The bands attributed to silica gel can be found at around 480 and 1080 $cm^{-1}$. The first band corresponds to the O-Si-O bond bending vibrations and is affected by the bond angle as well as by the occupancy of the neighboring sites or by the polymerization of the silica gel, while the second band corresponds to the stretching vibrations of the Si-O bond. The band at ~1080 $cm^{-1}$ deepens and broadens with the increasing carbonation parameter values thus indicating a higher polymerization degree of the silica gel.

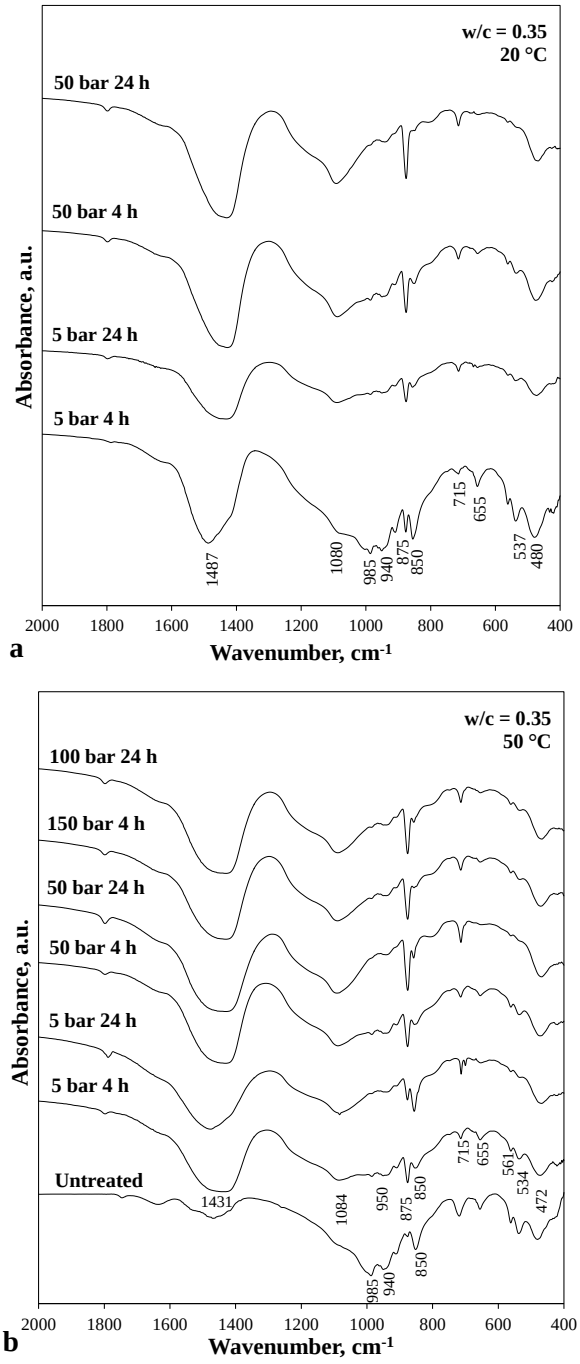


**Fig. 3.21** FTIR spectra of carbonated rankinite binder paste samples, w/c = 0.35, a – 20 °C, b – 50 °C

The obtained thermogravimetric (TG) analysis results (Fig. 3.22) showed a well-distinguished single step mass loss at around 700 °C attributed to the decomposition of calcium carbonate.

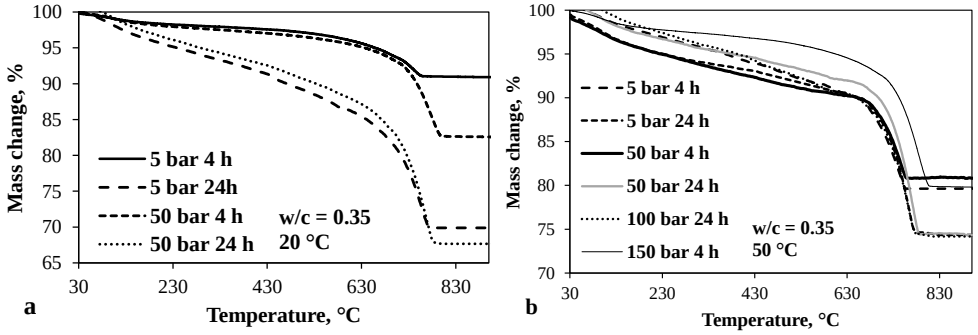


**Fig. 3.22** TG curves of carbonated rankinite binder paste samples, w/c = 0.35, a – 20 °C, b – 50 °C

To further determine the efficiency of the carbonation process, the carbonation degree was calculated based on the TG mass loss data. The mass loss due to the decomposition of calcium carbonate as well as the calculated degree of carbonation is provided in Table 3.5. The carbonation degree was calculated by using Equation 3.10 adapted from (93), where the maximum capacity of $CO_2$ uptake was calculated by using Equation 3.11 proposed by Steinour (172) since the $CO_2$ storing capacity of cementitious materials is dependent on their oxide content:

$$\text{Degree of carbonation, } \alpha = \frac{\text{CO}_2 \text{ content}}{\text{max. content of CO}_2} \times 100\ \% \quad (3.10)$$

$$CO_2\ (\%, \text{max}) = 0.785(CaO - 0.7SO_3) + 1.091Na_2O + 0.935K_2O = 37.65\% \quad (3.11)$$

It should also be noted that the impact of MgO in Eq. 3.11 was eliminated because it was determined that, in the binder composition, magnesium is combined into stable Ca, Mg silicates that do not participate in the carbonation reaction and remain inert.

**Table 3.5** Mass loss and degree of carbonation of the carbonated rankinite binder paste samples, %

| % | Mass loss | | | | Carbonation degree | | | |
|---|---|---|---|---|---|---|---|---|
| | 20 °C | | 50 °C | | 20 °C | | 50 °C | |
| | 4 h | 24 h | 4 h | 24 h | 4 h | 24 h | 4 h | 24 h |
| 5 bar | 3.00 | 12.72 | 10.72 | 15.52 | 7.97 | 33.80 | 28.46 | 41.23 |
| 50 bar | 10.60 | 18.02 | 9.06 | 16.98 | 28.15 | 47.87 | 24.06 | 45.11 |
| 100 bar | - | - | - | 14.83 | - | - | - | 39.39 |
| 150 bar | - | - | 12.90 | - | - | - | 34.26 | - |

As it can be seen in Table 3.5, the lowest carbonation degree of the paste samples was reached while carbonating at the lowest conditions – 5 bar, 4 h and 20 °C. Nonetheless, with the increasing carbonation parameter values, the carbonation degree increased as well. When carbonating the samples for 24 h at 50 °C, regardless of the pressure, all the samples seem to have reached a similar degree of carbonation at around 40%, which further confirms the XRD data that the paste samples were not fully carbonated. However, the obtained paste sample mass loss results and thus the calculated degree of carbonation, unfortunately, cannot be compared to the mortar carbonation degree in any way due to the limited carbonation of the paste samples, which is also evident in the XRD patterns in comparison to mortars and testifies an inaccurate amount of quartz remaining in the mortars.

The SEM images collected from powdered carbonated rankinite binder paste and mortar samples are shown in Figure 3.23. Energy dispersive X-ray (EDX) spectroscopy was performed on the SEM images to approximately determine the prevailing composition of the resulting compounds. The areas that were examined are marked from 1 to 7, and the obtained results are shown in Table 3.6.

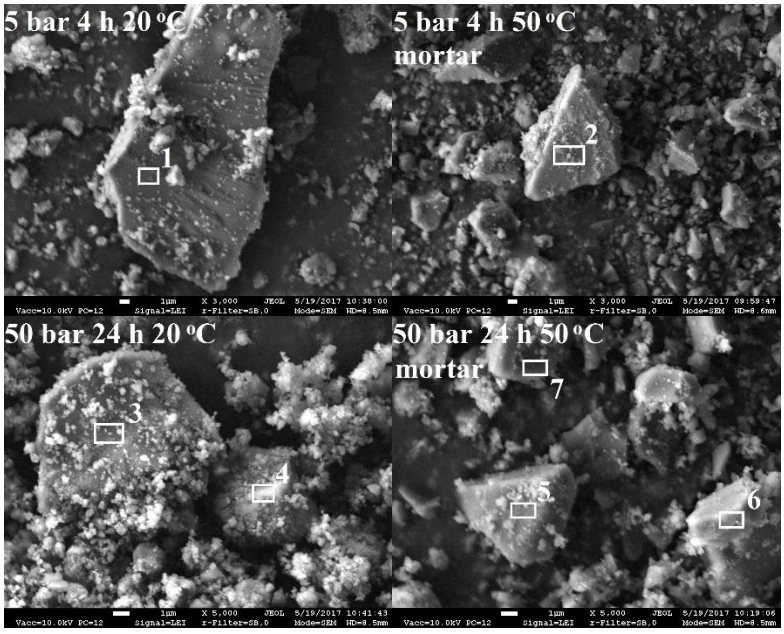


**Fig. 3.23** SEM images of carbonated rankinite binder samples, w/c = 0.35

**Table 3.6** EDX analysis of rankinite binder samples, areas 1–7 (Fig. 3.23)

| Area | | Element | | | |
|---|---|---|---|---|---|
| | | Ca | Si | O | C |
| 1 | Amount, wt% | 46.6 | 22.2 | 31.3 | - |
| 2 | | 5.8 | 55.4 | 20.2 | 18.7 |
| 3 | | 32.9 | 18.3 | 42.6 | 6.2 |
| 4 | | 25.00 | 12.8 | 53.5 | 8.7 |
| 5 | | 5.7 | 40.1 | 45.9 | 8.2 |
| 6 | | 7.2 | 38.9 | 44.5 | 9.5 |
| 7 | | 0.9 | 31.2 | 58.0 | 9.9 |

As can be seen in Figure 3.23 and Table 3.6, area No. 1 situated on a large scale crystal (~7×13 μm) from the sample carbonated at the lowest conditions (5 bar 4 h 20 °C) is most likely attributed to rankinite since no other elements than Ca, Si, and O were detected; also, when recalculating the elemental composition, as determined by EDX to oxide, the obtained results yielded molar C/S ratio of 1.37, which is fairly close to rankinite C/S. All of the other points showed the presence of carbon, which again confirms the formation of carbonates. Furthermore, supporting the previously made conclusion, the highest amount of carbon is detected in the mortar samples (Table 3.6, *area 2*) thus further demonstrating that mortars reached a higher carbonation degree than pastes. A relatively high amount of silica detected in the mortar samples (Table 3.7, *areas 2, 5–6*) is attributed to the presence of the remaining aggregate particles. The presence of all the key elements (Ca, Si, O and C) from the binder composition in all the analyzed areas leads to a conclusion that the carbonation reaction products – carbonates and silica gels – are intermingled and unevenly cover the unreacted binder particles. Figure 3.23 shows that all the visible crystals can be characterized as irregularly shaped and are covered in smaller scale (< 1 μm) brighter particles.

**********

According to the obtained results after this part of carbonation curing experiments, it can be concluded that process parameters have a considerable effect on the hardened concrete mechanical properties and mineral composition.

Even though the highest strength was reached after carbonating the samples at supercritical conditions, and although the practical benefits associated with the increased strength are self-evident, however, when considering a wider implementation, supercritical $CO_2$ may be impractical, and, since the strength values after carbonation at 50 bar and 24 h (at 50 °C) were almost equivalent, it would be much more economically viable to carry out the hardening process at a lower pressure for a longer period of time.

A higher temperature also had a positive impact on the sample properties, however, a wider range should also be taken into account in order to achieve not only an efficient but also an economically balanced process.

### 3.5. Carbonation process optimization

Due to the obtained results in the first part of the carbonation curing experiments, this part was dedicated to finding the variety of the optimum process as well as the sample preparation parameters in order to achieve the aforementioned balance. Owing to this, the range of the main parameters affecting the carbonation process and their intervals were expanded to further investigate the rankinite binder carbonation process. Besides, the pressure, duration, temperature, and w/c ratio, sample compaction and composition (binder/sand ratio) were also taken into account.

For this part of the carbonation curing experiments, the synthesized rankinite binder (further noted as $C_3S_2$) and industrial Portland cement CEM I 42.5 R (further referred to as OPC) were used. Since the samples of both binders were prepared in an identical procedure, in the further explanations, they will be referred to as the 'binder'.

In this stage of the carbonation process investigation, paste and mortar samples were prepared as well. However, when preparing the mortars, considering the previous experience, the methodology was slightly modified by increasing the ratio between the binder and the aggregates from 0.18 to 0.25 (unless indicated otherwise) and decreasing the mortar sample dimensions to 36×36 mm. The amount of the binder in the samples was increased to achieve a standard similar value, and the dimensions were reduced in order to attain full carbonation in a shorter period of time or at lower parameter values. The samples were prepared in a similar procedure as before – a mixture of the initial materials was prepared, immediately moulded and pressed (by using the same pressure as before, unless indicated otherwise, but a lower speed of 1 $N/mm^2$ and a longer exposure of 20 s). The water-to-binder ratio was maintained at 0.35 (unless indicated otherwise), and the w/s ratio was thus equal to 0.0875. What regards the paste samples, the procedure was adjusted as well: since the previously determined carbonation degree of the pastes was significantly lower than that of the mortars, most likely due to the absence of compaction, this time, the pastes were moulded and pressed as well by using the same parameters as for the mortars, only using ~10 g of the paste (same w/s as for the mortars) for one sample, which resulted in a circular-shaped disk samples with dimensions of ~36×6 mm. All of the samples were transported to the pressure reactor immediately after formation without any preconditioning.

The prepared samples were hardened in the pressure reactor with gaseous $CO_2$, by procedure described in Section 2.2. Carbonation curing was carried out at 5–25 bar (with steps of 5 bar), for 4, 16, and 24 h, with the process temperature of 25 to 55 °C; the compaction was changed from 5 to 17.5 MPa; the binder-to-sand ratio was changed from 15/85 to 30/70; the water-to-binder ratio varied from 0.15 to 0.4. The schematic relations between the chosen parameters are provided in Figure 3.24.

After the carbonation curing, the samples were prepared for the analysis in the same procedure as indicated in Section 3.4.

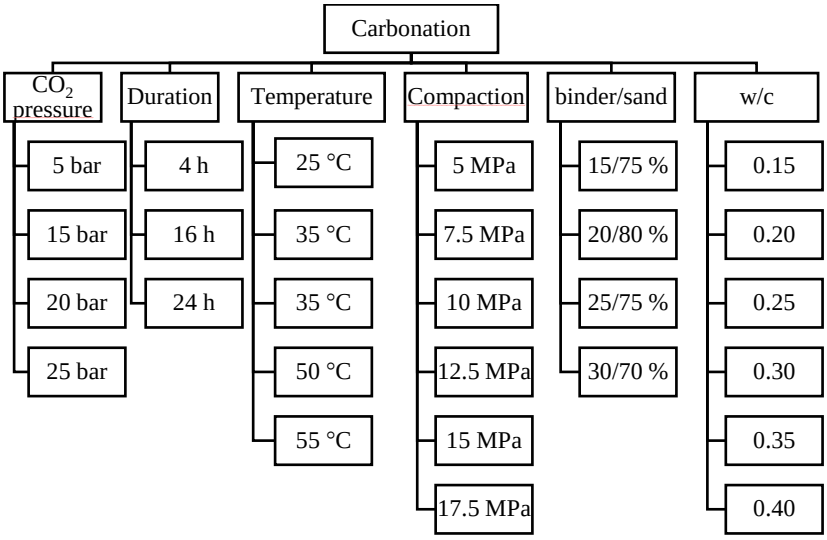


**Fig. 3.24** Carbonation parameter scheme

### 3.5.1. Compressive strength development of carbonated rankinite binder and cement mortars

In order to use the carbonated calcium silicate as an alternative binder, it is crucial to investigate the mechanical performance of such a system as well as the dependency of the mechanical strength on various conditions and process parameters. During this part of the research, the compressive strength of both of the binder – $C_3S_2$ and OPC – mortars was investigated based on the curing process parameters – $CO_2$ pressure, exposure duration, and temperature, along with the sample properties itself – the binder/sand ratio, the w/c ratio, and compaction. In order to detect the maximum conformity of all the parameters and to achieve the highest possible mechanical strength, after each experiment, the condition at which the highest result was reached, was chosen, and then the second parameter was changed, and so forth. Thus the primary parameters to be investigated were the $CO_2$ pressure and the exposure duration. Since carbonation is a diffusion-limited process, elevated pressure, combined with prolonged duration, promotes easier $CO_2$ penetration into the porous but rather dense material. However, over-pressurization can lead to the blockage of the pores thus hindering the entrance of gas into the inner parts of the material. Therefore, it is important to achieve the combined parameter balance. Considering the cost-effectiveness and practical implementation, in this part of the research, the pressure values were chosen from a considerably low range of 5–25 bar.

The evolution of the average compressive strength of $C_3S_2$ and OPC mortar samples based on the aforementioned curing parameters is shown in Figures 3.25–3.26. It can be seen that both binder systems reacted to the curing differently – the rankinite binder samples seem to follow a pattern of consistent strength increment with increasing curing parameter values, while the cement sample strength was rather fluctuating even though it reached higher strength values. When increasing the $CO_2$ pressure from 5 to 25 bar at the lowest exposure of 4 h, the $C_3S_2$ sample strength

increased by ~54%, still, it did not exceed 10 MPa. The cement sample strength, on the other hand, strangely did not seem to be directly dependent on the pressure value, although it reached a two-times-higher strength in comparison to the rankinite binder. Similarly as before, a much more significant impact stemmed from the increase of the exposure since, when increasing the duration from 4 to 16 h, the $C_3S_2$ sample strength increased by more than 100% at all the pressure values. A further increase of the duration up to 24 h led to no more than a 25% increase in the mortar strength of both binders. Considering the combined conditions, both OPC and $C_3S_2$ samples reached the highest strength after the carbonation at 15 bar for 24 h and remained virtually stable when further increasing the pressure. The samples hardened at these conditions visually seem to be fully carbonated, thus an increase of the pressure had no significant difference in a longer-term carbonation. Even though carbonation at 20 bar for 16 h had a similar impact on the sample strength, however, considering more practical and economically viable implementation, a lower pressure for a longer period of time might be more advantageous. Thus, in the following experiments, these pressure and duration parameter values – 15 bar and 24 h – were chosen as the most effective options.

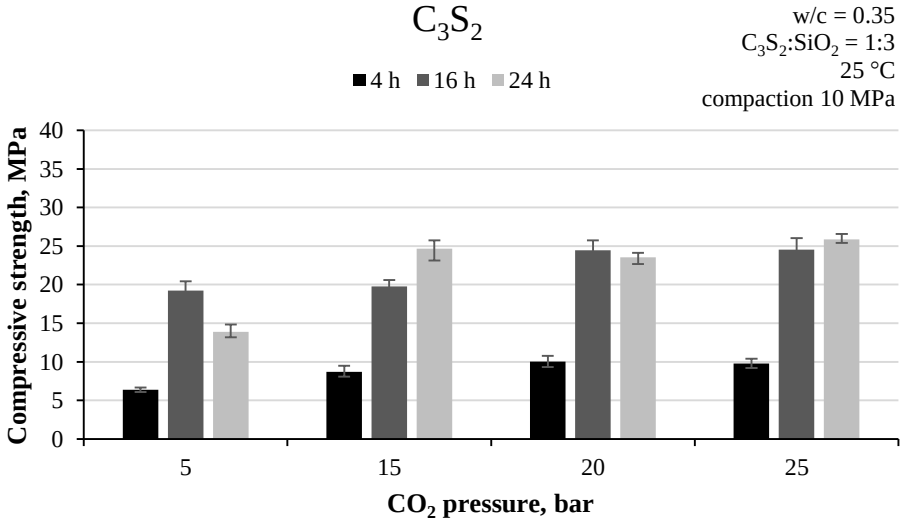


**Fig. 3.25** Compressive strength of the rankinite binder mortar samples carbonated at different $CO_2$ pressure and duration conditions

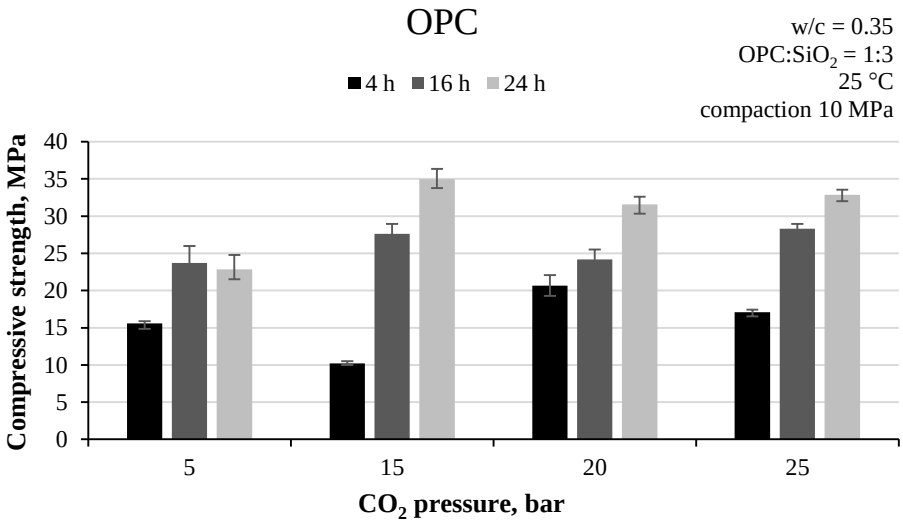


**Fig. 3.26** Compressive strength of the cement mortar samples carbonated at different $CO_2$ pressure and duration conditions

Since carbonation curing is a hardening process taking place in a gas environment, it is highly dependent on the diffusivity of the working gas. Thus the temperature has a significant impact on the attempt to reach a higher carbonation degree and to achieve increased mechanical properties of the system. A higher temperature increases $CO_2$ diffusivity and promotes ion leaching and chemical reaction, however, it can reduce the $CO_2$ solubility in water thus decreasing the rate of carbonation. Due to these reasons, it is important to find the right balance between these limitations.

The obtained compressive strength results (Fig. 3.27) showed that the temperature increase had a positive influence on the rankinite binder mortar strength: when increasing the temperature from 25 to 45 °C, the compressive strength of the samples increased by 25% and remained almost stable when further increasing the temperature up to 55 °C (Fig. 3.27). However, the OPC samples reacted to the temperature increase rather differently: even though higher strength values were reached, with each increase of the temperature, the results were fluctuating and did not exhibit a linear dependence, unlike the rankinite samples. As already stated above, early-age carbonation is a highly exothermic reaction with temperature increases of up to ~60 °C for concrete (100), thus the obtained cement result inconsistency may indicate that the ambient temperature of less than 60 °C may not exert a direct impact on the carbonation efficiency since the results fluctuated in a relatively low range of ±5 MPa, which is around 13.5% of the average strength value. Nevertheless, both binders showed the best performance when carbonated at 45 °C, therefore, this temperature value was chosen as the most efficient one for further experiments.

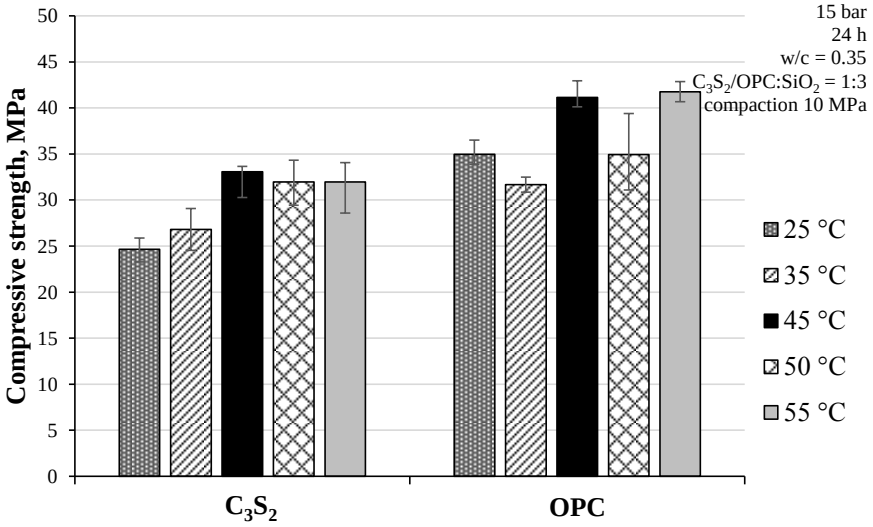


**Fig. 3.27** Compressive strength of rankinite binder and cement mortar samples carbonated at different temperature conditions

Diffusion efficiency of $CO_2$ gas is also highly reliant on the structure, i.e., the porosity of the material. Therefore, compaction of the material prior to its carbonation also influences the final product. The porosity and permeability of the structure decreases with the increasing compaction, which might lead to greater strength development, however, when the compaction is high, the reaction surface is lower, and the water layer in pores is thicker. Since the diffusion of $CO_2$ in water is slower than that in air, the early-age carbonation would be impeded (173). However, water evaporation would become difficult, and this would provide moisture for carbonation at a later stage – thus it would improve the total efficiency. On the other hand, the lower porosity hinders the diffusion of $CO_2$ in the bulk material, which results in a lower carbonation rate and degree. In addition, lower compaction provides a higher reaction surface since the structure is then looser; however, water in such looser systems may evaporate faster during the carbonation process. Accordingly, to reach the highest possible compressive strength, the samples must be compacted at an optimum pressure while ensuring sufficient porosity for easy gas penetration and access to moisture.

In this part of the work, the mortars were compacted by using different levels of pressure ranging from 5 to 17.5 MPa. The obtained compressive strength results are provided in Figure 3.28. As it can be seen in Fig. 3.28, the compressive strength of the rankinite binder mortars increased with the increasing compaction and reached their highest value at 12.5 MPa; the strength was reduced when further increasing the compaction pressure up to 17.5 MPa. At a low compaction pressure of 5 MPa, the microstructure of the sample is evidently too loose, and calcium carbonate does not seem to be able to occupy the entire pore volume, which leads to the low final porosity of the sample and directly relates to the lower compressive strength. In contrast, compaction at pressures higher than 12.5 MPa seems to result in an excess sample

density and low pore connectivity that most likely hindered the $CO_2$ penetration to the sample core. Moreover, at a higher compaction, the pore volume is lower, and pores are more likely to be fully saturated with water. If the pore connectivity is poor, water has no path to move, and since it does not directly participate in the carbonation reaction, the formation of carbonates due to the low free space is also limited. Accordingly, compaction at 12.5 MPa seems to provide sufficient porosity and pore connectivity for the carbonation reaction to successfully proceed. A similar observation can be made for the OPC mortars as well. Although cement samples were only compacted at a higher pressure, it can be seen that, with increasing the compaction from 10 to 17.5 MPa, the compressive strength decreases, with the exception for 15 MPa, at which, the samples reached the highest strength.

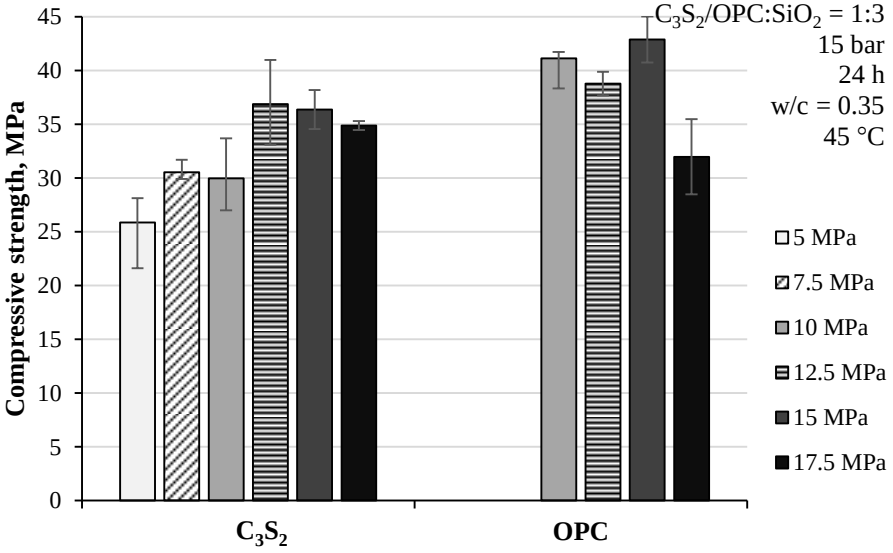


**Fig. 3.28** Compressive strength of the carbonated rankinite binder and cement mortar samples with different compaction

Other than compaction, the composition of the initial mixture plays a vital role in an attempt to obtain the required mechanical properties. In this part of the experiment, the sample composition, i.e., the impact of the binder and water content, on the compressive strength development was investigated. Initially, the w/c ratio was kept constant at 0.35, but the binder-to-sand ratio was changed from 15/85 to 30/70 wt%. Figure 3.29 shows the effect of the ratio modification on the average compressive strength of the rankinite binder samples. As it can be seen in Figure 3.29, increasing the binder content in the initial mixture composition from 15 to 25 wt% had a major effect on the compressive strength development since the strength increased by almost two times; however, a further increase of the binder content up to 30 wt% led to an almost equal decrease in the compressive strength value. Since the w/c ratio was kept constant, the amount of water was directly dependent on the binder content. Due to this, at a low binder content, scarcity of water was achieved. This resulted in an insufficient amount of moisture for the carbonation reaction to proceed. A higher

sand content may have offered higher porosity, thus further making it more difficult to maintain the water and not allowing it to evaporate in the early stage. Also, a lower amount of the binder leads to lower possible formation of carbonates, and thus evidently to a lower mechanical strength. Contrarily, with a higher binder content, the amount of water increased as well, which resulted in the reduced workability of the samples. The excess water not only caused poor workability that may have introduced more considerably larger pores, it also led to improper compaction and thus to lower compressive strength. Therefore, it is evident that the binder-to-sand ratio of 25/75% (1:3) is the most favorable, and it further supports the previously attempted experiments that were carried out with the same binder-to-sand ratio.

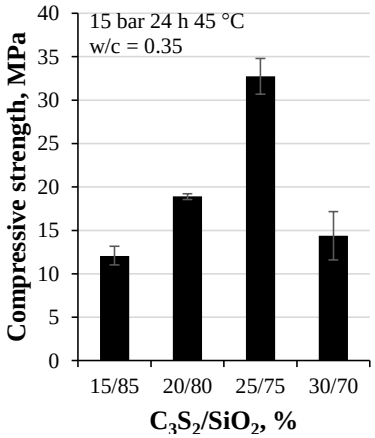


**Fig. 3.29** Compressive strength of the carbonated rankinite binder mortars with different composition

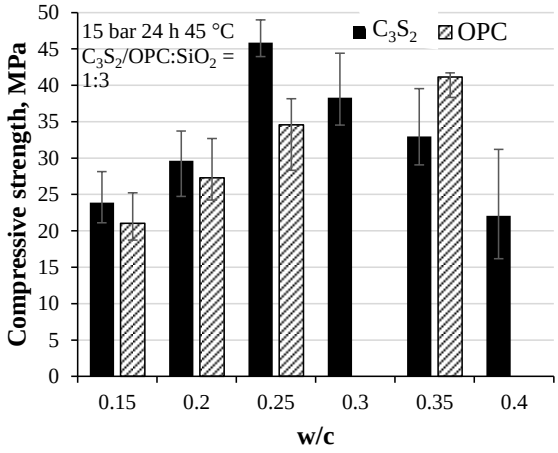


**Fig. 3.30** Compressive strength of the carbonated rankinite binder and cement mortars with different w/c ratios

Changing the water-to-binder ratio had a similar impact on the strength of the samples (Fig. 3.30). When increasing the w/c ratio from 0.15 to 0.25, the compressive strength of the rankinite binder mortars increased as well and reached the highest value of more than 45 MPa that for the first time was higher than the cement sample strength at the same conditions. However, a further increase of the w/c ratio up to 0.4 led to a decrease in the compressive strength value similar to that of w/c = 0.15. The cement samples, on the other hand, showed a continuous increase in the compressive strength value with the increasing water content and may have failed to reach the peak value. This may be due to the fact that cement is a hydraulic material that initially forms calcium hydroxide and C-S-H whose reactivity with $CO_2$ might be higher than that of the initial calcium silicates. In addition, the capillary (open) porosity of cement depends on the water-to-cement ratio which also determines the transition zone porosity in the concrete structure (174). Concrete with a high initial moisture level shows a much lower rate of carbonation due to diffusion of the $CO_2$; carbonation becomes difficult when pores are saturated with water. The carbonation rate also decreases at a lower initial water level since the water content necessary to form carbonic acid becomes insufficient (175). Therefore, pore saturation plays a crucial

role in the mechanism of carbonation. Considering the above discussed results, the water-to-binder ratio of 0.25 can be regarded as the optimum value for the rankinite binder system.

### 3.5.2. Durability of carbonated rankinite binder mortars

According to the obtained compressive strength results, it can be seen that it is possible to achieve considerably high results when working with a broad matrix of parameters. Combining the examined parameters, the rankinite binder system was able to achieve a compressive strength exceeding 45 MPa. This result was attained by carbonating the mortars at 15 bar $CO_2$ pressure for 24 h at 45 °C, with w/c = 0.25, binder/sand 1:3, and sample compaction of 12.5 MPa.

Even though the determined mechanical properties of the carbonated rankinite binder samples showed very favorable and promising results, the long-term durability performance of such a system plays no less important part in pursuing the improved alternative binder. Thus the carbonated samples featuring the best achieved mechanical properties were exposed to water absorption by immersion, freeze-thaw, and abrasion resistance determination in order to ascertain their durability.

The samples used for the aforementioned determinations were prepared as follows: tiles with dimensions of 100×100×20 mm, binder-to-sand ratio 1:3, w/c = 0.35 (for OPC) and w/c = 0.25 (for $C_3S_2$) were pressed (compaction of 12.5 N/mm$^2$) and cured at 15 bar for 24 h at 45 °C. Such sample dimensions were chosen in order to achieve a surface area between 7500–25000 mm$^2$ (according to Standard EN 1338:2003+AC:2006). After the carbonation curing, the samples were dried to a constant mass, weighed and afterwards immersed in tap water for 5, 30, 60, 1440, 2880 min, and up to 4 days, until the change in mass during a 24 h period was less than 0.1%. The obtained mass of the water-saturated sample was noted as $m_s$. After absorption, the saturated samples were dried at 105±5 °C until constant weight, the mass of the dried samples was noted as $m_d$. The water absorption by immersion $W$ is expressed as the water uptake relative to dry mass and was calculated according to the following Equation 3.12:

$$W = \frac{m_s - m_d}{m_d} \tag{3.12}$$

The calculated water absorption is provided in Figure 3.31 where each point of the results represents the mean value obtained from three different specimens. As it can be seen in Figure 3.31, both binder samples reached ~70% of the total absorbed water within the first 5 minutes of immersion. This shows that the sample can be characterized by high pore connectivity. After approximately 3 days of the continuing immersion, a plateau was reached, the samples were fully saturated with water, and the absorption no longer continued (Fig. 3.31). According to the obtained absorbance results, the total and open capillary porosity of the samples was calculated. The total porosity was calculated according to Equation 3.13:

$$P_t = \frac{\rho_m - \rho_0}{\rho_m} \tag{3.13}$$

where: $\rho_0$ – density of the cement mortar in the dry state, calculated from the mass and dimensions;

$\rho_m$ – density of the mortar crushed into powder, determined by the pycnometer method.

The open capillary porosity was calculated according to Equation 3.14:

$$P_0 = \frac{W \cdot \rho_0}{\rho_w} \quad (3.14)$$

where: $W$ – water absorption of cement mortar by mass;

$\rho_0$ – density of the cement mortar in the dry state, calculated from mass and dimensions;

$\rho_w$ – density of water.

The calculated total porosity of the rankinite binder samples was equal to $P_t$ = 17.27%, while the open capillary porosity was $P_0$ = 8.82%; for cement samples, we achieved $P_t$ = 17.81%, $P_0$ = 13.21%. Even though the initial porosity of both of the binder samples was rather similar, the calculated open porosity results are significantly dissimilar. According to the obtained results, it is evident that the rankinite sample pores were filled with a higher amount of carbonation reaction products than cement, which led to a lower capillary porosity. A reduction in porosity and the pore size distribution is due to the precipitation of the carbonation reaction products, such as calcium carbonates and silica gels, which have a bigger molar volume than the initial binder components (176). This increased volume of calcite fills the empty space in the capillary system thus densifying the system. This further confirms the obtained compressive strength results where rankinite binder samples reached a higher final compressive strength than cement.

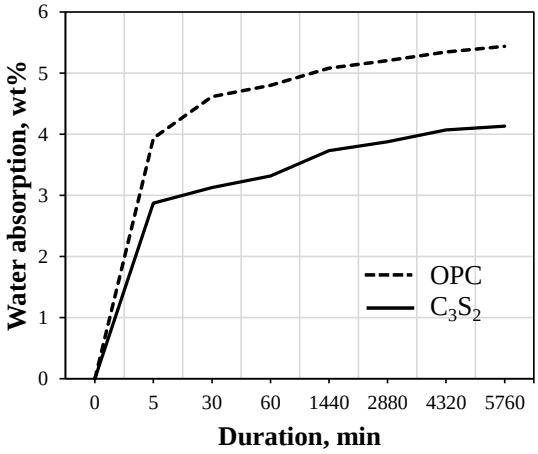


**Fig. 3.31** Carbonated rankinite binder and cement sample water absorption by immersion

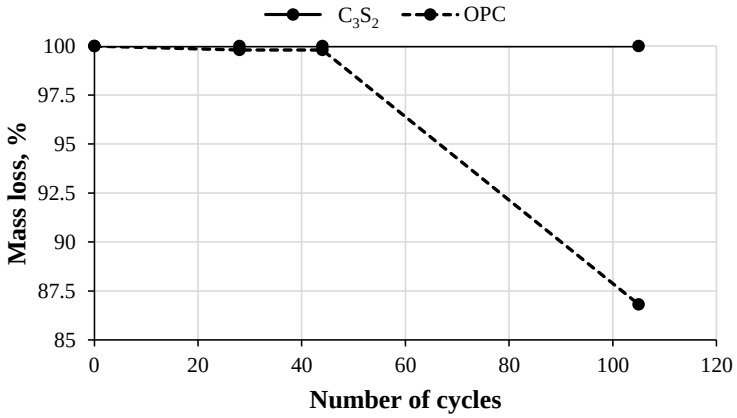


**Fig. 3.32** Freeze-thaw mass loss of the carbonated rankinite binder and cement samples

After determining the sample capability of water absorption, the same samples were used for the determination of the durability by freeze-thaw resistance while using de-icing salt. This method efficiently describes and imitates the natural conditions as concrete is usually exposed to high levels of moisture and temperature changes. Volume expansion in freezing water produces pressure in the pores of the concrete thus leading to cavity dilation and rupture which eventually causes expansion and cracking, scaling and crumbling of concrete. A commonly used de-icing chemical, including NaCl, reduces the freezing point of the precipitation thus reducing the freezing and thawing cycles and concrete durability. The addition of de-icing salt to water changes the behavior of the solution during freezing thus causing a more gradual formation of ice. NaCl is the most common de-icing salt used on roadways due to its comparably low cost. Generally, de-icing salts can alter the degree of saturation or react with the hydrated OPC, thus resulting in the expansive reaction products, which leads to the development of negative effects on the concrete structure (177). Therefore, the cement resistance to freeze-thaw cycles is of high importance, especially when considering the lower temperature climate zones.

For durability determination, the samples were prepared by insulating all but one wall, which was then poured over with 3% NaCl solution and exposed to freeze-thaw cycles when collecting the scaled material and calculating the average cumulative scaled mass.

The obtained results are provided in Figure 3.32 where it can be seen that the rankinite binder samples showed a significantly better performance compared to the cement samples. Even after more than 100 freeze-thaw cycles, the mass of the scaled rankinite binder samples was less than 1 g/m$^2$, while, for the OPC samples, it was significantly higher.

Another method to determine concrete durability is abrasion resistance. The wide wheel test method was applied to carbonated rankinite binder mortars, and it was determined that, after 70 abrasion cycles, using an abrasive material (corundum), the obtained groove was less than 20 mm wide.

All of the obtained durability results are in compliance with the requirements for concrete paving tiles according to Standard (EN 1338:2003+AC:2006) since water absorption was < 6%, freeze-thaw resistance when using de-icing salt was < 1 kg/m$^2$, and the abrasion resistance was < 20 mm.

### 3.5.3. Mineral composition of carbonated rankinite binder samples

XRD patterns of the rankinite binder paste and mortar samples carbonated at several condition scenarios are presented in Figure 3.33. Figure 3.33, *a*, shows carbonated rankinite binder paste sample mineral composition alteration with regard to the $CO_2$ pressure at the lowest exposure duration (4 h). It is evident that short-term carbonation is not efficient enough since all the diffraction patterns are similar regardless of the curing pressure – thus rankinite peaks slightly diminish, and the formation of calcite, as well as aragonite and vaterite, is observed. Extension of the duration, on the other hand, had a much higher impact on the paste sample carbonation (Figure 3.33, *b*). Although there is no significant difference between the samples carbonated for 4 and 16 h, there is a major contrast in comparison to the 24 h curing. The main calcite peak of *d*-spacing at around 0.3035 nm is visible in all the samples carbonated at higher conditions, i.e., at 24 h and ≥ 25 °C (Figure 3.33, *b 24 h, c*). However, calcite was not the only polymorph of the crystalline calcium carbonate detected in the carbonated paste samples – the appearance of metastable $CaCO_3$ polymorph – vaterite and aragonite – formation was detected as well. Since the carbonation reaction is exothermic, the heat of the reaction promotes the formation of these metastable polymorphs (55). Vaterite is a hexagonal crystal with a denser crystal structure whose pore filling is better than that of the other $CaCO_3$ polymorphs due to its larger volume, therefore, it should contribute to a denser structure and thus to the compressive strength development. However, vaterite is the least stable form of $CaCO_3$ and is denoted by a higher solubility in water than calcite and aragonite (178). Therefore, once exposed to water, vaterite should convert to calcite (at lower temperatures), or to aragonite at > 60 °C (179). This is evident in Figure 3.33, *c*, where the vaterite peak intensity increases with the increasing temperature up to 45 °C, however, when the temperature is increased further up to 55 °C, the peak typical to vaterite seems to diminish thus indicating that metastable polymorphs recrystallize into a more stable form of calcium carbonate. Aragonite, on the other hand, is stable at a higher pressure and is harder and less brittle than the other polymorphs. However, a higher temperature may cause aragonite transformation to calcite as well, which may lead to an increase in the free volume thus giving rise to micro crack formation that could reduce the compressive strength. Even though vaterite and aragonite have higher molar volumes than calcite, their influence on the compressive strength development is still somewhat debatable. In spite of this, a rather high residual amount of rankinite and pseudowollastonite in the paste samples indicates that, similarly as before, the pastes were not fully carbonated even after curing at the highest conditions. This indicates that the amount of moisture may have been insufficient, or that the compacted sample density was too high for $CO_2$ to penetrate it even though the dimensions of the sample were minimal. Additionally, as the coating of calcite around

the rankinite particles becomes denser, it prevents further diffusion of $CO_2$ gas to the unreacted particles thus limiting further carbonation.

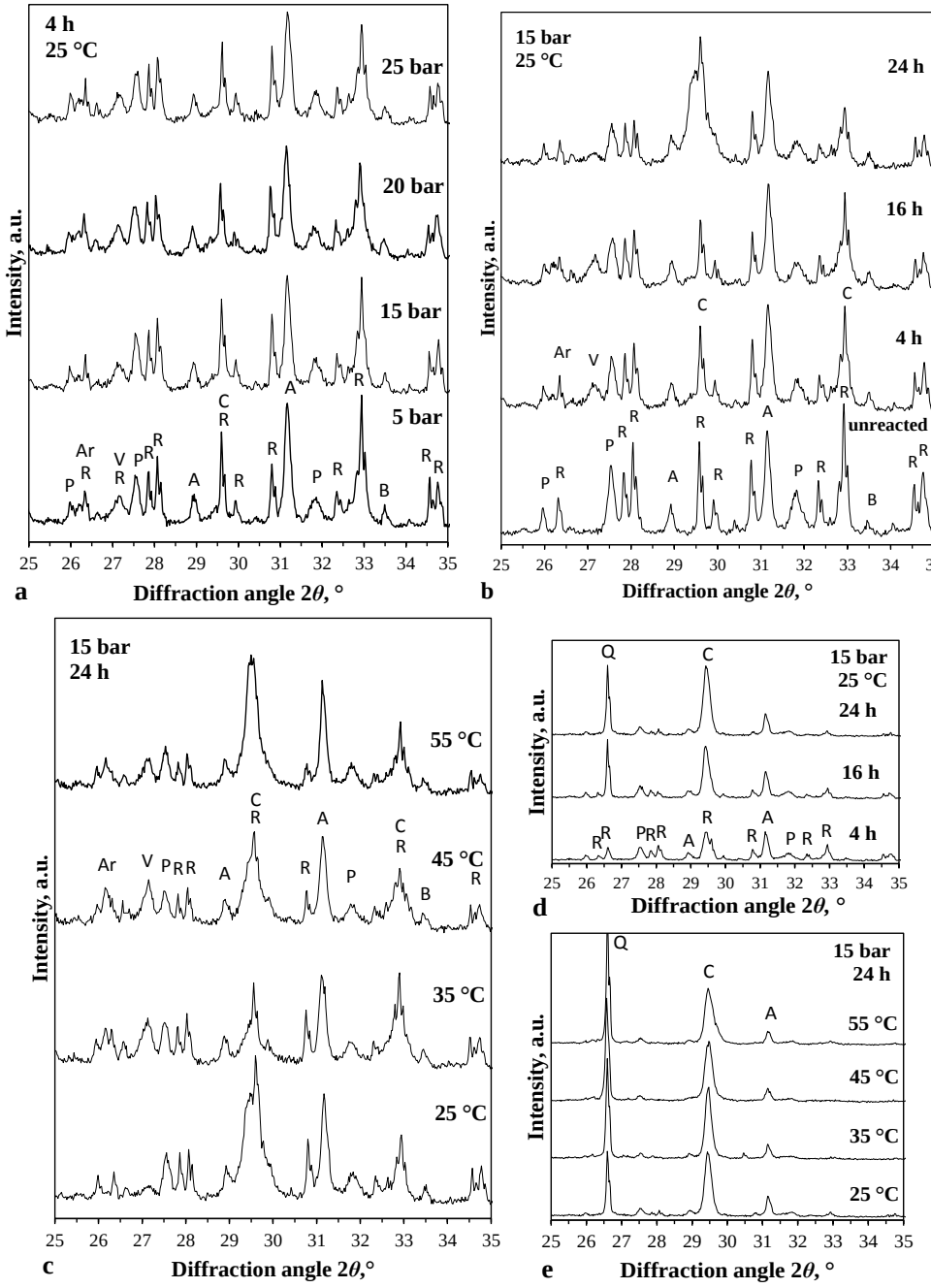


**Fig. 3.33** XRD patterns of carbonated rankinite binder paste (a–c) and mortar (d–e) samples. Indexes: R – rankinite, P – pseudowollastonite, A – akermanite, B – bredigite, C – calcite, V – vaterite, Ar – aragonite, Q – quartz

Apart from this, considering the mortar carbonation, entirely different XRD patterns were obtained. As it can be seen in Figure 3.33, *d* and *e*, the calcium carbonate peaks are much more intense, and the only detected polymorph of the crystalline $CaCO_3$ is calcite, whereas no presence of vaterite or aragonite was detected, contrary to the pastes. Because of this, an assumption that the presence of the aggregates, i.e., quartz, has a major impact on the formation of $CaCO_3$ can be made. Since both of these mineral structures fall under the same trigonal crystal shape category (180), it may be presumed that quartz affects calcium carbonate formation by exclusively supporting the formation of calcite rather than vaterite or aragonite. Additionally, the carbonation degree of the mortars, similarly as before, seems to be higher since only minimal peaks attributed to rankinite can be observed, which indicates that mortars most likely were fully carbonated as opposed to pastes. As the reasons for this have already been discussed in previous Section 3.4.2, no further interpretations will be made. However, it is evident that the exposure duration, which was the same as for the pastes, has a significant impact on the mortar carbonation as well. Fig. 3.33, *d* shows that mortars carbonated for the shortest period (4 h) did not reach full carbonation since the peaks attributed to rankinite and pseudowollastonite are still visible, which indicates that they did not react with $CO_2$. When increasing the duration up to 24 h, the samples seem to be fully carbonated since only a negligible amount of rankinite and pseudowollastonite can be detected in the XRD patterns. A temperature increase does not seem to have a considerable impact of the mortar mineral composition since calcite peak intensities in the obtained XRD patterns are fairly similar (Fig. 3.33, *e*).

The thermal analysis results of the samples carbonated at several conditions are provided in Figure 3.34. A clear endothermic effect in the DCS curves centred around 750 °C (Fig. 3.34 *a, c, e, g, i*) is due to decarbonation and is in good agreement with the TG mass loss data where well-distinguished decomposition is evident. Considering the shortest exposure (Fig. 3.34 *a, b*), it can be observed that, regardless of the $CO_2$ pressure, all the samples reached a similar carbonation degree since the mass loss in all the samples was very similar. Prior to further discussion, it should be noted that an exothermic effect in the DSC curves at around 870 °C is most likely due to the formation of wollastonite from CaO released after the decarbonation reaction and $SiO_2$ from the decomposition of rankinite (181), since, at this point, there is no evident mass loss; however, this effect is only visible in the paste samples rather than mortars due to the low carbonation degree. The endothermic effect of the samples carbonated at low conditions is at a lower temperature at around 735 °C thus confirming that lower crystallinity or even amorphous calcium carbonate is formed. Moreover, the small-scale effect visible at around 650 °C is probably due to the decomposition of poorly crystalline forms of calcium carbonate, i.e., vaterite and aragonite (140), which is in good agreement with the XRD results where these polymorphs were indicated. Thiery *et al*. (182) suggest that metastable and amorphous forms of $CaCO_3$ in the carbonated area seems to be a feature of accelerated carbonation. As previously stated, prolonging the $CO_2$ treatment led to higher amounts of $CaCO_3$ to be formed (Fig. 3.34 *c, d*). When increasing the carbonation duration from 4 to 24 h, the total amount of carbonates increased by 5%. Moreover, with prolonged carbonation, decarbonation is shifted to a higher temperature range, thus likely indicating that carbonates of a higher degree of

crystallinity are formed. A similar effect was observed regarding the increase of the temperature – while increasing the process temperature from 25 to 55 °C, the total carbonate amount increased by ~10%.

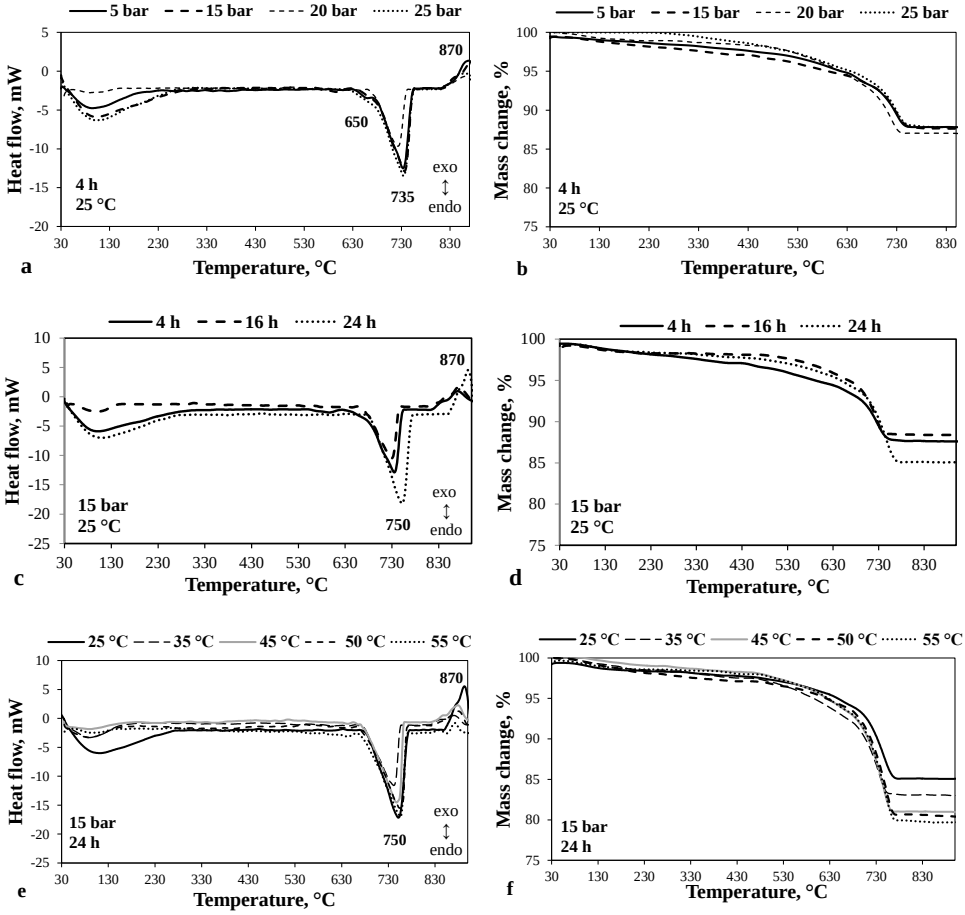


**Fig. 3.34** DSC and TG curves of rankinite binder pastes carbonated at different pressures (a–b), durations (c–d), and temperatures (e–f)

Considering the results obtained from the mortar samples (Fig. 3.35), it is evident that the exposure duration here also had a major impact on the carbonate formation since prolongation of the exposure from 4 to 24 h led to the overall carbonate amount increase by more than 10%. The temperature, on the other hand, did not seem to have a significant impact on the total amount of formed $CaCO_3$ since the mass loss data yielded very similar results. However, when comparing the TG data with the compressive strength development (Fig. 3.27), it is evident that even though the total amount of $CaCO_3$ remained similar in all the samples, the degree of $CaCO_3$ crystallinity in the samples carbonated at higher temperature was most likely higher thus increasing the compressive strength.

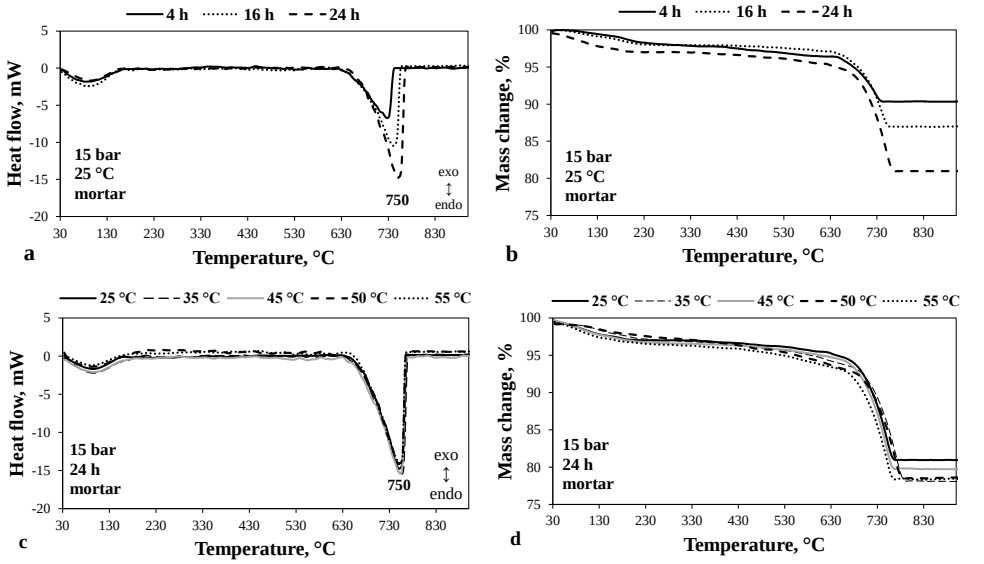


**Fig. 3.35** DSC and TG curves of carbonated rankinite binder mortars

The degree of the carbonation of the paste samples was calculated by Equation (3.10) considering the same maximum binder $CO_2$ storing capacity calculated by Equation (3.11). The obtained results are provided in Table 3.7.

**Table 3.7** Degree of carbonation of the rankinite binder paste samples, %

| Temperature, °C → | | 25 | | | 35 | 45 | 50 | 55 |
|---|---|---|---|---|---|---|---|---|
| $CO_2$ pressure, bar ↓ | Duration, h → | 4 | 16 | 24 | | | | |
| 5 | | 14.95 | 15.19 | 17.48 | - | | | |
| 15 | | 17.80 | 17.40 | 24.28 | 24.73 | 33.44 | 35.19 | 42.76 |
| 20 | | 16.44 | 24.56 | 26.67 | - | | | |
| 25 | | 19.89 | 18.86 | 21.14 | | | | |

As it can be seen in Table 3.7, the carbonation degree increased with the increasing carbonation parameter values, however, even at the highest conditions (15 bar 24 h, 55 °C), the maximum obtained carbonation degree only slightly exceeded 40%. This degree of carbonation is similar to, however, slightly lower than, that obtained in the first part of the carbonation experiments (Table 3.5), which shows that, similarly as before, the paste samples were not fully carbonated despite the compaction. In this case, such a low carbonation degree may be an indication of an overly dense structure that prevented the $CO_2$ penetration into the interior of the sample. However, since both compacted and loose powder paste samples reached a similarly low degree of carbonation, it can be concluded that the primary limitation was, most probably, the scarcity of water. From a sample of minimal dimensions, water could have as easily evaporated as from the loose powder. Unfortunately, this makes it highly challenging to measure the actual carbonation degree development and process evolution, especially considering the mortar samples.

The utilized FTIR spectra of carbonated rankinite binder paste samples are shown in Figure 3.36. Due to the carbonation reaction, bands at around 715, 875, and 1480 $cm^{-1}$ were indicated. These bands are attributed to calcium carbonate phases that are due to the planar $CO_3^{-2}$ ion and are already discussed in the previous section. Even though in this part of the experiments not only calcite but also vaterite and aragonite were determined as well, the bands corresponding to different $CaCO_3$ polymorphs appear at similar wavenumbers and tend to overlap thus making it difficult to distinguish them apart. Moreover, the wavenumber at around 1100 $cm^{-1}$ corresponding to the silica gel phase is also attributed to vaterite and aragonite as well, complicating the analysis (183). The bands at around 1100 and 480 $cm^{-1}$ are associated with the silica gel phase. The band at 1100 $cm^{-1}$ corresponds to the Si-O vibrations and increases with the increasing polymerization of the silica gel, while the band at around 480 $cm^{-1}$ corresponds to the O-Si-O bond bending vibrations and is affected by the bond angle and occupancy of the neighboring sites or silica gel polymerization (122). Hidalgo *et al.* (122) suggests that these bands are likely to change in frequency and intensity according to the silica gel polymerization. It can be seen in Figure 3.36 that the band at 480 $cm^{-1}$ only appears at a higher temperature (> 25 °C) and reaches its maxima at 45–50 °C thus suggesting that at these conditions the silica gel reaches its highest polymerization, since, with a further increase of the temperature, this peak decreased. This may indicate that the degree of silica gel polymerization is also related to the compressive strength development, since, considering the result obtained in Fig. 3.27, it is evident that the best strength results were reached at these conditions.

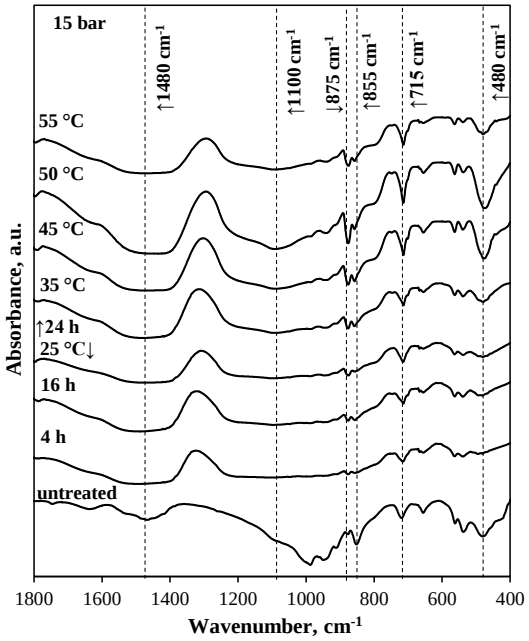


**Fig. 3.36** FTIR spectra of carbonated rankinite binder paste samples

## 3.6. Investigation of carbonated rankinite binder paste phase evolution and strength development

The main objective of this part of the carbonation curing experiments was to determine the rankinite binder carbonation kinetics and mineral composition alterations based on the process duration and temperature as the main parameters affecting the hardening process. This part of the research was dedicated to investigating rankinite binder paste carbonation and diffusion processes as well as the phase evolution during the ongoing reactions. Since it was previously determined that aggregates have a significant effect on the carbonation reaction products, therefore, in this part of the experiment, sand was eliminated, and the samples were prepared solely from the moistened rankinite binder. Since, in the previous experiments, the highest compressive strength of the rankinite binder samples was reached with the w/c = 0.25 (w/s = 0.0625) (Fig. 3.30), this ratio was considered for further investigations as well. However, it was also determined that the same w/s ratio for the mortars and pastes is insufficient on account of pastes reaching a much lower carbonation degree than the mortars. Based on the assumption that the reason for this is most likely the scarcity of water, in further experiments, the w/s ratio was doubled due to assuming that this approach would lead to a higher carbonation degree. Also, in this part of the experiment, the sample dimensions remained the same as for the mortars (36×36 mm), and, considering the absence of the aggregates, a higher water content should lead to a higher compaction and thus to pore saturation thus promoting the process development. Hence, the paste samples were prepared in a similar procedure as before, only this time we set w/c = w/s = 0.125. The samples were compacted by the previously determined compaction pressure of 12.5 MPa and immediately cured for 2 to 48 h, at 25 to 55 °C while using the $CO_2$ pressure of 15 bar. The obtained compressive strength of the sample was determined immediately after the carbonation hardening, simultaneously, a few samples of each batch were left for further investigation by XRD, LA-ICP-MS, NMR, SEM/EDX, and chemical analysis.

### 3.6.1. Compressive strength development of carbonated rankinite binder samples

Compressive strength development of the rankinite binder paste samples carbonated at different conditions is provided in Figure 3.37. As it can be seen in Fig. 3.37, carbonation at a low duration (2–8 h) led to the development of lower compressive strength, and the samples reached a strength value of around 50 MPa; however, it was visually evident that the samples were not fully carbonated since fragments of the crushed samples showed a brittle uncarbonated core. Upon increasing the duration up to 16 h, the sample compressive strength increased by 26%, yet, unfortunately, the samples were still not fully carbonated yet. A much more significant impact upon the strength development was made by carbonation extension up to 24 h. After 24 h of curing, the sample acquired a compressive strength exceeding 100 MPa; thus the samples were evidently fully carbonated, and the structure of the sample fragments seemed to be uniform. Even though the highest strength value was reached by the samples carbonated for 36 h, with a further extension of the duration to 48 h, the sample strength still decreased to a similar value to that obtained after 24 h.

However, an extended duration from 24 to 48 h did not seem to have a significant impact on the further compressive strength development. Thus it can be concluded that 24 h is the optimum duration for rankinite binder samples to reach full carbonation and a considerably high compressive strength.

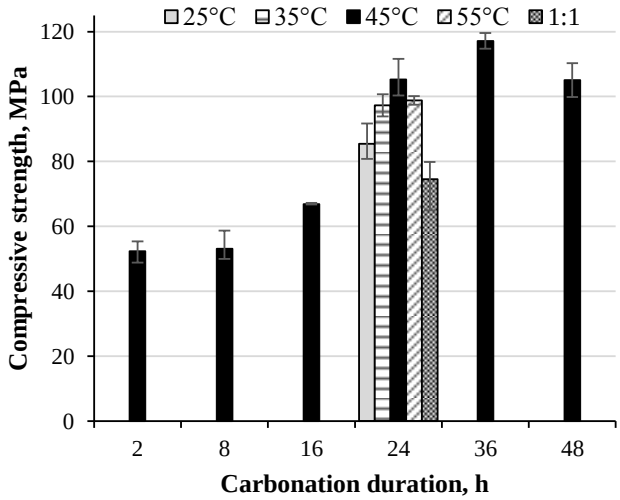


**Fig. 3.37** Compressive strength development of rankinite binder paste samples carbonated at 15 bar at different durations and temperatures; w/c = 0.125

In order to investigate the effect of the temperature, the samples carbonated for 24 h were cured at 25–55 °C. Similarly as before with the mortars, the highest compressive strength value was obtained by the samples cured at 45 °C (Fig. 3.37). Increasing the process temperature from 25 to 45 °C led to a 23% increase in the strength value, while a further increase of the temperature up to 55 °C led to a 6% decrease in the obtained strength value. This further confirms the previous assumption that 45 °C is the optimum temperature for rankinite binder carbonation in order to achieve the optimal outcome.

For a comparison, additional mortar samples were prepared with a higher binder-to-sand ratio of 1:1. These samples were cured at 15 bar for 24 h at 45 °C (Figure 3.37, *1:1*). In comparison to the paste samples carbonated at the same conditions, the mortars demonstrated results of a significantly lower strength. The peak mortar sample (binder/sand 1:3) compressive strength visible in Figure 3.30 only reached ~45 MPa, which, in comparison with the mortar sample (binder/sand 1:1) treated for the same time, showed a strength that was 40% lower, while, in comparison with the paste sample (binder/sand 1:0), the strength value is more than two times lower. This extreme compressive strength improvement is naturally associated with the sample microstructure. It is evident that, without the aggregates, the structure of the sample is much denser, and, even in spite of this, the samples were able to reach full carbonation. Due to the absence of sand, the sample was solely composed of the binder particles that, later on, recrystallized to calcium carbonate and silica gel thus making the structure much more enhanced. The mortars with a lower ratio of the aggregates, on the other hand, also reached a considerably higher compressive strength, which was

also due to a higher amount of the binder leading to a higher density microstructure. However, the obtained mechanical strength of the mortar was still far lower than that of the paste. This can be explained by the properties of the interfacial transition zone (ITZ) between the binder and the aggregate particles that, in the case of the conventional OPC system, is considered to be the weakest link that significantly affects the properties of the concrete (184). However, when comparing the OPC and carbonated CSC mortar, similar to that of our research, Ashraf *et al*. (107) states that CCSC mortar system ITZ should be stronger than that of OPC due to the absence of the deposits around the aggregate particles that can dissolve in water, which results in the formation of a weak zone in the microstructure of the material. Moreover, the ITZ can be affected by the adhesion of the binder to the aggregate particle as well. The paste sample microstructure should be much better bonded since the system is composed entirely of one material, while, in the mortars, the presence of the aggregates that do not react either with the binder or with $CO_2$ results in weaker bonding and thus in the weakened microstructure.

The compressive strength results were supplemented by the determination of the sample porosity and pore size distribution. It should be noted that the sample parts for the determination of porosity were taken from the outer part of the sample (around 10 mm from the edge) and as close to the same spot of the samples as possible in order to achieve comparable results. The obtained results are provided in Figure 3.38, where it can be seen that the highest total porosity was determined in the samples carbonated for 16 h (Fig. 3.38). As these samples were not fully carbonated and as they achieved considerably lower mechanical data values, the porosity results only further confirm the obtained results. The pore size distribution in these samples was also much different, with a two times higher amount of larger pores. However, it is not entirely clear why the samples carbonated for an extended duration – 36 and 48 h – had a higher porosity even though they also exhibited a higher compressive strength. The pore size distribution of the samples carbonated at prolonged durations also showed similar results, although the samples carbonated for 24 h had relatively smaller pore volumes (Fig. 3.38).

Furthermore, if comparing these results with the ones obtained in the previous section (Fig. 3.16), it can be seen that the carbonated paste samples had much smaller pores (< 10 μm) than the mortars (> 10–< 100 μm); this phenomenon is evidently observed due the absence of the aggregates.

The obtained results confirm that the chosen water-to-solid ratio was also successful by enabling easy $CO_2$ penetration into the sample core and leading to full carbonation. This opens up great opportunities for wide implementation of the rankinite binder since it is possible to control the process development while working with different initial mixture properties. This enables to reach considerably high mechanical properties.

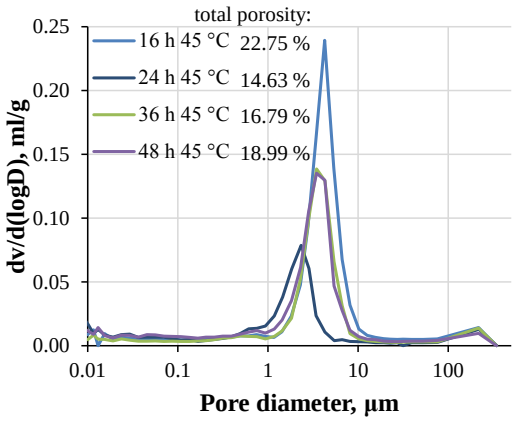


**Fig. 3.38** Porosity and pore size distribution of carbonated rankinite binder paste and mortar samples, dependence on duration

### 3.6.2. Mineral composition of carbonated rankinite binder samples

The mineral composition of the carbonated rankinite binder paste samples was further investigated by the XRD, LA-ICP-MS, NMR, SEM, and chemical analysis.

The XRD analysis was performed on the cross section of the sample while moving from the surface to the centre of the sample where 9 positions were analyzed from 0.5 to 16.5 mm (Fig. 3.39). The obtained mineral composition results from the sample carbonated for 8 h with different cross section positions are provided in Figure 3.39.

After preparing the cross section of the samples carbonated for the shortest durations (up to 16 h), by using a precision saw, the cross section appeared to consist of a brighter inner core with a diameter of ~10–15 mm surrounded with a transition zone of ~2 mm and a darker outer layer. The carbonation products were primarily found within the darker outer layer, however, they did not seem to be evenly distributed within the layer. Rankinite was found in every measurement position and had higher concentrations in the inner core of the sample as that is evidently the uncarbonated part of the sample. Pseudowollastonite seems to be distributed similarly to rankinite, while akermanite was found to be equally distributed within the entire cross section of the sample. This shows that pseudowollastonite is similarly reactive to $CO_2$ as rankinite, while the even distribution of the akermanite phase shows that this mineral is non-reactive during the carbonation process, which was also previously suggested by Ashraf *et al*. (107). Considering the carbonation reaction products, two polymorphs of crystalline calcium carbonate – calcite and aragonite – were detected (Fig. 3.40). Calcite showed a significant contrast in the concentration: it had high concentrations in the darker outer layer, with the highest concentrations being detected at 6.5 and 8.5 mm positions, while, within the brighter inner core, its concentration dropped down to a low level. Aragonite, on the other hand, appeared in the darker outer layer, but not within the inner core of the sample, with a noticeable maximum at the 4.5 mm position. Similar observations of the mineral composition distribution were made in all the sample cross sections.

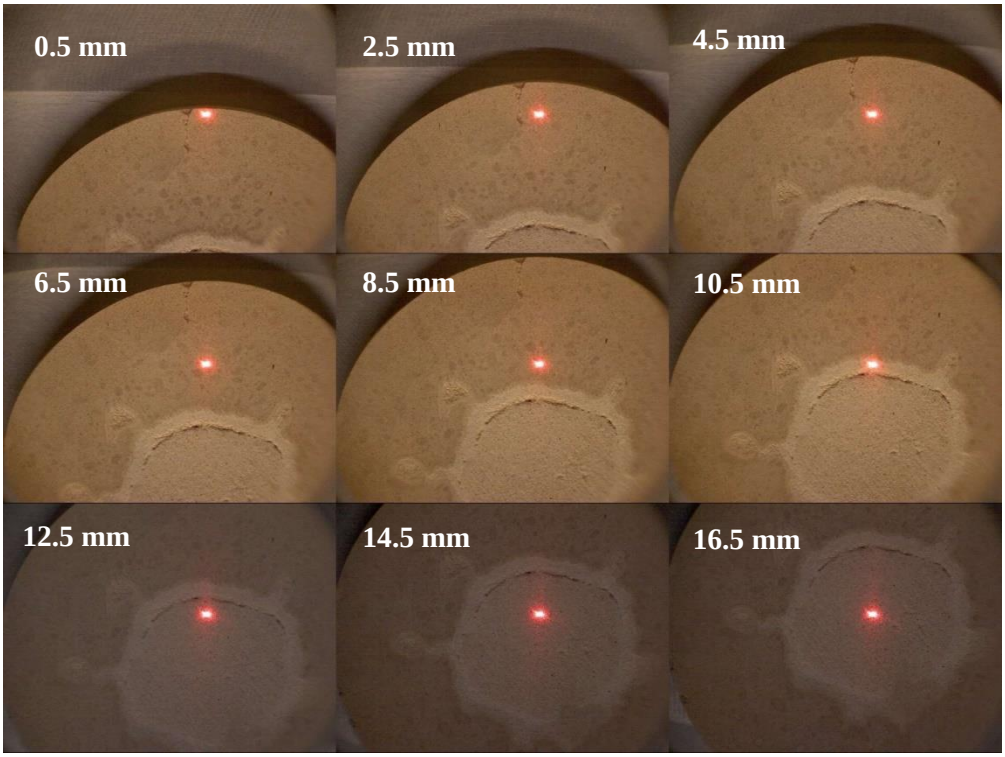


**Fig. 3.39** Measurement positions for XRD analysis within the cross section of the rankinite binder sample carbonated for 8 h

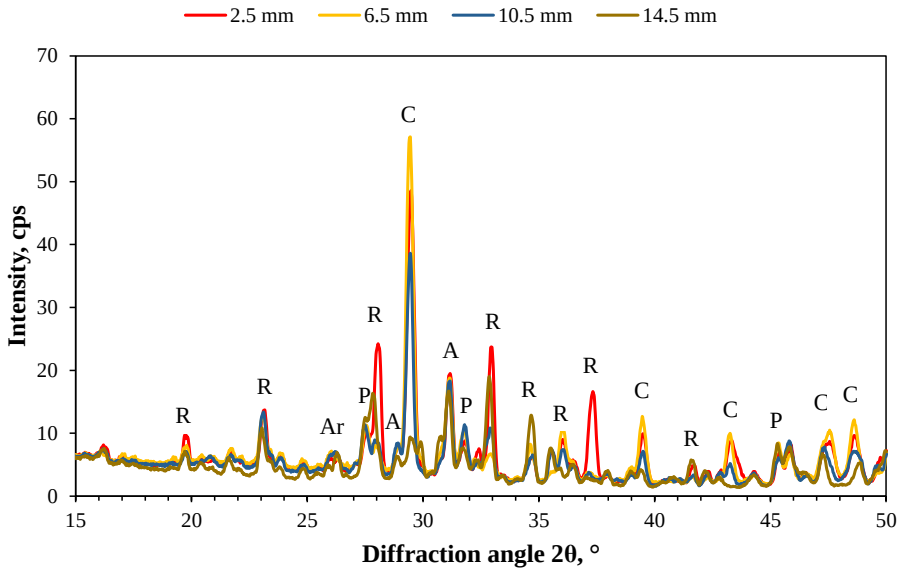


**Fig. 3.40** XRD patterns of the rankinite binder sample carbonated for 8 h at different cross section positions. Indexes: R – rankinite, P – pseudowollastonite, A – akermanite, C – calcite, Ar – aragonite

Since the main compound after the carbonation reaction that best describes the ongoing process is calcite, its distribution throughout the sample cross sections is provided in Figure 3.41. Only the main calcite peak (d-spacing = 0.3027 nm, 2θ = 29.48 °) net area was taken into account. However, it should also be noted that the first outermost position at 0.5 mm had to be omitted since, during the measurement, the beam hit the sample holder material thus distorting the results.

In Figure 3.41, it can be seen that calcite distribution in the sample cross section is highly dependent on the carbonation process parameters. It is evident that in the samples that were not fully carbonated (Fig. 3.41 *a*, <24 h and *b*, <45 °C), calcite reaches a maximum at around 8.5 mm position, after which it drops to a negligible amount. According to the obtained results, it can be seen that only samples carbonated for 24 h at 45 °C and higher were fully carbonated. In these samples, calcite seems to be evenly distributed throughout the entire cross section. However, samples carbonated for 36 h evidently reached a higher carbonation degree since the calcite peak net area, and thus also the intensity, is higher than in the areas carbonated for different periods of time. These results are in good agreement with the compressive strength development, where it was determined that the samples carbonated for 36 h reached the highest strength value. Even though the calcite distribution is rather different in the samples carbonated at different conditions, all the samples seem to have reached a similar carbonation degree in the 6.5–8.5 mm positions. This position may be a breakthrough point, at which, the carbonation process changes from phase-boundary controlled to diffusion controlled. It has been previously stated (93) that, at the beginning, the carbonation reaction is occurring very rapidly and is mostly dependent on the nucleation of the reaction product. However, the second stage of the carbonation reaction is believed to be diffusion controlled (185). At this point, the layer of the reaction products around the unreacted particles becomes so thick that the $CO_2$ diffusion through the product layer becomes the limiting step for further carbonation development.

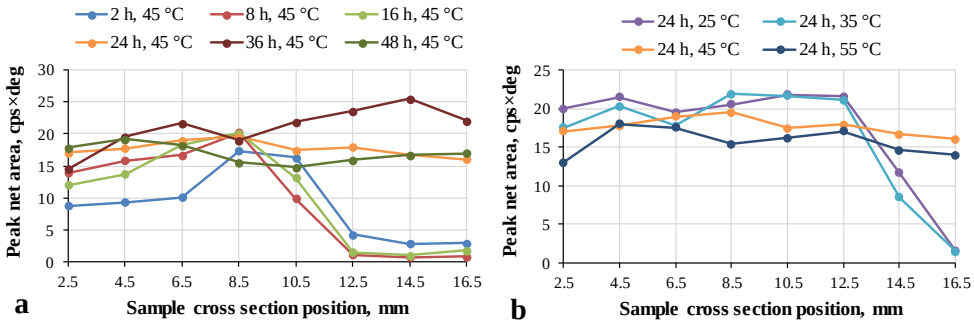


**Fig. 3.41** Calcite peak (d-spacing = 0.3027 nm, 2θ = 29.48 °) net area in positions throughout the sample cross section, dependence on duration (a) and temperature (b)

The carbonated rankinite binder sample cross sections with plotted carbon distributions were determined by LA-ICP-MS. Since all of the elements other than carbon are distributed evenly in the cross section of samples, only the distribution and alteration of carbon is provided. The color plot indicating the element signal intensity is provided in Figure 3.42, where the purple color represents the lowest signal, and the red color is attributed to the highest signal intensity. The intensity of the signal directly corresponds to the element appearance in the specific position.


**Fig. 3.42** Color scheme for the element color plots

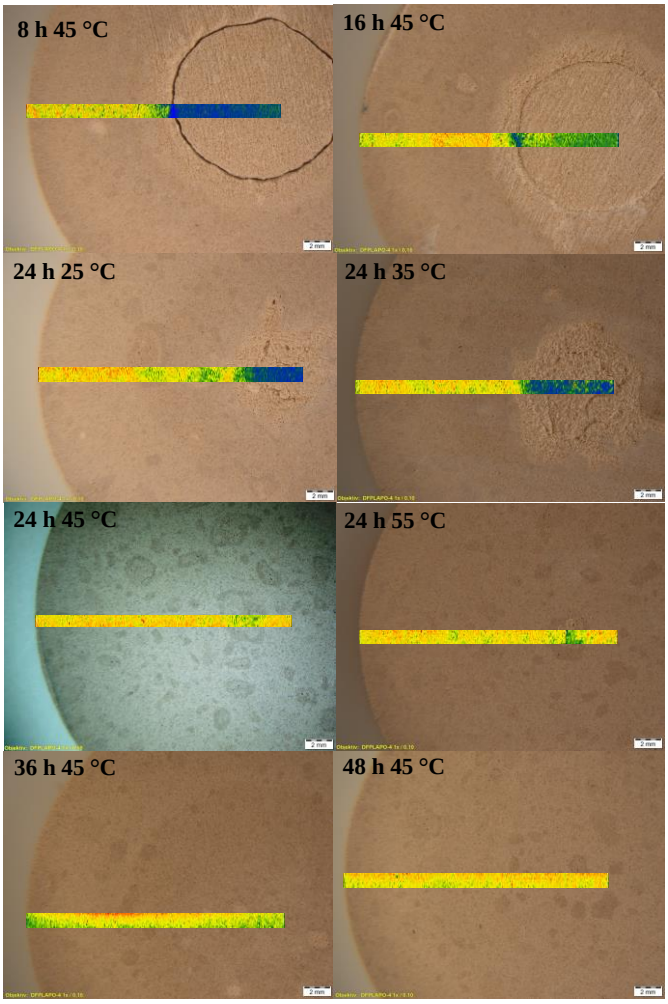


**Fig. 3.43** Carbonated rankinite binder sample cross section with plotted carbon distribution

The obtained results are provided in Figure 3.43, and, as it can be seen, the samples that are not fully carbonated have a lighter-colored brittle core, in which, the appearance of carbon is low (blue/green color), while the outer parts of those samples can be identified by a darker color, in which, the appearance of carbon is much higher (yellow/red color). It is evident that, with the extended carbonation duration, the uncarbonated core is shrinking, the semi-carbonated transition zone around the core disappears, and the sample seems to have completely reacted after 24 h of carbonation at 45 °C. A further increase of the carbonation duration does not seem to affect the appearance of the sample cross section. Accordingly, in the samples carbonated for 24 (at 45 and 55 °C), 36, and 48 h, carbon appears to be evenly disturbed in the entire sample cross section thus indicating that the samples are fully carbonated. The temperature, on the other hand, also seems to have a significant influence on the carbonation process development since only the samples carbonated at 45 °C and higher were fully carbonated.

The chemical analysis was carried out to further analyze the carbonated samples. The chemical composition of the unreacted (raw) rankinite binder and samples carbonated for 8 (inner and outer parts) and 48 h is provided in Table 3.8. As it can be seen in the provided table, the sample carbonated for 8 h featured a composition that was highly contrasting if comparing its outer and inner parts. The composition of the inner part almost did not differ from raw rankinite. The total amount of carbon in the outer part of the sample is almost nine times higher than in the inner part, thus indicating a much higher degree of carbonation. Since the sample carbonated for 48 h featured a chemical composition that was rather evenly distributed, the total determined carbon amount reached 4.23%, which is equal to roughly 35.25% of calcium carbonate based on the molar mass. Since the previously calculated (Eq. 3.11) maximum amount of $CO_2$ that can react to the rankinite binder, according to its chemical composition, was equal to 37.65%, this leads to around 85% of calcium carbonate that can be formed from the $CO_2$ reactive components from the binder composition. However, it is evident that only a half of this amount actually formed. This suggests a conclusion that, as the coating of the reaction products around the surface of the unreacted rankinite particle becomes thicker, the particle is surrounded with a densified layer thus preventing further permeation and diffusion of $CO_2$ to the unreacted particle and subsequently limiting the carbonation extent. Due to this, a considerably large share of the rankinite particles remains unreacted due to being preserved by a dense layer of carbonation reaction products. Even though the sample seems to be fully carbonated throughout the entire volume, less than a half of the binder mass actually reacted. However, the formed reaction products appear to provide a highly densified structure that leads to a significantly improved compressive strength. While summarizing the obtained results in Figure 3.43, it can be seen that the carbonation process stops to proceed after 24 h at temperatures higher than 45 °C since neither the chemical composition nor the compressive strength is significantly altering after that point. At this time, the reaction products most likely reached a point at which no further reaction can proceed, and the carbonation process is impeded.

Considering the previously obtained degree of carbonation of the paste samples in the previous stages (Tables 3.5 and 3.7), it was concluded that the samples were not

fully carbonated since only ~40% maximum degree of carbonation was reached. However, according to the latest results, it can be seen that only a half of the binder particles need to react for the sample to reach full carbonation. Since for the determination of the carbonation degree in the previous stages the TG mass loss results were taken into account and the whole sample was ground and used for the analysis, it is evident that this operation may fail to correctly reflect the real situation. Since the samples were fully grounded, this way, all the sample volume, including the binder particles that could no longer react with $CO_2$, were involved in the analysis, thus distorting the obtained results. Based on the latest results, it can be observed that the paste samples in the previous parts most likely were fully carbonated, especially considering their minimal dimensions in comparison to the last stage paste samples. However, there is still a matter of difference considering the paste and the mortar samples. As it was determined that the mortars reached full carbonation, as opposed to the paste samples, the higher degree of carbonate formation in the mortars can be explained by the difference in the sample structure, i.e., the thickness of the binder layer between the aggregate particles. Since the mortar sample porosity, due to the presence of the relatively coarse aggregate particles, was much higher than that of the paste samples, the particle distribution was also different. The sand particles in the mortars provided a much higher surface area for the binder particles to attach to thus contributing to the thinner final layer of the binder around them. Due to this, $CO_2$ was able to react much more efficiently resulting in full binder carbonation. Meanwhile, the paste samples consisting only of the binder developed a dense layer of the binder particles thus preventing the $CO_2$ penetration throughout the entire volume of the binder layer.

**Table 3.8** Chemical analysis results of uncarbonated and carbonated rankinite binder samples

| Composition, wt% | Raw rankinite binder | 8 h carbonation outer part | 8 h carbonation inner part | 48 h carbonation |
|---|---|---|---|---|
| Total carbon | - | 3.60 | 0.41 | 4.23 |
| LOI 1000 °C | - | 15.34 | 2.64 | 17.51 |
| $Na_2O$ | 0.21 | 0.08 | 0.09 | 0.07 |
| $K_2O$ | 0.62 | 0.49 | 0.43 | 0.46 |
| CaO | 49.48 | 42.17 | 49.03 | 41.19 |
| MgO | 2.79 | 1.67 | 1.93 | 1.55 |
| $Fe_2O_3$ | 1.28 | 1.45 | 1.70 | 1.43 |
| $Al_2O_3$ | 2.34 | 1.69 | 1.92 | 1.59 |
| $SiO_2$ | 42.49 | 38.27 | 44.49 | 37.61 |
| $P_2O_5$ | 0.09 | 0.09 | 0.10 | 0.09 |
| $SO_3$ | 0.20 | 0.22 | 0.13 | 0.25 |
| $TiO_2$ | 0.09 | 0.09 | 0.10 | 0.09 |
| BaO | 0.01 | 0.01 | 0.01 | 0.01 |
| SrO | 0.09 | 0.09 | 0.09 | 0.08 |
| MnO | 0.02 | 0.02 | 0.02 | 0.02 |
| $Cr_2O_3$ | 0.01 | 0.01 | 0.02 | 0.01 |

However, the structure of the carbonated sample depends not only on the formation of the calcium carbonate but on the formation and polymerization of the silica gel as well. Silica gel formation and development was investigated by $^{29}$Si MAS NMR, and the obtained results are provided in Figure 3.44. The unreacted rankinite binder (noted as *untreated*) contained three major sharp peaks, two of which seem to be overlapping: at -74.47 and -75.77 ppm, and the third peak is at -83.56 ppm. According to the literature (140; 107; 186), the first two peaks are assigned to $Q_1$ species and are assigned to rankinite since this mineral consists of the array of $Si_2O_7^{6-}$ groups linked by Ca atoms (187), while the third peak is assigned to $Q_2$ species and is assigned to pseudowollastonite due to its chain silicate tetrahedron (186). The intensities of the peaks at -74.47 and -75.77 ppm decreased with prolonged carbonation, while the peak at -83.56 ppm remained of similar intensity. Along with the carbonation reaction, new peaks at around -101 and -111 ppm appeared. The peak at -101 ppm is attributed to the hydroxylated surface sites of the silica gel and is assigned to $Q_3$ species, while the peak at -111 ppm is attributed to the $Q_4$ sites of the polymerized 3D network of the silicate tetrahedrons (140). After 16 h carbonation, the peaks at -101 and -111 ppm are of a similarly low intensity to those of uncarbonated rankinite, whereas, with a prolonged carbonation (24, 36, and 48 h), the intensity of these peaks is much higher, thus indicating that carbonation caused a significant formation of $Q_3$ and $Q_4$ silicate species. Although all the carbonated samples still contained considerably high fractions of $Q_0$, $Q_1$, and $Q_2$ species, these could be not only from the uncarbonated binder, but also from the formation of a C-S-H like phase (188). However, since it was previously determined that only a half of the binder particles react with $CO_2$, the remaining peaks are most likely due to the unreacted binder particles.

The degree of polymerization of the silica gel can be described by calculating the ratio of integrated areas of $Q_3/Q_4$, where the lower values of $Q_3/Q_4$ represent the higher fraction of fully condensed silicate clusters, and, therefore, a higher degree of polymerization (140). As the silicate condensation reaction proceeds, the amount of partially condensed silica tetrahedrons ($Q_3$ species, with three bridging and one non-bridging oxygen negatively charged) decreases, whereas that of the fully condensed tetrahedrons ($Q_4$ species, with four bridging oxygens) increases (189). The silica tetrahedrons are fully condensed by their four corners in a lattice extending over the three directions in space.

For samples carbonated for 16 h, this ratio was equal to 1.03, while the prolonged carbonation duration led to a decrease in the ratio value to 0.58, 0.74, and 0.71 for 24, 36, and 48 h, respectively. It is evident that the highest degree of Ca-modified silica gel was obtained by the samples carbonated for 24 h. However, these results do not seem to be directly related to the compressive strength development where the highest strength was achieved by the samples carbonated for 36 h (Fig. 3.37) which had a lower degree of silica gel polymerization than the 24 h sample. Nevertheless, the compressive strength and silica gel polymerization values of all the samples carbonated for highest durations – 24, 36, and 48 h – are rather similar, and they fall into the deviation values.

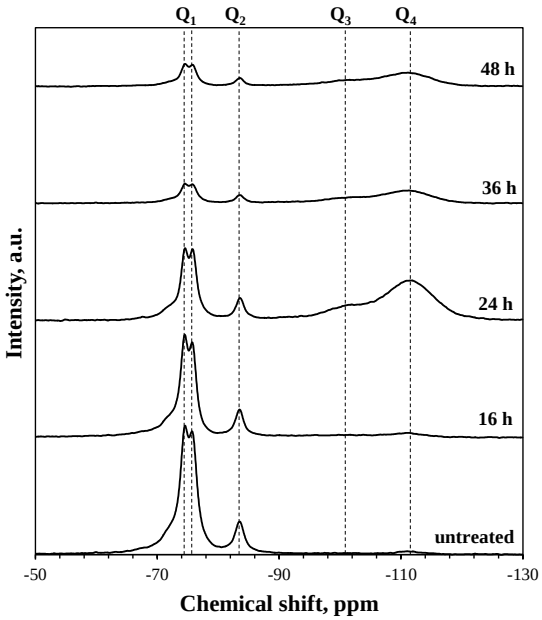


**Fig. 3.44** $^{29}$Si MAS NMR spectrum of untreated and carbonated for 16, 24, 36, and 48 h at 15 bar and 45 °C rankinite binder samples

The microstructure of the carbonated binder paste samples was further investigated by SEM analysis, by collecting backscattered electron (BSE) images and mapping the elemental distribution on the obtained images. Figure 3.45 shows a BSE image of the sample carbonated for 24 h at 45 °C with the mapping of the prevailing elemental distribution provided below. Four different sites were identified based on the scale of the grey color and the obtained element mapping results: the darkest grey regions are most likely attributed to the silica gel, while the brightest grey is attributed to the unreacted binder particles; calcium carbonate was described by the medium light grey in between the large particles, and the pores, although easily visible, due to a better phase contrast, are in bright white. The large dark grey particle is most definitely attributed to silica gel since no other elements were detected in that area. Silica gel seems to be distributed as a rim around the unreacted (or partially reacted) binder particles with a dimension of around 1–5 μm. This formation of silica gel around the binder particles was also previously reported by Ashraf *et al*. (107). Calcium carbonates, on the other hand, seem to fill the spaces between the particles without any specific dimensions and are distributed rather evenly throughout the volume. The mapping also showed that, in the areas of silica gel, the amount of Ca is negligible, thus indicating that the silica gel contains only an insignificant amount of calcium in its structure. However, the carbon distribution cannot be reliably taken into account since the samples were coated with graphite before the measurement.

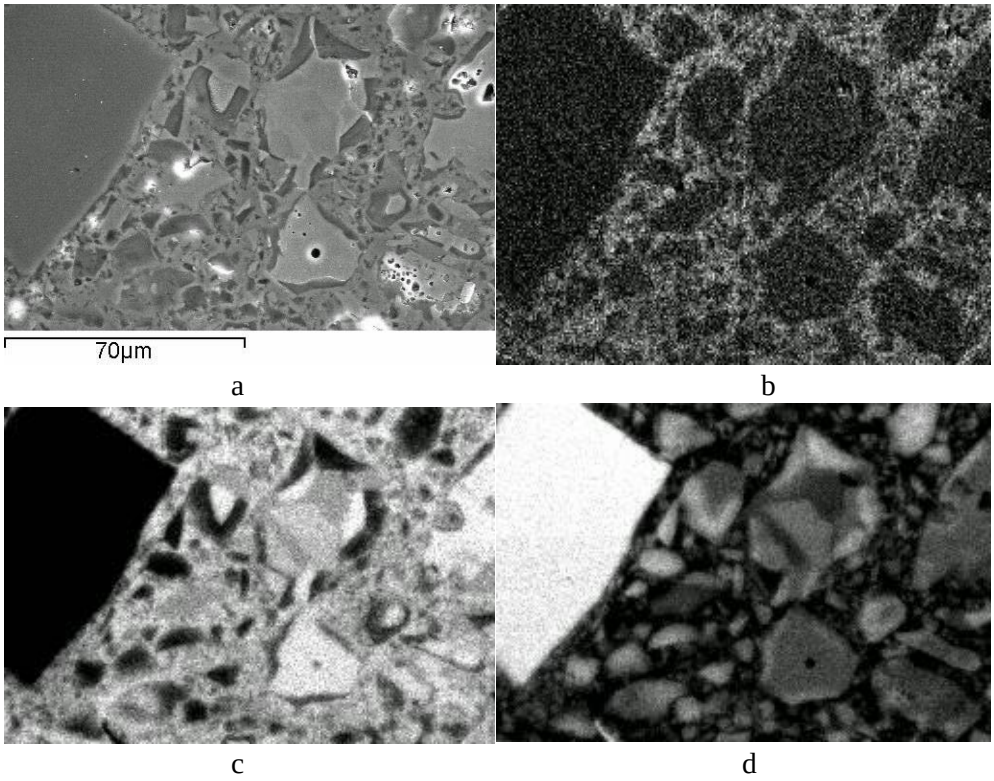


**Fig. 3.45** BSE image (a) of the carbonated rankinite binder sample (for 24 h at 45 °C) in the fully carbonated area near the edge with mapping of the element distribution: b – C, c – Ca, d – Si

Therefore, it is evident that carbon is distributed between the unreacted binder particles and outside the silica gel layer (Fig. 3.45, b).

From the obtained images, the microstructure of the carbonated material was determined to be considerably porous, with pore diameters from 50 μm to less than 5 μm. From all of the obtained SEM images, it was determined that the first layer surrounding the unreacted binder particle is silica gel followed by the layer of calcium carbonates filling the remaining volume and thus densifying the microstructure of the material. However, as previously mentioned, at some point, the layer of carbonation reaction products around the unreacted binder particles becomes so thick that it obstructs $CO_2$ from further diffusion to the unreacted particles thus hindering the further carbonation reaction and restricting the material from additional microstructure development.

## 4. Conclusions

1. After compacting the OPC the raw meal, clinker calcination temperature could be reduced from 1450 to 1400 °C. Pressing has a positive influence on the clinker mineral formation and hydration reactions since, in the samples calcined at 1400 °C, the amount of $CaO_{free}$ after pressing was reduced from 1.6% to 1.1%, and the amount of alite and heat released after hydration increased by ~2.5%.
2. The optimal conditions determined for rankinite binder synthesis from the locally available materials of opoka and limestone is: initial mixture molar ratio $CaO/SiO_2$ = 1.5, isothermal treatment at 1250 °C for 45 min. The obtained binder is mainly composed of rankinite with small amounts of additional compounds – pseudowollastonite, akermanite, and bredigite.
3. Concrete with a compressive strength of ~45 MPa can be produced from rankinite binder and sand mixtures, while carbonating was performed at the following conditions: 15 bar $CO_2$ pressure, 24 h duration, 45 °C, w/c = 0.25, binder/sand = 1:3, compaction of 12.5 MPa.
4. It was determined that rankinite binder mortars and pastes deliver different carbonation reaction products. The only polymorph of crystalline calcium carbonate obtained in the mortars was calcite, while pastes contained three of the polymorphs, i.e., calcite, vaterite, and aragonite. These considerable differences were due to the presence of quartz, acting as a buffer for calcite formation, as well as a highly different microstructure and moisture content.
5. Rankinite binder paste samples reached significantly high compressive strength values exceeding 100 MPa as a result of calcium carbonate, especially calcite, formation and silica gel polymerization that leads to a denser microstructure and thus a higher compressive strength.
6. The degree of carbonation highly depends on the thickness of the binder layer in the sample microstructure. It was found that only ~40% of the binder particles need to react for the paste sample to reach the maximum carbonation degree. This is due to the fact that, at some point of the carbonation process, the layer of the reaction products on the surface of the unreacted binder particle becomes so thick that it impedes $CO_2$ diffusion and finally suspends further carbonation.
7. It was determined that the rankinite binder is a suitable cementitious material for high strength, highly durable carbonated concrete products which opens up a great opportunity for $CO_2$ mitigation by permanent sequestration in the concrete structure in the form of stable carbonates.

## REFERENCES


1. Gao, T.; Shen, L.; Liu, L.; *et al*. Analysis of material flow and consumption in cement production. *Journal of Cleaner Production*. 2016, 112, 553-565. ISSN: 0959-6526.
2. Schneider, M.; Romer, M.; Tschudin, M.; *et al*. Sustainable cement production – present and future. *Cement and Concrete Research*. 2011, 41(7), 642-650. ISSN: 0008-8846.
3. Benhelal, E.; Zahedi, G.; Shamsaei, E.; *et al*. Global strategies and potentials to curb $CO_2$ emissions in cement industry. *Journal of Cleaner Production*. 2012, 51, 142-161. ISSN: 0959-6526.
4. Damtoft, J.S.; Lukasik, J.; Herfort, D.; *et al*. Sustainable development and climate change initiatives. *Cement and Concrete Research.* 2008, 38(2), 115-127. ISSN: 0008-8846.
5. Huntzinger, Deborah N.; Eatmon, Thomas D. A life-cycle assessment of Portland cement manufacturing: comparing the traditional process with alternative technologies. *Journal of Cleaner Production*. 2009, 17(7), 668-675. ISSN: 0959-6526.
6. Oda, J.; Akimoto, K.; Tomoda, T.; *et al*. International comparisons of energy efficiency in power, steel, and cement industries. *Energy Policy*. 2012, 44, 118-129. ISSN: 0301-4215.
7. Juenger, M.; Provis, J.; Elsen, J.; *et al*. Supplementary Cementitious Materials for Concrete: Characterization Needs. *Materials Research Society Proceedings*. 2012, 1488. DOI 10.1557/opl.2012.1536.
8. Yuksel, I.; Bilir, T.; Ozkan, O. Durability of concrete incorporating non-ground blast furnace slag and bottom ash as fine aggregate. *Building Environment*. 2007, 42(7), 2651-2659. ISSN: 0360-1323.
9. Qasrawi, H. The use of steel slag aggregate to enhance the mechanical properties of recycled aggregate concrete and retain the environment. *Construction and Building Materials*. 2014, 54, 298-304. ISSN: 0950-0618.
10. Komljenovic, M.; Petrasinovic-Stojkanovic, L.J.; Bascarevic, Z.; *et al*. Fly ash as the potential raw mixture component for Portland cement clinker synthesis. J*ournal of Thermal Analysis and Calorimetry*. 2009, 96(2), 363-368. ISSN: 1572-8943.
11. Wongkeo, W.; Thongsanitgarn, P.; Ngamjarurojana, A.; *et al*. Compressive strength and chloride resistance of self-compacting concrete containing high level fly ash and silica fume. *Materials and Design*. 2014, 64, 261-269. ISSN: 0261-3069.
12. Lilkov, V.; Rostovsky, I.; Petrov, O.; *et al*. Long term study of hardened cement pastes containing silica fume and fly ash. *Construction and Building Materials*. 2014, 60, 48-56. ISSN: 0950-0618.

13. Mohammadhosseini, H.; Yatim, Jamaludin M.; Sam, A.R.M.; et al. Durability performance of green concrete composites containing waste carpet fibers and palm oil fuel ash. *Journal of Cleaner Production.* 2017, 144, 448-458. ISSN: 0959-6526.
14. Awal, A.S.M. Abdul; Mohammadhosseini, H. Green concrete production incorporating waste carpet fiber and palm oil fuel ash. *Journal of Cleaner Production.* 2016, 137, 157-166. ISSN: 0959-6526.
15. Ul Islam, M. M.; Mo, K. H.; Alengaram, U. J.; *et al*. Durability properties of sustainable concrete containing high volume palm oil waste materials. *Journal of Cleaner Production.* 2016, 137, 167-177. ISSN: 0959-6526.
16. Torres, A.; Bartlett, L.; Pilgrim, C. Effect of foundry waste on the mechanical properties of Portland Cement Concrete. *Construction and Building Materials*. 2017, 135, 674-681. ISSN: 0950-0618.
17. Siddique, R.; de Schutter, G.; Noumowe, A. Effect of used-foundry sand on the mechanical properties of concrete. *Construction and Building Materials*. 2017, 23(2), 976-980. ISSN: 0950-0618.
18. Fiore, S.; Zanetti, M.C. Foundry wastes reuse and recycling in concrete production. *American journal of environmental sciences*. 2007, 3(3), 135-142. ISSN: 1558-3910.
19. Sengul, O. Mechanical behavior of concretes containing waste steel fibers recovered from scrap tires. *Construction and Building Materials*. 2016, 122, 649-658. ISSN: 0950-0618.
20. Aprianti, Evi S. A huge number of artificial waste material can be supplementary cementitious material (SCM) for concrete production – a review part II. *Journal of Cleaner Production.* 2017, 142, 4178-4194 Part: 4. ISSN: 0959-6526.
21. Letelier, V.; Marcos Ortega, J.; Munoz, P.; *et al*. Influence of Waste Brick Powder in the Mechanical Properties of Recycled Aggregate Concrete. *Sustainability*. 2018, 10(4), article number: 1037. ISSN: 2071-1050.
22. Hanif, A.; Kim, Y.; Lee, K.; *et al*. Influence of cement and aggregate type on steam-cured concrete – an experimental study. *Magazine of Concrete Research*. 2017, 69(13), 694-702. ISSN: 0024-9831.
23. Chatziaras, N.; Psomopoulos, C.S.; Themelis, N.J. Use of waste derived fuels in cement industry: a review. *Management of Environmental Quality.* 2016, 27(2), 178-193. ISSN: 1477-7835.
24. Mokrzycki, E; Uliasz-Bochenczyk, A. Alternative fuels for the cement industry. *Applied Energy*. 2003, 74(1-2), 95-100. ISSN: 0306-2619.
25. Asamany, E.A.; Gibson, M.D.; Pegg, M.J. Evaluating the potential of waste plastics as fuel in cement kilns using bench-scale emissions analysis. *Fuel*. 2017, 193, 178-186. ISSN: 0016-2361.
26. Madlool, N. A.; Saidur, R.; Hossain, M. S.; et al. A critical review on energy use and savings in the cement industries. *Renewable and Sustainable Energy Reviews.* 2011, 15(4), 2042-2060. ISSN: 1364-0321.

27. Benhelal, E.; Zahedi, G.; Hashim, H. A novel design for green and economical cement manufacturing. *Journal of Cleaner Production.* 2012, 22(1), 60-66. ISSN: 0959-6526.
28. AZO Materials. Using XRF to Determine Free Lime Content in Clinker for Cement Quality Control [interactive]. 2011. [last viewed 2016 02 12]. Access: https://www.azom.com/article.aspx?ArticleID=5728.
29. Popescu, C.D.; Muntean, M.; Sharp, J.H. Industrial trial production of low energy belite cement. *Cement and Concrete Composites.* 2003, 25(7), 689-693. ISSN: 0958-9465.
30. Bouzidi, M. A.; Tahakourt, A.; Bouzidi, N.; *et al*. Synthesis and Characterization of Belite Cement with High Hydraulic Reactivity and Low Environmental Impact. *Arabian Journal of Science and Engineering.* 2014, 39(12), 8659-8668. ISSN: 2193-567X.
31. Stanek, T.; Sulovsky, P. Active low-energy belite cement. *Cement and Concrete Research.* 2015, 68, 203-210. ISSN: 0008-8846.
32. Kacimi, L.; Simon-Masseron, A.; Salem, S.; *et al*. Synthesis of belite cement clinker of high hydraulic reactivity. *Cement and Concrete Research.* 2009, 39(7), 559-565. ISSN: 0008-8846.
33. Ashraf, W., Jan, O. Carbonation behavior of hydraulic and non-hydraulic calcium silicates: potential of utilizing low-lime calcium silicates in cement-based materials. *Journal of Material Science.* 2016, 51(13), 6173-6191. ISSN: 0022-2461.
34. Sahu, S.; DeCristofaro, N. Solidia Cement, in: Solidia Technol. White Paper. [interactive]. 2013. [last viewed May 17, 2016]. Access: http://solidiatech.com/wp-content/uploads/2014/02/Solidia-Cement-White-Paper-12-17-13-FINAL.pdf.
35. Dambrauskas, T.; Baltakys, K.; Eisinas, A.; *et al*. A study on the thermal stability of kilchoanite synthesized under hydrothermal conditions. *Journal of Thermal Analysis and Calorimetry.* 2017, 127(1), 229-238. ISSN: 1388-6150.
36. Hillert, M.; Sundman, B.; Wang, X.Z.; *et al*. A reevaluation of the rankinite phase in the $CaO$-$SiO_2$ system. *Calphad-Computer Coupling of Phase Diagrams and Thermochemistry*. 1991, 15(1), 53-58. ISSN: 0364-5916.
37. Minghua, W.; Chao, L.; Yuchun, Z. Sorption-Desorption Behavior of $CO_2$ on $Ca_3Si_2O_7$ Absorbent. In: *The Second China Energy Scientist Forum*. Institute of Metallurgy and Physical Chemistry, China. Science Research, 2010, 315-319.
38. Qian, B.; Li, X.; Shen, X. Preparation and accelerated carbonation of low temperature sintered clinker with low Ca/Si ratio. *Journal of Cleaner Production.* 2016, 120, 249-259. ISSN: 0959-6526.
39. Daval, D.; Martinez, I.; Guigner, J.M.; *et al*. Mechanism of wollastonite carbonation deduced from micro- to nanometer length scale observations. *American Mineralogist.* 2009, 94(11-12), 1707-1726. ISSN: 0003-004X.

40. Daval, D.; Martinez, I.; Corvisier, J.; et al. Carbonation of Ca-bearing silicates, the case of wollastonite: Experimental investigations and kinetic modelling. *Chemical Geology*. 2009, 265(1-2), 63-78. ISSN: 0009-2541.
41. Seryotkin, Y.V.; Sokol, E.V.; Kokh, S.N. Natural pseudowollastonite: Crystal structure, associated minerals, and geological context. *Lithos*. 2012, 134, 75-90. ISSN: 0024-4937.
42. Warda, A.; Jan, O.; Hyungu, J.;Vahit, A. Effects of High Temperature on Carbonated Calcium Silicate Cement (CSC) and Ordinary Portland Cement (OPC) Paste. In: *5th International Conference on the Durability of Concrete Structures.* Shenzhen University, Shenzhen, Guangdong Province, P.R.China, 2016. DOI: 10.5703/1288284316153.
43. Jang, J. G.; Kim, G. M.; Kim, H. J.; *et al*. Review on recent advances in $CO_2$ utilization and sequestration technologies in cement-based materials. *Construction and Building Materials.* 2016, 127, 762-773. ISSN: 0950-0618.
44. Kainiemi, L.; Eloneva, S.; Toikka, A.; *et al*. Opportunities and obstacles for $CO_2$ mineralization: $CO_2$ mineralization specific frames in the interviews of Finnish carbon capture and storage (CCS) experts. *Journal of Cleaner Production.* 2015, 94, 352-358. ISSN: 0959-6526.
45. Xuan, D.; Zhan, B.; Poon, C.S. Development of a new generation of eco-friendly concrete blocks by accelerated mineral carbonation. *Journal of Cleaner Production.* 2016, 133, 1235-1241. ISSN: 0959-6526.
46. Mazzella, A.; Errico, M.; Spiga, D. $CO_2$ uptake capacity of coal fly ash: Influence of pressure and temperature on direct gas-solid carbonation. *Journal of Environmental Chemical Engineering.* 2016, 4(4), 4120-4128. ISSN: 2213-2929.
47. Sormeh, K.H.; Subhasis, G. $CO_2$ Sequestration in Concrete through Accelerated Carbonation Curing in a Flow-through Reactor. *Industrial and Engineering Chemistry Research*. 2009, 49(3), 1143-1149. ISSN: 1520-5045.
48. Naik, T.N.; Kumar, R.; Kraus, N.R. Carbon dioxide sequestration in cementitious products. In: Report Submitted to the Electric Power Research Institute, Palo Alto, California. [interactive]. 2009. [last viewed June 06, 2016]. https://www4.uwm.edu/cbu/Papers/2009%20CBU%20Reports/REP-640.pdf.
49. Garcia-Gonzalez, C.A.; el Grouh, N.; Hidalgo, A.; *et al*. New insights on the use of supercritical carbon dioxide for the accelerated carbonation of cement pastes. *Journal of Supercritical Fluids.* 2008, 43(3), 500-509. ISSN: 0896-8446.
50. Ashraf, W. Carbonation of cement-based materials: Challenges and opportunities. *Construction and Building Materials.* 2016, 120, 558-570. ISSN: 0950-0618.
51. Rostami, V.; Shao, Y.; Boyd, A. J. Durability of concrete pipes subjected to combined steam and carbonation curing. *Construction and Building Materials.* 2011, 25(8), 3345-3355. ISSN: 0950-0618.

52. Heinz, D.; Urbonas, L. Modification of cementitous building materials by treatment with $CO_2$. *Cheminė Technologija.* 2016, 1(67), 46-52. ISSN: 1392-1231.
53. Urbonas, L.; Heinz, D.; Hilbig, H.; Reger, J. The effect of supercritical carbon dioxide on the properties of hardened cement paste. *Cement International.* 2010, 8(4), 72-81. ISSN: 1610-6199.
54. Zhang, D.; Shao, Y. Early age carbonation curing for precast reinforced concretes. *Construction and Building Materials.* 2016, 113, 134-143. ISSN: 0950-0618.
55. Fernandez Bertos, M.; Simons, S.J.R.; Hills, C.D.; Carey, P.J. A review of accelerated carbonation technology in the treatment of cement-based materials and sequestration of $CO_2$. *Journal of Hazardous Materials.* 2004, 112(3), 193-205. ISSN: 0304-3894.
56. Huet, B.; Tasoti, V; Khalfallah, I. A review of Portland cement carbonation mechanisms in $CO_2$ rich environment. In: *$10^{th}$ International Conference on Greenhouse Gas Control Technologies*. 2010, Amsterdam, Netherlands. Book Series: Energy Procedia, 2011, 4, 5275-5282. ISSN: 1876-6102.
57. Leemann, A.; Moro, F. Carbonation of concrete: the role of $CO_2$ concentration, relative humidity and $CO_2$ buffer capacity. *Materials and Structures.* 2017, 50(1), Article Number: UNSP 30. ISSN: 1359-5997.
58. Galan, I.; Andrade, C.; Mora, P.; *et al*. Sequestration of $CO_2$ by Concrete Carbonation. *Environmental Science and Technology.* 2010, 44(8), 3181-3186. ISSN: 0013-936X.
59. Mahoutian, M.; Ghouleh, Z.; Shao, Y. Synthesis of waste-based carbonation cement. *Materials and Structures.* 2016, 49(11), 4679-4690.
60. Neves Junior, A.; Toledo Filho, R.D.; Rego F., de Eduardo M.; *et al*. A study of the carbonation profile of cement pastes by thermogravimetry and its effect on the compressive strength. *Journal of thermal Analysis and Calorimetry.* 2014, 116(1), 69-76. ISSN: 1388-6150.
61. Hussain, S.; Bhunia, D.; Singh, S.B. Comparative study of accelerated carbonation of plain cement and fly-ash concrete. *Journal of Building Engineering.* 2017, 10, 26-31. ISSN: 2352-7102.
62. Wang, X.Y. Modeling of Hydration, Compressive Strength, and Carbonation of Portland-Limestone Cement (PLC) Concrete. *Materials*. 2017, 10(2), Article Number: 115. ISSN: 1996-1944.
63. Yoshioka, I.; Obata, D.; Nanjo, H.; *et al*. New ecological concrete that reduces $CO_2$ emissions below zero level; new method for $CO_2$ capture and storage. In: *International Conference on Greenhouse Gas Technologies (GHGT-11)*. Kyoto, Japan, 2012. *Energy Procedia*. 2013, 37, 6018-6025. ISSN: 1876-6102.
64. Calera [interactive] [last viewed May 30, 2017]. http://www.calera.com/.
65. Evans, S.M.; Vlassopoulos, N. Novacem – carbon negative cement to transform the construction industry [interactive] 2008. [last viewed 2017 05 30]. Energy

Futures Lab, Imperial College, London. http://www3.imperial.ac.uk/pls/portallive/docs/1/50161701.PDF.
66. Telschow, S.; Frandsen, F.; Theisen, K.; Dam-Johansen K. Cement Formation-A Success Story in a Black Box: High Temperature Phase Formation of Portland Cement Clinker. *Industrial and Engineering Chemistry Research*. 2012, 51(34), 10983-11004. ISSN: 1520-5045.
67. Chang, J.; Fang, Y.; Shang, X. The role of β-$C_2S$ and γ-$C_2S$ in carbon capture and strength development. *Materials and Structures*. 2016, 49(10), 4417-4424. ISSN: 1359-5997.
68. Benmohamed, M.; Alouani, R.; Jmayai, A.; *et al*. Morphological Analysis of White Cement Clinker Minerals: Discussion on the Crystallization-Related Defects. *International Journal of Analytical Chemistry*. 2016, Article Number: 1259094. ISSN: 1687-8760.
69. Tantawy, M.A., Shatat, M.R.A.; El-Roudi, A.M.; *et al*. Low Temperature Synthesis of Belite Cement Based on Silica Fume and Lime. *International Scholarly Research Notices*. 2014. DOI: 10.1155/2014/873215.
70. Cuesta, A.; Losilla, E.R.; Aranda, M.A.G.; *et al*. Reactive belite stabilization mechanisms by boron-bearing dopants. *Cement and Concrete Research.* 2012, 42(4), 598-606. ISSN: 0008-8846.
71. Joong Kim, Y.; Nettleship, I.; Kriven, W.M. Phase Transformations in Dicalcium Silicate. II: TEM Studies of Crystallography, Microstructures and Mechanisms. *Journal of the American Ceramic Society.* 2005, 75(9), 2407-2419. ISSN: 1551-2916.
72. Davraz, M. The Effect of Boron Compound to Cement Hydration and Controllability of this Effect. *Acta physica Polonica A*. 2015, 128(2B), B26-B33. ISSN: 0587-4246.
73. Stemmermann, P.U.; Schweike, U.; Garbev, K.; *et al*. Celitement – a sustainable prospect for the cement industry. *Cement International*. 2010, 8(5), 52-66. ISSN: 1610-6199.
74. Taylor, H. F. W. The Chemistry of Cements. London: Academic Press, 1964.
75. Garbev, K.; Beuchle, G.; Schweike, U.; Stemmermann P. Hydration behavior of Celitement®: Kinetics, phase composition, microstructure and mechanical properties. In: *3rd International Congress on the Chemistry of Cement*. Madrid, Spain, 2011.
76. Garbev, K.; Beuchle, G.; Schweike, U.; *et al*. Preparation of a Novel Cementitious Material from Hydrothermally Synthesized C–S–H Phases. *Journal of American Ceramic Society*. 2014, 97(7), 2298-2307. ISSN: 1551-2916.
77. Garbev, K.; Gasharova, B.; Beuchle, G.; *et al*. First observation of α-$Ca_2[SiO_3(OH)](OH)$- $Ca_6[Si_2O_7][SiO_4](OH)_2$ phase transformation upon thermal treatment in air. *Journal of American Ceramic Society*. 2008, 91(1), 263-271. ISSN: 1551-2916.

78. Garbev, K.; Gasharova, B.; Stemmermann, P. A Modular Concept of Crystal Structure Applied to the Thermal Transformation of alpha-$C_2SH$. *Journal of American Ceramic Society*. 2014, 97(7), 2286-2297. ISSN: 1551-2916.
79. Link, T.; Bellmann, F.; Ludwig, H.M.; *et al*. Reactivity and phase composition of $Ca_2SiO_4$ binders made by annealing of alpha-dicalcium silicate hydrate. *Cement and Concrete Research.* 2015, 67, 131-137. ISSN: 0008-8846.
80. Siauciunas, R.; Gendvilas, R.; Prichockiene, E.; *et al*. Synthesis of low-energy cement based on α-$C_2SH$. *Advances in Cement Research*. 2015, 28(4), 1-10. ISSN: 0951-7197.
81. Siauciunas, R.; Gendvilas, R.; Mikaliunaite, J.; *et al*. Heat flow and strength properties of perspective hydraulic binder material. *Journal of Thermal Analysis and Calorimetry*. 2015, 121(1), 57-65. ISSN1572-8943.
82. Gendvilas, R.; Siauciunas, R.; Baltakys, K. Quantitative thermal analysis of a-$C_2SH$ as a precursor analysis of alfa-$C_2SH$ as a precursor. *Journal of Thermal Analysis and Calorimetry*. 2015, 121(1). DOI: 10.1007/s10973-015-4570-8. ISSN1572-8943.
83. Siauciunas, R.; Mikaliunaite, J.; Urbonas, L.; *et al*. Tribochemical and thermal activation of alfa-$C_2S$ hydrate as precursor for cementitious binders. *Journal of Thermal Analysis and Calorimetry*. 2014, 118(2), 817-823. ISSN1572-8943.
84. Deer, W.A.; Howie, R.A.; Zussman J. Rock-Forming Minerals – Disilicates and Ring Silicates, Volume 1B Second Edition. London: The Geological Society, 1997.
85. Freitas, A.A.; Santos, R.L.; Colaco, R.; *et al*. From lime to silica and alumina: systematic modeling of cement clinkers using a general force-field. *Physical Chemistry Chemical Physics*. 2015, 17(28), 18477-18494. ISSN: 1463-9076.
86. Kusachi, I. The structure of rankinite. *Mineralogical Journal.* 1975, 8(1), 38-47. ISSN: 0544-2540.
87. Sahu, S.; DeCristofaro, N. Part two of a T series exploring the chemical properties and performance results of Sustainable Solidia Cement™ and Solidia Concrete™. Solidia Technologies [interactive]. 2013 [last viewed May 25, 2017]. https://pdfs.semanticscholar.org/691a/16464fff1a9379e23f30f487cc0e9c846f5e.pdf.
88. Hicks, J.K.; Caldarone, M.A.; Bescher, E. Opportunities from Alternative Cementitious Materials. [interactive] 2015 [last viewed May 26, 2017]. https://www.concreteinternational.com.
89. Sahu, S.; Quinn, S.; Atakan, V.; *et al*. $CO_2$-Reducing Cement Based on Calcium Silicates. In: *The 14th International Congress on the Chemistry of Cement*. Beijing, China, 2015.
90. Wang, K.; Ren, L.; Yang, L. Excellent Carbonation Behavior of Rankinite Prepared by Calcining the C-S-H: Potential Recycling of Waste Concrete Powders for Prefabricated Building Products. *Materials*. 2018, 11(8), Article Number: 1474. ISSN: 1996-1944.

91. Zhang, H.; Chen, J.; Shao, R.; *et al*. The usage of rankinite for carbon capture and storage and carbonation kinetics. *Energy Sources Part A – Recovery Utilization and Environmental Effects*. 2018, 40(13), 1629-1646. ISSN: 1556-7036.
92. Lu, B.; Shi, C.; Hou, G. Strength and microstructure of $CO_2$ cured low-calcium clinker. *Construction and Building Materials*. 2018, 188, 417-423. ISSN: 0950-0618.
93. Ashraf, W.; Olek, J. Carbonation activated binders from pure calcium silicates: Reaction kinetics and performance controlling factors. *Cement and Concrete Composites*. 2018, 93, 85-98. ISSN: 0958-9465.
94. Mazzucato, E.; Gualtieri, A.F. Wollastonite polytypes in the $CaO$-$SiO_2$ system. *Physics and Chemistry of Minerals.* 2000, 27(8), 565-574. ISSN: 0342-1791.
95. Abd Rashid, R.; Shamsudin, R.; Hamid, M.A.A.; *et al*. In-vitro bioactivity of wollastonite materials derived from limestone and silica sand. *Ceramics International*. 2014, 40(5), 6847-6853. ISSN: 0272-8842.
96. Wang, Y.; Song, J.; Guo, Q.; *et al*. The environmental sustainability of synthetic wollastonite using waste from zirconium oxychloride production. Journal of Cleaner Production. 2018, 172, 2576-2584. ISSN: 0959-6526.
97. Ashraf, W.; Olek, J.; Tian, N. Multiscale characterization of carbonated wollastonite paste and application of homogenization schemes to predict its effective elastic modulus. *Cement and Concrete Composites*. 2016, 72, 284-298. ISSN: 0958-9465.
98. Savija, B.; Lukovic, M. Carbonation of cement paste: Understanding, challenges, and opportunities. *Construction and Building Materials.* 2016, 117, 285-301. ISSN: 0950-0618.
99. Lagerblad, B. Carbon dioxide uptake during concrete life cycle – State of the art. Stockholm: Swedish Cement and Concrete Research Institute, 2005.
100. Zhang, Duo; Ghouleh, Zaid; Shao, Yixin Review on carbonation curing of cement-based materials. *Journal of $CO_2$ Utilization*. 2017, 21, 119-131. ISSN: 2212-9820.
101. Johannesson, B; Utgenannt, P. Microstructural changes caused by carbonation of cement mortar. *Cement and Concrete Research*. 2001, 31(6), 925-931. ISSN: 0008-8846.
102. Bernal, Susan A.; Provis, John L.; Brice, David G.; *et al*. Accelerated carbonation testing of alkali-activated binders significantly underestimates service life: The role of pore solution chemistry. *Cement and Concrete Research*. 2012, 42(10), 1317-1326. ISSN: 0008-8846.
103. Goni, S; Gaztanaga, MT; Guerrero, A. Role of cement type on carbonation attack. *Journal of Materials Research*. 2002, 17(7), 1834-1842. ISSN: 0884-2914.
104. Rostami, V.; Shao, Y.; Boyd, Andrew J. Carbonation Curing versus Steam Curing for Precast Concrete Production. *Journal of Materials in Civil Engineering*. 2012, 24(9), 1221-1229. ISSN: 0899-1561.

105. Klemm, W.A.; Berger, R.L. Accelerated curing of cementitious systems by carbon dioxide: Part I. Portland cement. *Cement and Concrete Research*. 1972 2(5), 567-576. ISSN: 0008-8846.
106. Shao, Y.; Mirza, M. S.; Wu, X. $CO_2$ sequestration using calcium-silicate concrete. *Canadian Journal of Civil Engineering.* 2006, 33(6), 776-784. ISSN: 0315-1468.
107. Ashraf, W.; Olek, J.; Jain, J. Microscopic features of carbonated calcium silicate based cement paste and mortar. *Cement and Concrete Research*. 2017, 100, 361-372. ISSN: 0008-8846.
108. Shi, C.; Wu, Y. Studies on Some Factors Affecting $CO_2$ Curing of Lightweight Concrete Products. *Resources Conservation and Recycling.* 2008, 52(8-9), 1087-1092. ISSN: 0921-3449.
109. Taylor, C.M.V.; Rubin, J.B.; Carey, J.W.; *et al*. Next Generation Enhancement of Cements by the Addition of Industrial Wastes and Subsequent Treatment with Supercritical $CO_2$. In: *1997 Green Chemistry and Engineering Conference: Implementing Vision 2020 for the Environment*. American Chemical Society, Washington D.C., 1997.
110. Wang, T.; Huang, H.; Hu, X.; *et al*. Accelerated mineral carbonation curing of cement paste for $CO_2$ sequestration and enhanced properties of blended calcium silicate. *Chemical Engineering Journal.* 2017, 323, 320-329. ISSN: 1385-8947.
111. Garcia-Gonzalez, C.A.; Hidalgo, A.; Andrade, C.; *et al*. Modification of Composition and Microstructure of Portland Cement Pastes as a Result of Natural and Supercritical Carbonation Procedures. *Industrial and Engineering Chemistry Research.* 2006, 45(14), 4985-4992. ISSN: 0888-5885.
112. Leemann, A.; Nygaard, P.; Kaufmann, J.; *et al*. Relation between carbonation resistance, mix design and exposure of mortar and concrete. *Cement and Concrete Composites.* 2015, 63, 33-43. ISSN: 0958-9465.
113. Galan, I.; Andrade, C.; Castellote, M. Natural and accelerated $CO_2$ binding kinetics in cement paste at different relative humidities. *Cement and Concrete Research*. 2013, 49, 21-28. ISSN: 0008-8846.
114. Asavapisit, S.; Fowler, G.; Cheeseman, C.R. Solution chemistry during cement hydration in the presence of metal hydroxide wastes. *Cement and Concrete Research*. 1997, 27, 1249-1260. ISSN: 0008-8846.
115. Liu, L.; Ha, J.; Hashida, T.; *et al*. Development of a $CO_2$ solidification method for recycling autoclaved lightweight concrete waste. *Journal of Materials Science Letters.* 2001, 20(19), 1791-1794. ISSN: 0261-8028.
116. Van-Loc, T.; Bonnet, S.; Kiesse, T.S.; *et al*. A new meta-model to calculate carbonation front depth within concrete structures. *Construction and Building Materials.* 2016, 129, 172-181. ISSN: 0950-0618.
117. Silva, R.V.; Neves, R.; de Brito, J.; *et al*. Carbonation behaviour of recycled aggregate concrete. *Cement and Concrete Composites*. 2015, 62, 22-32. ISSN: 0958-9465.

118. Thiery, M.; Dangla, P.; Belin, P.; et al. Carbonation kinetics of a bed of recycled concrete aggregates: A laboratory study on model materials. *Cement and Concrete Research*. 2013, 46, 50-65. ISSN: 0008-8846.
119. Duguid, A.; Scherer, G.W. Degradation of oilwell cement due to exposure to carbonated brine. *International Journal of Greenhouse gas Control.* 2010, 4(3), 546-560. ISSN: 1750-5836.
120. Urbonas, L.; Leno, V.; Heinz, D. Effect of carbonation in supercritical $CO_2$ on the properties of hardened cement paste of different alkalinity. *Construction and Building Materials.* 2016, 123, 704-711. ISSN: 0950-0618.
121. Liu, Q.; Liu, J.; Qi, Li. Effects of temperature and carbonation curing on the mechanical properties of steel slag-cement binding materials. *Construction and Building Materials.* 2016, 124, 999-1006. ISSN: 0950-0618.
122. Hidalgo, A.; Domingo, C.; Garcia, C.; *et al*. Microstructural changes induced in Portland cement-based materials due to natural and supercritical carbonation. *Journal of Materials Science.* 2008, 43(9), 3101-3111. ISSN: 0022-2461.
123. Short, N.R.; Purnell, P.; Page, C.L. Preliminary investigations into the supercritical carbonation of cement pastes. *Journal of Materials Science.* 2001, 36(1), 35-41. ISSN: 0022-2461.
124. Chang, C.F.; Chen, J.W. The experimental investigation of concrete carbonation depth. *Cement and Concrete Research*. 2006, 36(9), 1760-1767. ISSN: 0008-8846.
125. Shamsad, S.; Assaggaf, R.A.; Maslehuddin, M.; *et al*. Effects of carbonation pressure and duration on strength evolution of concrete subjected to accelerated carbonation curing. *Construction and Building Materials.* 2017, 136, 565-573. ISSN: 0950-0618.
126. Wigand, M.; Kaszuba, J.P.; Carey, J.W.; *et al*. Geochemical effects of $CO_2$ sequestration on fractured wellbore cement at the cement/caprock interface. *Chemical Geology*. 2009, 265(1-2), Special Issue: SI, 122-133. ISSN: 0009-2541.
127. Kjellsen, K.O.; Guimaraes, M.; Nilson, A. The $CO_2$ Balance of Concrete in a Life Cycle Perspective. Danish Technological Institute: Nordic Innovation Center, 2005.
128. Santra, A.; Sweatman, R. Understanding the Long-Term Chemical and Mechanical Integrity of Cement in a CCS Environment. In: *10th International Conference on Greenhouse Gas Control Technologies*. Amsterdam, Nettherlands, 2010. *Energy Procedia*. 2011, 4, 5243-5250. ISSN: 1876-6102.
129. Bukowski, J.M.; Berger, R.L. Reactivity and Strength Development of $CO_2$ Activated Non-hydraulic Calcium Silicates. *Cement and Concrete Research*. 1979, 9(1), 57-68. ISSN: 0008-8846.
130. Hyvert, N.; Sellier, A.; Duprat, F.; et al. Dependency of C–S–H carbonation rate on $CO_2$ pressure to explain transition from accelerated tests to natural carbonation. *Cement and Concrete Research*. 2010, 40(11), 1582-1589. ISSN: 0008-8846.

131. Borges, P. H. R.; Costa, J. O.; Milestone, N. B.; et al. Carbonation of CH and C–S–H in composite cement pastes containing high amounts of BFS. *Cement and Concrete Research*. 2010, 40(2), 284-292. ISSN: 0008-8846.
132. Zhou, Q.; Glasser, F.P. Kinetics and mechanism of the carbonation of ettringite. *Advnaces in Cement Research.* 2000, 12(3), 131-136. ISSN: 0951-7197.
133. Jang, J.G.; Lee, H.K. Microstructural densification and $CO_2$ uptake promoted by the carbonation curing of belite-rich Portland cement. *Cement and Concrete Research*. 2016, 82, 50-57. ISSN: 0008-8846.
134. Fang, Y.; Chang, J. Rapid hardening beta-$C_2S$ mineral and microstructure changes activated by accelerated carbonation curing. *Journal of Thermal Analysis and Calorimetry*. 2017, 129(2), 681-689. ISSN: 1388-6150.
135. Guan, X.; Liu, S.; Feng, C.; *et al*. The hardening behavior of gamma-$C_2S$ binder using accelerated carbonation. *Construction and Building Materials.* 2016, 114, 204-207. ISSN: 0950-0618.
136. Saito, T.; Sakai, E.; Morioka, M.; *et al*. Carbonation of γ-$Ca_2SiO_4$ and the Mechanism of Vaterite Formation. *Journal of Advanced Concrete technology.* 2010, 8(3), 273-280. ISSN: 1346-8014.
137. Saito, T.; Saphouvong, K.; Yumoto, T.; *et al*. Permeability of sulfate ions in cementitious materials containing γ-$Ca_2SiO_4$ after autoclave curing and accelerated carbonation. *Journal of Advanced Concrete technology.* 2010, 8(3), 273-280. ISSN: 1346-8014.
138. Mabudo, G.M.; Lee, S.; Kang, S.; *et al*. Physical properties and carbon dioxide capture of synthetic gamma-$C_2S$ cement composites in the early days of curing. *Magazine of Concrete Research.* 2016, 68(21), 1079-1084. ISSN: 0024-9831.
139. Engel'sht, V. S.; Muratalieva, V. Zh. Thermal Interaction between Limestone and Silica. *High Temperature*. 2013, 51(6), 769-775. ISSN: 0018-151X.
140. Ashraf, W.; Olek, J. Elucidating the accelerated carbonation products of calcium silicates using multi-technique approach. *Journal of $CO_2$ Utilization.* 2018, 23, 61-74. ISSN: 2212-9820.
141. Pizzol, V.D.; Mendes, L.M.; Savastano, H., Jr.; *et al*. Mineralogical and microstructural changes promoted by accelerated carbonation and ageing cycles of hybrid fiber–cement composites. *Construction and Building Materials*. 2014, 68, 750-756. ISSN: 0950-0618.
142. Mo, L.; Panesar, D.K. Accelerated carbonation – A potential approach to sequester $CO_2$ in cement paste containing slag and reactive MgO. *Cement and Concrete Composites*. 2013, 43, 69-77. ISSN: 0958-9465.
143. Lackner, K.S.; Wendt, C.H.; Butt, D.P. Carbon dioxide disposal in carbonate minerals. *Energy*. 1995, 20(11), 1153-1170. ISSN: 0360-5442.
144. Huijgen, W.J.J.; Witkamp, G.; Comans, R.N.J. Mechanisms of aqueous wollastonite carbonation as a possible $CO_2$ sequestration process. *Chemical Engineering Science.* 2006, 61(13), 4242-4251. ISSN: 0009-2509.

145. Min, Y.; Li, Q.; Voltolini, M.; *et al*. Wollastonite Carbonation in Water-Bearing Supercritical $CO_2$: Effects of Particle Size. *Environmental Science and Technology*. 2017, 51(21), 13044-13053. ISSN: 0013-936X.
146. Miller, Q.R.S.; Thompson, C.J.; Loring, J.S.; *et al*. Insights into silicate carbonation processes in water-bearing supercritical $CO_2$ fluids. *International Journal of Greenhouse gas Control.* 2013, 15, 104-118. ISSN: 1750-5836.
147. Whitfield, P.S.; Mitchell, L.D. *In situ* laboratory X-ray powder diffraction study of wollastonite carbonation using a high-pressure stage. *Applied Geochemistry*. 2009, 24(9), 1635-1639. ISSN: 0883-2927.
148. Siauciunas, R.; Gendvilas, R.; Mikaliunaite, J.; *et al*. Application of Isomorphic Ca-Si Rocks for the Synthesis of α-$C_2S$ Hydrate. *Material Science*. 2014, 20(3), 321-327. ISSN: 1068-820X.
149. Longa-Avello, L.; Pereyra-Zerpa, C.; Andres Casal-Ramos, J.; *et al*. Study of the calcination process of two limonitic iron ores between 250 °C and 950 °C. *Revista Facultad de Ingenieria, Universidad Pedagogica y Technologica de Colombia*. 2017, 26(45), 33-45. ISSN: 0121-1129.
150. Chandra, S. Waste Materials Used in Concrete Manufacturing. London: Elsevier, 1996. T. 1st Edition.
151. Armand, P.; Lignie, A.; Beaurain, M.; *et al*. Flux-Grown Piezoelectric Materials: Application to α-Quartz Analogues. *Crystals*. 2014, 4(2), 168-189. ISSN: 2073-4352.
152. Dyatlova, E. M.; Minenkova, G. Ya.; Mikhal'skaya, T. I. Obtaining facing tiles based on low-fusing clays. *Glass and Ceramics*. 1994, 51(9-10), 308-311. ISSN: 0361-7610.
153. Pesonen, J.; Myllymaki, P.; Toumikoski, S.; *et al*. Use of Calcined Dolomite as Chemical Precipitant in the Simultaneous Removal of Ammonium and Phosphate from Synthetic Wastewater and from Agricultural Sludge. *ChemEngineering*. 2019, 3, 40. ISSN: 2305-7084.
154. Gaudette, H.E.; Eades, J.L.; Grim, R.E. The Nature of Illite. In: *Thirteenth National Conference on Clays and Minerals*. Madison, 1964.
155. Saxena, S.K.; Chatterjee, N.; Fei, Y.; *et al*. Thermodynamic Data on Oxides and Silicates. Heidelberg: Springer Verlag, 1993.
156. Haynes, M.W. CRC Handbook of Chemistry and Physics (92nd ed.). Haboken: CRC Press, 2011.
157. Kubachewski, O.; Alcock, C.B. Metallurgical Thermochemistry. Oxford: Pergamon Press, 1979.
158. Na, S.; Kang, S.; Lee, S.; *et al*. Gamma-$C_2S$ Synthesis from Fly Ash of Fluidize-Bed Boiler for $CO_2$ Capture. *Acta Physica Polonica A*. 2015, 127(4), 1282-1285. ISSN: 0587-4246.
159. Pontikes, Y.; Jones, P.T.; Geysen, D.; *et al*. Options to Prevent Dicalcium Silicate-Driven Disintegration of Stainless Steel Slags. *Archives of Metallurgy and Materials.* 2010, 55(4), 1167-1172. ISSN: 1733-3490.

160. Jansen, D.; Goetz-Neunhoeffer, F.; Lothenbach, B.; *et al*. The early hydration of Ordinary Portland Cement (OPC): An approach comparing measured heat flow with calculated heat flow from QXRD. *Cement and Concrete Research*. 2012, 42(1), 134-138. ISSN: 0008-8846.
161. Joachim, B; Gardes, E.; Abart, R.; *et al*. Experimental growth of akermanite reaction rims between wollastonite and monticellite: Evidence for volume diffusion control. *Contributions to Mineralogy and Petrology*. 2010, 161(3), 389-399. ISSN: 0010-7999.
162. Mirhadi, S.M.; Tavangarian, F.; Emadi, R. Synthesis, characterization and formation mechanism of single-phase nanostructure bredigite powder. *Mineral Science and Engineering C-materials for Biological Applications*. 2012, 32(2), 133-139. ISSN: 0928-4931.
163. Zhang, N.; Molenda, J.A.; Mankoci, S.; *et al*. Crystal Structures of $CaSiO_3$ Polymorphs Control Growth and Osteogenic Differentiation of Human Mesenchymal Stem Cells on Bioceramic Surfaces. *Biomaterials Science*. 2013, 1(10), 1101-1110. ISSN: 2047-4830.
164. Grapes, R. Pyrometamorphism. Berlin: Springer-Verlag Berlin Heidelberg, 2006.
165. Fang, Y.; Chang, J. Rapid hardening β-$C_2S$ mineral and microstructure changes activated by accelerated carbonation curing. *Journal of Thermal Analysis and Calorimetry*. 2017, 129(2), 681-689. ISSN: 1388-6150.
166. Fernandez-Carrasco, L.; Torrens-Martin, D.; Morales, L.M.; *et al*. Infrared Spectroscopy in the Analysis of Building and Construction Materials. Infrared Spectroscopy – Materials Science, Engineering and Technology: In Tech, 2011, 369-381.
167. Fernandez, L.; Alonso, C.; Hidalgo, A.; *et al*. The role of magnesium during the hydration of $C_3S$ and C-S-H formation. Scanning electron microscopy and mid-infrared studies. *Advances in Cement Research*. 2005, 17(1), 9-21. ISSN: 0951-7197.
168. Choudhary, R.; Koppala, S.; Swamiappan, S. Bioactivity studies of calcium magnesium silicate prepared from eggshell waste by sol-gel combustion synthesis. *Journal of Asian Ceramic Societies*. 2015, 3(2), 173-177. ISSN: 2187-0764.
169. Kouhi, M.; Shamanian, M.; Fathi, M.; *et al*. Synthesis, Characterization, *In Vitro* Bioactivity and Biocompatibility Evaluation of Hydroxyapatite/Bredigite ($Ca_7MgSi_4O_{16}$) Composite Nanoparticles. *JOM: the Journal of the Minerals, Metals & Materials Society*. 2016, 68(4), 1061-1070. ISSN: 1047-4838.
170. Purnell, P.; Short, N.R.; Page, C.L. Super-critical carbonation of glass-fibre reinforced cement. Part 1: mechanical testing and chemical analysis. *Composites Part A – Applied Science and Manufacturing*. 2001, 32(1), 1777-1787. ISSN: 1359-835X.

171. Fernandez-Carrasco, L.; Rius, J.; Miravitlles, C. Supercritical carbonation of calcium aluminate cement. *Cement and Concrete Research*. 2008, 38(8-9), 1033-1037. ISSN: 0008-8846.
172. Steinour, H.H. Some effects of carbon dioxide on mortars and concrete-discussion. *Journal of the American Concrete*. 1959, 50, 905-907. ISSN: 0002-8061.
173. Fang, Y.; Chang, J.; Cao, M. Influence of compaction pressure on the accelerated carbonation of calcium hydroxide. *Journal of Wuhan University of Technology-Materials Science Edition*. 2016, 31(6), 1187-1192. ISSN: 1000-2413.
174. Kumar, R; Bhattacharjee, B. Porosity, pore size distribution and *in situ* strength of concrete. *Cement and Concrete Research*. 2003, 33(1), 155-164. ISSN: 0008-8846.
175. St. John, D.A.; Poole, A.B.; Sims, I. Concrete Petrography – A Handbook of Investigative Techniques. London: Arnold, 1998.
176. Morandeau, A.E.; Thiery, M.; Faure, P.F.; *et al*. Effect of Carbonation on the Microstructure and Moisture Properties of Cement-Based Materials. In: XII DBMC Conference. Porto, Portugal, 2011.
177. Farnam, Y.; Villani, C.; Washington, T.; *et al*. Performance of carbonated calcium silicate based cement pastes and mortars exposed to NaCl and $MgCl_2$ deicing salt. *Construction and Building Materials*. 2016, 111, 63-71. ISSN: 0950-0618.
178. Liu, S.; Dou, Z.; Zhang, S.; *et al*. Effect of sodium hydroxide on the carbonation behavior of β-dicalcium silicate. *Construction and Building Materials*. 2017, 150, 591-594. ISSN: 0950-0618.
179. Shen, Q; Wei, H; Zhou, Y; *et al*. Properties of Amorphous Calcium Carbonate and the Template Action of Vaterite Spheres. *Journal of Physical Chemistry B*. 2006, 110(7), 2994-3000. ISSN: 1520-6106.
180. Lioliou, M.G.; Paraskeva, C.A.; Koutsoukos, P.G.; *et al*. Heterogeneous nucleation and growth of calcium carbonate on calcite and quartz. *Journal of Colloid and Interface Science*. 2007, 308(2), 421-428. ISSN: 0021-9797.
181. Nour, W.M.N.; Mostafa, A.A.; Ibrahim, D.M. Recycled wastes as precursor for synthesizing wollastonite. *Ceramics International*. 2008, 34(1), 101-105. ISSN: 0272-8842.
182. Thiery, M.; Villain, G.; Dangla, P.; *et al*. Investigation of the carbonation front shape on cementitious materials: Effects of the chemical kinetics. *Cement and Concrete Research*. 2007, 37(7), 1047-1058. ISSN: 0008-8846.
183. Andersen F. A.; Brecevic, L. Infrared Spectra of Amorphous and Crystalline Calcium Carbonate. *Acta Chemica Scandinavia*. 1991, 45(10), 1018-1024. ISSN: 0904-213X.
184. Zheng, J.J.; Li, C.Q.; Zhou, X.Z. Characterization of Microstructure of Interfacial Transition Zone in Concrete. *Aci Materials Journal*. 2005, 102(4), 265-271. ISSN: 0889-325X.

185. Ashraf, W.; Olek, J.; Sahu, S. Phase evolution and strength development during carbonation of low-lime calcium silicate cement (CSC). *Construction and Building Materials*. 2019, 210, 473-482. ISSN: 0950-0618.
186. Hansen, M.R.; Jakobsen J.H.; Skibsted, J. 29Si Chemical Shift Anisotropies in Calcium Silicates from High-Field 29Si MAS NMR Spectroscopy. *Inorganic Chemistry*. 2003, 42(7), 2368-2377. ISSN: 0020-1669.
187. Deer, W.A.; Howie, R.A.; Zussman, J. Rock-forming Minerals: Disilicates and Ring Silicates, vol. 1B. London: Geological Society of London, 1997.
188. Cong, X.; Kirkpatrick, R.J. 29Si MAS NMR study of the structure of calcium silicate hydrate. *Advanced Cement Based Materials*. 1996, 3(3-4), 144-156. ISSN: 1065-7355.
189. Avérous, L.; Pollet, E. Environmental Silicate Nano-Biocomposites. London: Springer-Verlag, 2012.

**List of Scientific Publications**

**Articles published in journals indexed in the Clarivate Analytics web of Science with Impact Factor:**

1. Šmigelskytė, Agnė; Šiaučiūnas, Raimundas; Parameter influence on the rankinite binder paste and mortar accelerated carbonation curing // Journal of Thermal Analysis and Calorimetry. ISSN 1388-6150. eISSN 1588-2926. 2019, DOI 10.1007/s10973-019-08590-1.
2. Šmigelskytė, Agnė; Šiaučiūnas, Raimundas; Wagner, Matthias; Urbonas, Liudvikas. Synthesis of rankinite from natural Ca-Si rocks and its hardening in $CO_2$ atmosphere // Revista Romana de materiale – Romanian journal of materials. Bucurest: ISSN 1583-3186. eISSN 2457-502X. 2019, vol. 49, iss. 1, p. 111-119.
3. Šmigelskytė, Agnė; Šiaučiūnas, Raimundas. Influence of raw meal compaction pressure on OPC clinker mineral composition and heat flow // Journal of Thermal Analysis and Calorimetry. ISSN 1388-6150. eISSN 1588-2926. 2018, Vol. 131, iss. 1, p. 513-519.

**Articles published in conference proceedings**

1. Šiaučiūnas R.; Šmigelskytė A. Carbonation parameter influence on rankinite hardening process // 15th international congress on the chemistry of cement: Prague, Czech Republic, September 16-20, 2019: papers and posters proceedings. Prague: CONFEA. ISSN 2523-935X. 2019.

**Publications of International Scientific Conferences**

1. Šmigelskytė, A.; Takulinskas, Ž.; Skirbutas, J. Influence of raw meal composition on sintering and carbonation of calcium silicates // Chemistry and chemical technology: Lithuanian chemists conference, May 16, 2019, Lithuanian Academy of Sciences, Vilnius: conference book. Vilnius: Vilnius University, 2019. eISBN 9786090701676. p. 119.
2. Šiaučiūnas, Raimundas; Šmigelskytė, Agnė. Thermal gravimetric studies of rankinite binder carbonation process // 12$^{th}$ European symposium on thermal analysis and calorimetry, 27-30 August 2018, Brasov, Romania / editors: Andrei Rotaru, Crisan Popescu. Greifswald: Academica, 2018, PS1.051. ISBN 9783940237507. p. 235.
3. Šmigelskytė, Agnė; Šiaučiūnas, Raimundas. Accelerated carbonation curing of rankinite binder and OPC // 38$^{th}$ Cement and concrete science conference: 10 – 11 September 2018, Coventry University, UK. Coventry: Coventry University, 2018, art. no. 06. ISBN 9781846000881. p. 25.
4. Šmigelskytė, Agnė; Šiaučiūnas, Raimundas. Temperature influence on rankinite carbonation hardening process // BaltSilica 2018: book of abstracts of the 8$^{th}$ international conference on silicate materials, May 30 – June 1,

2018, Riga, Latvia / organized by: Riga Technical University, Kaunas University of Technology, Adam Mickiewicz University in Poznan. Riga: RTU Publishing House. ISSN 2243-6057. 2018, O2, p. 25.
5. Šmigelskytė, Agnė; Šiaučiūnas, Raimundas. Investigation of rankinite activation and hardening in $CO_2$ atmosphere // Chemistry and chemical technology 2017: proceedings of the international conference, April 28, 2017, Kaunas. Kaunas: Kauno technologijos universitetas. ISSN 2538-7359. 2017, p. 85.
6. Šmigelskytė, Agnė; Šiaučiūnas, Raimundas. Influence of forming pressure on the hydration of clinker minerals // BaltSilica 2016 : book of abstracts of the 7th Baltic conference on silicate materials, 26-27 May 2016, Kaunas, Lithuania / Kaunas University of Technology, Riga Technical University, Adam Mickiewicz University in Poznan. Kaunas: Kauno technologijos universitetas. ISSN 2243-6057. 2016, p. 35.
7. Šmigelskytė, Agnė; Šiaučiūnas, Raimundas. Influence of forming pressure on the synthesis of clinker minerals // Chemistry and chemical technology: international conference of Lithuanian Society of Chemistry: Lithuanian Academy of Science, Vilnius, Lithuania, April 28-29, 2016: book of abstracts / Fizinių ir technologijos mokslų centras, Vilniaus universitetas, Lietuvos mokslų akademija, Kauno technologijos universitetas. 2016. ISBN 9786099551135. p. 220.
8. Šmigelskytė, Agnė; Šiaučiūnas, Raimundas. Influence of initial mixture pressing pressure on OPC clinker mineral composition and heat flow // International conference on thermal analysis and calorimetry in Russia (RTAC-2016), 16-23 September, 2016, St. Petersburg, Russia. Vol 1: book of abstracts. St. Petersburg: St. Petersburg Polytechnic University, 2016. ISBN 9785742254478. p. 357-359.

**Acknowledgments**

The foremost thank you to my supervisor prof. Raimundas Šiaučiūnas, for his respect, attention, knowledge, patience, and care during all the years of my PhD studies. None of this would have happened if it were not for him.

A sincere thank you to all the colleagues at the Department of Silicate technology, for their help and support.

Huge thanks to my family and friends for supporting and comforting me and a very special thank you to my partner Andrius for always being there for me.

I am truly grateful for this opportunity to whomever else contributed to making this happen. Thank you all!

SL344. 2019-10-30, 13,5 leidyb. apsk. l. Tiražas 12 egz. Užsakymas 234.
Išleido Kauno technologijos universitetas, K. Donelaičio g. 73, 44249 Kaunas
Spausdino leidyklos „Technologija“ spaustuvė, Studentų g. 54, 51424 Kaunas